UNIVERSITÀ DI PARMA

UNIVERSITÀ DEGLI STUDI DI PARMA

DOTTORATO DI RICERCA IN INGEGNERIA INDUSTRIALE

CICLO XXXVII

Vibration-based damage detection strategies using piezoelectric sensors

Coordinatore:

Chiar.mo Prof. Gianni Royer Carfagni

Tutore:

Chiar.mo Prof. Marcello Vanali

Dottorando:

Carlotta Rossi

Anni Accademici: 2021/2022 – 2023/2024

Abstract

Structural Health Monitoring (SHM) techniques aim to evaluate the structural integrity of civil, mechanical and aerospace systems. All these systems have a predicted service life which can be heavily reduced because of damage occurrence; their safety, serviceability and performance need to be ensured through the most suitable techniques. Once some damage emerges in the structures, the changes in the physical properties can cause detectable changes in modal parameters such as natural frequencies, modal damping and mode shapes, which can be used to detect, characterise and localise the damage itself.

During the last few years, many techniques have been developed to identify suitable and reliable damage indices, and vibration-based structural health monitoring (VBSHM) has achieved great success and widespread adoption. The main goal is to remove or minimise environmental and operational influences such as temperature variations which can affect the quality and reliability of the analysis. Structures under investigation are typically laboratory ones representing plausible structures on a laboratory scale.

This PhD thesis studies the possibility of implementing piezoelectric transducers for SHM techniques suiting a model-based approach. The structure under investigation is a laboratory truss girder specifically designed to develop VBSHM techniques. The possibility of exploiting the electromechanical coupling between the structure and piezoelectric transducer, specifically the variation of the so-called Modal Electro-Mechanical Coupling Factor (MEMCF) between undamaged and damaged conditions to evaluate the structural health status is investigated. This scalar parameter, which measures the effectiveness of the transducer's sensing and actuating capabilities, has been proven to be sensible to structural alterations and not to temperature variations, being a reliable damage index. Moreover, it can be easily estimated by measuring the eigenfrequencies of the electromechanical system.

This study provides numerical and experimental analysis: first, a Finite Element (FE) analysis of the electromechanical system, in different healthy conditions, has been performed to identify the best transducer and its best placement in the structure. After that, experimental tests were performed to validate the model and to estimate the variation of the MEMCF from undamaged to damaged condition of the structure. Ambient vibration excitation has been simulated with a shaker input signal control strategy to perform an Operational Modal Analysis (OMA) and properly estimate modal parameters such as eigenfrequencies. Different damage scenarios have been tested to evaluate the sensitivity of the damage indexes chosen to the damage's entity and location.

Table of contents

List of Figures

List of tables

1. Introduction

In this chapter, a brief introduction to Structural Health Monitoring and piezoelectricity is reported. After that, the modal electromechanical coupling factor (MEMCF) is defined and analysed as a possible damage index. Subsequently, the purpose and the outline of this thesis are presented.

1.1. Structural Health Monitoring

During the last few years, structural and mechanical systems such as bridges, rotating machinery, and power generation systems have become increasingly important for modern society. As all the systems, these structures have a predicted service life which can be heavily reduced because of damage occurrence. Damage can be defined as changes to the material and/or geometric properties of these systems, including changes to the boundary conditions and system connectivity, which adversely affect their current or future performance [1]. They need to be monitored to ensure their safety and serviceability and, if possible, avoid their replacement, which cannot be economically done. Monitoring structures by using integrated sensor networks, not only at scheduled inspection intervals but on demand, could bring several benefits, such as discovering the damage at an earlier stage of advancement and tracing its further development.

The process of implementing a damage identification strategy for aerospace, civil and mechanical engineering infrastructures is referred to as Structural Health Monitoring (SHM). Unlike the conventional techniques of inspection, where an operator periodically evaluates the structural integrity by external equipment, in SHM sensors and actuators are permanently attached to the structure, collecting data almost continuously during the entire service life of the structure. SHM, indeed, involves the observation of the system under investigation over time using periodically spaced measurements, the extraction of damage-sensitive features from these measurements and the statistical analysis of these features to determine the current state of the system health [2]. So, the concept of damage and SHM would be meaningless without comparing at least two different states of the system, one of which represents the undamaged state. During the last years, among many different non-destructive techniques that have been developed, vibration-based structural health monitoring (VBSHM) is the one that has gained the most success and spread. The reason of its diffusion is its global damage identification approach. Compared with other techniques, such as ultrasound testing (C-Scan) or radiographic detection (X-ray), VBSHM doesn't require the knowledge a priori of the position of damage, or its readily accessibility for testing. Any structure can be studied as a dynamic system with stiffness, mass and damping. Once some damage emerges in the structures, the changes in the physical properties will cause detectable changes in modal parameters as natural frequencies, modal damping and mode shapes [3]. These changes in modal parameters can be used to detect, characterise, and, to a certain extent, localise damage of a structure in operation [3],[4]. Many research studies about the extraction and the processing of natural frequencies, mode shapes, damping coefficients or a combination of them can be found in the literature. Natural frequency-based methods are attractive because natural frequencies can be conveniently measured from a few accessible points on the structure by low-cost sensors. Another critical limitation is that the frequency changes caused by damage are usually very small and may be buried in the changes caused by environmental and operational conditions. In [5] [6] and is discussed how frequency variation due to ambient vibration and environmental effects can be as high as 5-10%. To account for this effect, most successful damage identification methods using frequency are verified only in a controlled laboratory scale, and statistical damage detection models are needed to distinguish damage-induced changes from environment-induced changes [7]. Compared to the natural-frequencies model-based methods, those based on mode shapes take advantage of the fact that mode shapes contain local information, which makes them more sensitive to local damages and they are less sensitive to environmental effects, such as temperature, than natural frequencies [8]. However, their measurement is more complex and more prone to noise contamination than natural frequencies. It has been shown by many researchers that the displacement mode shape itself is not very sensitive to small damage, even with high density mode shape

measurement [9], [10]. These methods are both used for global and local damage detection. The first one deals with the overall structure response, while the second one is focused on screening components and subcomponents.

Data acquisition can be obtained through experimental measurements like an accelerometer network or computationally via numerical methods like the Finite Element method. Consequently, SHM methods can be divided into two categories: model-based methods and data-driven methods. Compared with data-driven SHM, where the system under investigation is like a "black box" whose response is analysed, model-based methods provide an updated physics-based numerical model that can be used for damage prognosis. In both cases, data have to be as representative as possible of the structure's status and the number of data sets must be adequate. For these reasons, experimental analysis is more attractive, since the performance of model-based methods is susceptible to modelling error due to model simplification and omission. However, due to practical limitations, data acquisition usually happens on lab-scale structures. On the other hand, given FE models accurate enough, several damage types and load cases can be simulated at virtually no cost and effort. Updated model techniques [11], [12] offer solutions to the problem of FE accuracy by using experimental measurements of the actual structure to numerically modify the physical parameters of a FE model [13]. So, once the optimal FE model on the healthy status is reached, it can be used to simulate damage status too.

Another fundamental aspect of SHM concerns the choice of sensors applied. Wireless sensor networks are often preferred to traditional high-cost wired SHM systems because of their ease of placement, high spatial resolution and wireless data transmission ([7]). Despite this, they have certain limitations, such as difficulties implementing large-scale sensor networks and accurate damage localization[14] .

To improve the quality of SHM and solve these problems, several solutions employing smart materials as sensing components have been developed. Smart materials work with fundamentally different principles and they owe their increasingly widespread adoption to their unique ability to respond to stimuli such as loads or environment [14]. Smart materials include optical fibres, piezoelectric polymers and ceramics, electro-rheological (ER) fluids, magneto-strictive materials and shape memory alloys (SMAs). The employment of piezoelectric materials witnessed significant growth in SHM of civil and mechanical structures because of their special ability to respond to stimuli, embeddability and compatibility with construction materials [14], [15]. They are also cost-effective and capable of detecting ambient vibrations in the host structures in which they are embedded. By tuning the piezoelectric mode of operation, advanced sensors have been developed, such as piezoelectric electromechanical impedance sensors [16]. Some examples of laboratory experiments employing piezoelectric sensors are those of Baptista [17], Park [18] and Giurgiutiu [19] in which impedance-based methods were used for damage detection for composite-reinforced concrete walls and the detection of a loosening bolt on an experimental three-story moment-resisting frame structure, adhesive defect monitoring of lass fibre epoxy [18], [20]. Other studies focus on the wave lamb waves generated by piezoelectric materials which also detect the reflected Lamb wave using the pulse-echo method. For example, it has been applied for corrosion and crack detection, bolt loosening and delamination [21], [22].

In the next section, a brief introduction about piezoelectricity and piezoelectric sensors in SHM will be presented.

1.2. Piezoelectricity

Piezoelectricity is the ability of some materials to transform mechanical energy into electrical energy and vice versa. Some examples of piezoelectric materials are many monocrystalline materials such as quartz, tourmaline or topaz, and some man-made polycrystalline ceramic materials, as the lead zirconate titanate (PZT). When a poled piezoelectric ceramic is mechanically strained it turns electrically polarised and an electric charge is produced on its surface. This property is referred to as "direct piezoelectric effect" and it is the basis on which piezo-sensors are based on. In fact, if two electrodes are attached to the surface of the material, the generated

charge can be collected and use. Otherwise, we refer to "converse piezoelectric effect" when the piezoelectric element strains mechanically because of a voltage applied to it. In this case the device is used as an actuator.

The constitutive equations describing the piezoelectric property are based on the assumption that the total strain in the transducer is the sum of mechanical strain induced by the mechanical stress and the controllable actuation strain caused by the applied electric voltage [23]. Thus, the electromechanical equations for a linear piezoelectric material can be written, referring to Figure 1 for the converse and direct effect respectively, as [24], [25]:

$$\varepsilon_i = S_{ij}^E \sigma_j + d_{mi} E_m \quad and \quad \varepsilon_i = S_{ij}^D \sigma_j + g_{mi} D_m$$

Eq. 1

$$D_m = d_{mi} \sigma_i + \xi_{ik}^\sigma E_k \quad and \quad E_i = g_{mi} \sigma_i + \beta_{ik}^\sigma D_k$$

Eq. 2

where:

- σ is the stress vector [N/m^2]
- ε is the strain vector [m/m]
- E is the vector of applied electric field [V/m]
- ξ is the permittivity [F/m]
- d is the matrix of piezoelectric strain constants [m/V]
- S is the matrix of compliance coefficients [m^2/N]
- D is the vector of electric displacement [C/m^2]
- g is the matrix of piezoelectric constants [m^2/C]
- β is the impermittivity [m/F]
- Indexes i,j=1_6 and m,k=1_3 refer to different directions of the material coordinate system
- Superscripts D, E, σ indicate measurements taken at constant electric displacement, constant electric field and constant stress respectively

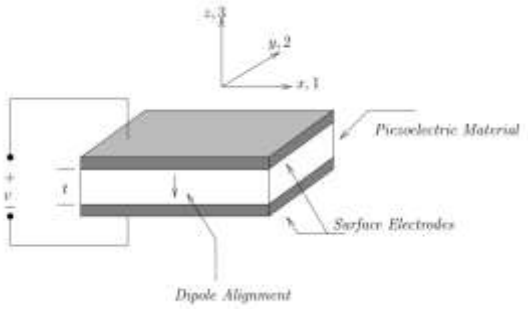

Figure 1: Scheme of a piezoelectric transducer

The converse piezoelectric effect describes the situation in which the piezoelectric transducer is used as an actuator, while the direct effect is when it is used as a sensor.

Piezoelectric transducers are available in many forms and shapes [26].Thin sheets generally called "patches" and the "stack" form, where many layers of piezoelectric materials and electrodes are assembled together are the most used. Since in this thesis work the interaction between a host structure and piezoelectric sensors in the form of stacks is investigated, from now on every reference will be addressed to them.

The efficiency of the conversion of mechanical energy into electrical energy and vice versa can be measured through the so-called electromechanical coupling factor of the transducer. For a piezoelectric stack composed of n layers, characterised by the capacitance C and the stiffness K_a, this parameter can be defined as:

$$\hat{k}^2 = \frac{n^2 d_{33}^2 K_a}{C}$$

Eq. 3

While other material properties, such as stiffness, permittivity, and piezoelectric coefficients, can vary with temperature, the coupling factor itself is a dimensionless quantity that reflects the relationship between these properties in a specific mode of vibration. It can be considered independent of temperature in many practical scenarios.

As reported above, in the literature there are many studies which exploit piezoelectric characteristics for SHM. In this work, the possibility of the implementation of the so-called modal electromechanical coupling factor (MEMCF) as a damage index has been investigated. In the next section, this parameter is defined.

1.3. The Modal Electromechanical Coupling Factor (MEMCF)

There is a wide range of possible implementations of piezoelectric transducers, owing to the coupled electro-mechanical behaviour, manifested in terms of direct or indirect piezoelectric effect. Some examples of these applications are vibration measurement, energy harvesting, active vibration control or, as in this case, vibration-based damage detection in SHM. These materials are also preferred in micro/nano electromechanical systems (M/NEMS) as an alternative to the traditional electrostatic transduction technique [27], [28], [29].

Several authors, as Berardengo et al. [30], [31], [32], [33], highlight the importance of the modal electromechanical coupling factor (MEMCF) in designing a performant shunt for structural vibration reduction by means of piezoelectric patches. In fact, it is demonstrated that the performances of the shunts are measured in terms of added damping factor for free vibrations and gain reduction for forced vibrations, which depend only on the MEMCF and structural damping (in most cases a problem data). It is also shown that MEMCF are very close to the effective electromechanical coupling factor (EEMCF) defined in [24]. To better understand what the MEMCF means we can consider a random elastic structure as the one depicted in Figure 2 with one piezoelectric transducer (patch or stack) bonded to it.

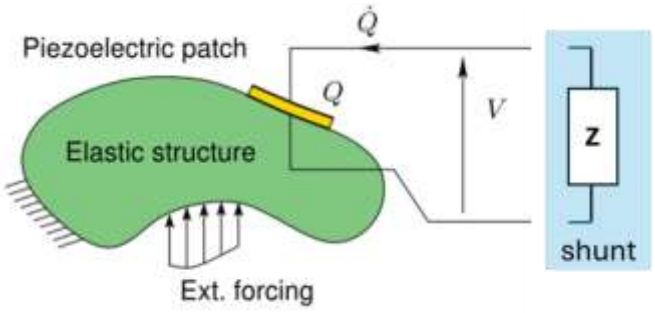

Figure 2:Random structure with piezoelectric patches on it

This coupled electromechanical system can be modelled as a reduced order model extending the displacement $\boldsymbol{U}(\boldsymbol{x}, t)$ of any point $\boldsymbol{x}$ at time t into N vibration eigenmodes (with piezoelectric patch short-circuited) as

$$U(x,t) = \sum_{i=1}^{N} \boldsymbol{\Phi}_i(x) q_i$$

Eq. 4

Thus, the modal coordinates q_i are the solutions of the problem

$$\ddot{q}_i + 2\xi_i\omega_i\dot{q}_i + \omega_i^2 q_i - \chi_i V = F_i \; \forall \; i \in \{1, \_, N\}$$

Eq. 5

$$CV - Q + \sum_{i=1}^{N} \chi_i q_i = 0$$

Eq. 6

where V is the voltage between the electrodes, Q is the electric charge in one of the electrodes and C is the electric capacitance of the patch. Moreover, ξ_i is the modal structural damping term, ω_i and Φ_i are the angular natural frequency and mode shape of the corresponding ith mode, respectively. Finally, the modal coupling coefficient χ_i represents the electromechanical coupling, so the energy transferred between the ith mode shape and the piezoelectric patch.

Eq. 5 can be rewritten introducing a dimensionless modal electromechanical coupling factor k_i as:

$$\ddot{q}_i + 2\xi_i\omega_i\dot{q}_i + \omega_i^2 q_i - \omega_i k_i \sum_{j=1}^{N} \omega_j k_j q_j - \omega_j k_i \frac{Q}{\sqrt{C}} = F_i$$

Eq. 7

$$V\sqrt{C} - \frac{Q}{\sqrt{C}} + \sum_{i=1}^{N} \omega_i k_i q_i = 0$$

Eq. 8

with

$$k_i = \frac{\chi_i}{\omega_i\sqrt{C}}$$

Eq. 9

So, assuming that the natural frequencies are far enough from one another, and so a single mode approximation can be adopted, $q_i = 0 \; \forall \; i \neq j$ and the equation N became

$$\ddot{q}_j + 2\xi_i\omega_i\dot{q}_i + \hat{\omega}_j^2 q_i - \omega_j k_j \frac{Q}{\sqrt{C}} = F_j$$

Eq. 10

Where

$$\hat{\omega}_j = \omega_j\sqrt{1 + k_j^2}$$

Eq. 11

which is the natural frequency of the mechanical oscillator with Q=0, and so it approximates the jth system's natural frequency in open circuit. Denoting and ω_j^{SC} and ω_j^{OC} the natural frequencies of the electromechanical system in short circuit (SC) and open circuit (OC) conditions, it is possible to observe that the MEMCF k_j is close, in absolute value, to the jth effective coupling factor $k_{eff\,j}$

$$|k_j| \cong k_{eff\ j} = \sqrt{\frac{\left(\omega_j^{OC}\right)^2 - \left(\omega_j^{SC}\right)^2}{\left(\omega_j^{SC}\right)^2}}$$

Eq. 12

This formula shows that k_j can be quickly evaluated with good approximation since ω_j^{SC} and ω_j^{OC} can be easily measured in practice.

The higher the $MEMCF_j$, the higher the electromechanical coupling, and so the higher the vibration reduction of jth mode. For this reason, recent studies have been developed to enhance this parameter. For example, Berardengo et al. [34], [35] investigates the implementation in the shunt circuit of negative capacitances in different configurations such as series, parallel or series-parallel ones.

The analytical definition of the $MEMCF_s$ so highlights their dependency to the natural frequencies of the system and to the mode shapes. As said in Section 1.1, many SHM techniques are based on variations in the frequency response function to assess the health and the well-functioning of the structures and a possible damage insurgence. For example, several studies focus on the alteration of the natural frequencies and curvature alteration of the mode shapes, such as the Curvature Damage Factor (CDF), the Damage Index Method (DMI) [36]. For this reason, it is plausible to think that the MEMCF could be used as an index to identify potential damage in a structure.

Moreover, the modal electromechanical coupling factor is a dimensionless quantity derived from the resonance frequencies of a particular mode of vibration evaluated at the same time, at the same environmental condition in two different electric configurations. Being evaluated as a frequency shift, it can be considered independent of temperature and its variations, as opposed to other indices as for example the simple natural frequencies estimation in different healthy conditions. Precisely because of this, it could be considered a good indicator for possible damage.

Relying on this, Manzoni, Berardengo et al. [37], [38], [39], [40] have actually shown in their work that this parameter varies as a damage occurs in the structures, and thus it can be used as index of damage's presence in a structure. Specifically, Brambilla [37] studied the case of a metallic beam with piezoelectric patches tied on in, while Schena [38] studied a case in which piezoelectric stacks were bonded on a truss.

1.4. Aim of this thesis

This PhD thesis aims to study and verify the possibility of implementing piezoelectric stack actuators for Structural Health Monitoring techniques. Specifically, the possibility of using the MEMCFs as a damage index in SHM of complex three-dimensional structures, specifically a truss girder one is investigated. The object of this study is a laboratory structure designed for the development of SHM technique based on vibration analysis. These types of structures owe their diffusion in the mechanical, aerospace and civil engineering field because they can be very strong and stable without being excessively heavy, thanks to the reduction of material used. Some examples of structures built suiting the truss girder scheme are for example bridges, roofs, floors, aerospace and mechanical components. Their popularity justifies the interest in developing techniques to monitor their serviceability and safety.

Recently, researchers have investigated further the employment of piezoelectric materials in SHM, because of their special ability to respond to external forces, compatibility with structures' materials, cost efficiency and ability to sense ambient vibration in the structure in which they are embedded. Some examples are piezoelectric-excited guided wave and piezoelectric electromechanical impedance sensors. In this work, piezoelectric stacks embedded in a truss structure are investigated. Indeed, the variation of the so-called modal

electromechanical coupling factor (MEMCF) due to the occurrence of damages in the host structure is analysed. This parameter measures the quality of the coupling between the piezoelectric element and the host structure, and it depends on the natural frequencies and the mode shapes of the entire electromechanical system. It is known from the literature that changes in modal parameters can be attributed to damages, and thus also the variation of MEMCFs could be employed as damage index for SHM. Some reasons that can justify this choice are the fact that it can be easily evaluated in practice, by simply measuring the natural frequencies with the piezoelectric stack in short circuit and open circuit configurations, and its low dependency on temperature variations despite its high sensitivity to physical, and thus vibration parameters, alterations.

Moreover, since the structure under investigation is a modular one, several damages, such as corrosion or breaks, can be considered; additionally, the piezoelectric sensors can be placed in different positions with different layouts. Unlike the piezoelectric patches that are glued to the host structure, the mechanical mounting of the stacks requires more attention. They can be easily damaged if subjected to mechanical action different from the ones they were designed to undergo. This is the reason why they are also preloaded in compression.

The approach taken in this work is reported below. A model-based method has been adopted, studying the problem through a Finite Element Analysis. First, a FE Model of the truss girder under investigation has been developed. It was validated by comparing the mode shapes evaluated numerically with those evaluated experimentally through an operational modal analysis applied to vibration measurements acquired experimentally. The MAC indices were evaluated too. Once the model has been validated, several damages have been simulated, such as cracks or breaks, in order to have at least two healthy conditions (damaged and undamaged) to compare. Then piezoelectric stacks have been modelled and added to them. In both configurations, the best geometrical layout of the piezoelectric sensors and their best placement have been evaluated. The best ones ensure the greatest magnitude of MEMCFs and their variation; for this reason, the dynamic response to ambient vibration of the EMS has been studied in different electrical configurations such as with the piezo actuators in Short Circuit and Open Circuit configuration. Once the most suitable actuator from those available from the main manufacturers and the best layout had been identified the experimental tests were performed. Ambient vibration excitation has been simulated with a shaker input signal control strategy to perform an Operational Modal Analysis (OMA) and correctly estimate modal parameters such as eigenfrequencies. Different damage scenarios have been tested to assess the sensitivity of the damage indexes chosen to the damage's entity and location.

1.5. Outline

The thesis is organised as follows:

- **Section 1**: a short introduction about the two main themes of this thesis, so structural health monitoring techniques and piezoelectricity is presented. The analytical definition of the MEMCF is exposed too. After that, the aim of the thesis is declared.
- **Section 2**: a brief introduction to piezoelectric stack sensors operation and main material characteristics is provided. The Fe model and analysis of the piezoelectric stacks are presented, focusing on the electrical and mechanical boundaries applied to reach the Short Circuit and Open Circuit electrical configurations. These configurations have been evaluated to determine the MEMCFs for several modes of the structure. Starting from those available in the main companies, different geometrical layouts have been added to the structure model in different placements, to find out the best ones.
- **Section 3**: After a brief introduction to truss girder structures, their theoretical background and application in mechanical, civil and aerospace engineering the subject of this study, a laboratory truss girder designed ad hoc for the development of SHM techniques is presented. The FE model of the structure is presented. This model has been updated and validated comparing its results from free

vibrations analysis with experimental tests. The modal parameters employed for the validation are natural frequencies, mode shapes and MAC index values.

- **Section 4**: After the validation of the undamaged model some possible damage scenarios have been simulated. The first goal has been to check if and where these damages could induce a variation in the mode shapes, to find the best placements for the piezo actuators. MAC indices were evaluated to match the modes between different electrical and damaged/undamaged configurations.
- **Section 5**: The Fe model of the electromechanical system is presented. Different piezoelectric actuators and different placements have been tested. The MEMCFs for several modes of the structure and then their variation between damaged and undamaged conditions have been estimated. Preliminary results are reported and analysed. Then, the best actuators were chosen as a trade-off between effectiveness, costs, number of modes detectable and MEMCFs magnitude reached.
- **Section 7**: based on the availability of piezoelectric actuators and on their mechanical mounting requirement, PZTs with similar geometrical and electrical characteristics were tested as for the precious ones. The PZT to implement was then chosen between these.
- **Section 8**: The experimental test setup is presented. A suitable structure for mounting the piezo was designed to ensure its correct functioning and preserve it from damage. The OMA technique used to analyse the data collected to correctly identify modal parameters such as eigenfrequencies is presented too.
- **Section 9**: The different damaged and undamaged scenarios tested and their results are presented. First experimental and numerical results were compared. After that, the reliability and effectiveness of the damage indexes chosen are analysed. The sensitivity to damage's entities and location was examined too.

2. Piezoelectric stack

As already introduced above, in this work the possibility of implementing piezoelectric stacks and exploiting their electromechanical coupling with structures to which they are bonded to for developing SHM technique is investigated. Specifically, since the electromechanical coupling can be estimated through the so-called MEMCF, the possible variation of this index between the undamaged and damaged condition of the structure is analysed. The FE model developed in this thesis is presented after a brief theoretical introduction to the piezoelectric stacks and their functionality.

2.1. Piezoelectric stacks

Piezoelectric sensors owe their diffusion to their higher signal-to-noise ratio and better high-frequency noise rejection than strain gauges. Moreover, they are compact, easy to embed and require moderate signal conditioning circuitry. Piezoelectric stacks are multilayer constructions, each composed of several piezoelectric layers [25]. Thus, several heights and thicknesses can be obtained. Dimensions and aspect ratio depend on the application requirements: in particular, the height leads to the desired movement, and the area of the cross-section depends on the force required. Typically, these stacks generate large forces but small displacements in the direction normal to the top and bottom surfaces. Piezoelectric films are connected in parallel, as shown in Figure 3.

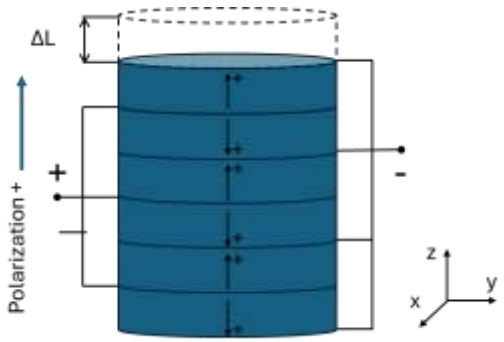

Figure 3:Piezoelectric stack

The piezoelectric stack operates in the so-called 33 mode, which means that according to the reference system in Figure 1, the electric field is applied along the same direction (3) in which the considered stress and strain developed, or that the stress and strain are applied along the direction in which the electric field develops. Thus, according to [15], the linear constitutive equation of a piezoelectric stack can be simplified as:

$$Q = CV + nd_{33}F$$

Eq. 13

$$\Delta L = nd_{33}V + \frac{F}{K_a}$$

Eq. 14

Considering a stack with *n* layers, a stiffness K_a (with short-circuited electrodes) and an unloaded capacitance C. V is the voltage between the electrodes, Q is the electric charge on them, F is the force exerted on the transducer and ΔL its axial elongation.

The efficiency of the conversion between mechanical energy and electrical one and vice versa is expressed via the electromechanical coupling factor k, defined by

$$\hat{k}^2 = \frac{n^2 d_{33}^2 K_a}{C}$$

Eq. 15

The capacitance and the stiffness of the PZT also change based on the mechanical and electrical boundary conditions (BC). Some examples of mechanical BC are the free strain and the blocked stressed ones, which are, respectively, the case in which the PZT is free to move and in which it is constrained.

The electrical conditions are the Short-Circuit (SC) and Open-Circuit (OC) conditions. In the SC, shown in Figure 4, the voltage between the electrodes is zero, and the charge Q can flow between them until equipotentiality is reached. On the other hand, in the OC the electrodes are not connected, so no charge flow is possible. A non-zero voltage is present.

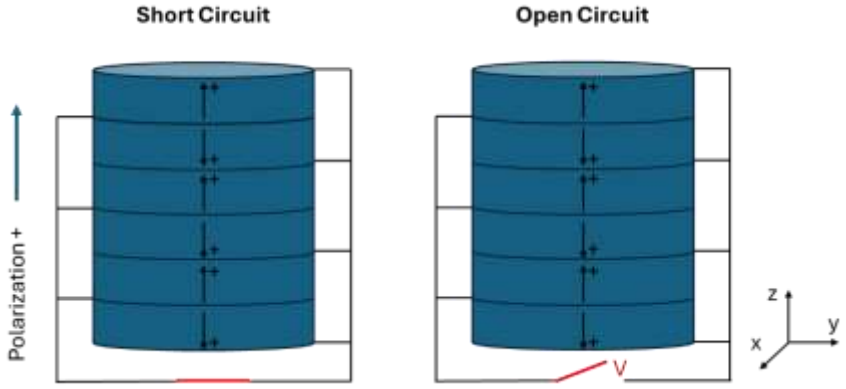

Figure 4: Piezoelectric stack in Short and Open circuit

The choice of employing piezoelectric stacks (so, multilayer structures) and not patches for developing SHM techniques in truss structures as in this work is mandatory due to its three-dimensional shape and the dimension of the structure that should be monitored. Indeed, individual layers provide relative low displacements, while when they are mechanically connected in series and electrically connected in parallel higher and useful displacement can be achieved.

2.2. Geometry and material parameters of the stack

The piezoelectric transducers analysed are based on the actuators produced by PI Instruments since it represents one of the main manufacturers of such transducers. Piezoelectric actuators are made of piezoelectric ceramic based on modified lead zirconate and barium titanate (PZT), especially in PIC 255 piezoceramics. This “soft PZT” has an extremely high Curie temperature, high permittivity, high coupling factor and high charge constant. Its material data are reported in Table 1.

Material characteristic of PIC 255		
Parameter	**Symbol**	**Value**
Physical and dielectric properties		
Density [Kg/m^3]	ρ	7800
Poisson's coefficient	ν	0.34
Permittivity (in the polarisation direction)	ε_{33}	1.55E-08
Permittivity (perpendicular to the polarity)	ε_{31}, ε_{32}	1.46E-08
Electromechanical properties		
	d_{31}	-1.80E-10
Piezoelectric charge constants [C/N]	d_{32}	4.00E-10
	d_{15}	5.50E-10
Mechanical properties		
Elastic constants (compliance) [m^2/N]	S^E_{11}	1.61E-11

S^E_{33}	2.07E-11

Table 1: PIC 255 material data

Several layouts and geometries have been tested, starting from the catalogue of Piezo Actuators produced by PI Physical Instruments. So, the geometrical characteristics will be described in each case. Moreover, since this kind of transducer is available both as parallelepipeds and as cylinders, the first form was chosen to be simulated. This is because it allows FE elements of the same size in the piezo stack and greater accuracy in selecting the areas where the PZT are bonded.

In the next section, the FE model of the piezo stack will be presented.

2.3. Finite element model of the stack

Unlike the structure, which model has been developed with different CAD and FE software, the piezoelectric stacks have been directly modelled in Abaqus software and then added to the model of the structure imported in it. Their geometry is easier than the structure's, so the CAD and meshing features of the software can be used. Real piezoelectric stacks are created by glueing the plates together and interposing a thin metal contact plate between each two ceramic plates in order to contact the attached electrodes. In the FE model stacks have been simplified creating a unique solid and then dividing it into several features to simulate the layers with opposite poling. An example is shown in Figure 5 where layers with opposite posing are distinguishable thanks to different colours.

Each PZT item has been discretized using quadratic brick elements (i.e. 20 nodes), specifically C3D20ER, with approximate side dimensions equal to 2 mm, where R is for reduced integration and E is for electric, were used. This solution was chosen because it is a good compromise between reaching the convergence of the mesh and performing simulation in a short amount of time.

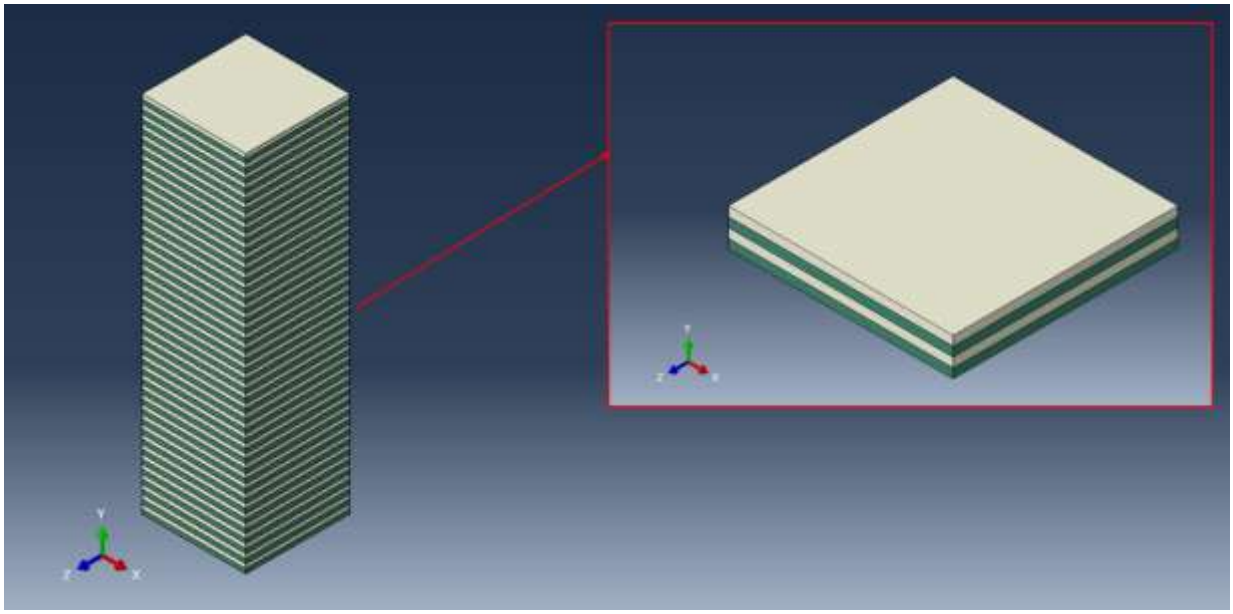

Figure 5: FEM of a PZT stack and zoom on the different layers

To understand the electrical connections of the stack, a single layer as the one depicted in (Figure 6) can be considered.

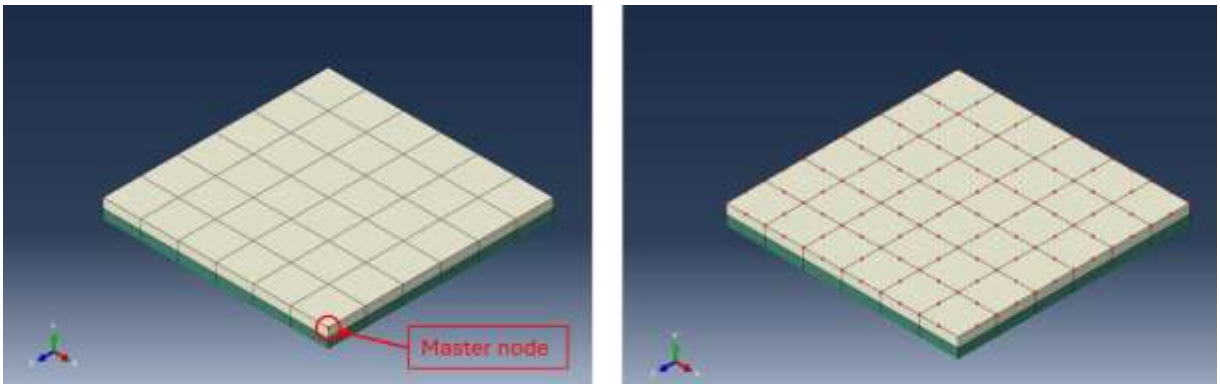

Figure 6: Zoom on single-layer constraints for electrical equipotentiality of the electrodes

The equipotentiality of the electrodes was reached using the kinematics linear relation via ABAQUS constraints command in terms of the electric degree of freedom, DOF9. All the nodes except one, both in the upper and in the lower surface, are referred to that node, typically called the "*master node*". This equipotentiality is exploited also for the electrical boundary conditions, such as Short Circuit (SC) and Open Circuit (OC) since it is enough to apply the electrical boundary condition to the master node. Hence, for the SC condition, a zero potential must be applied to both the upper and lower master nodes. While, for the OC condition, electrodes are charge free, so one face has no electric boundary condition applied while the other has a zero potential applied.

As mentioned before, consecutive layers of the stack have opposite poling orientations, creating a parallel electric connection of the layers. Referring to Figure 7, white layers, which can be identified as "A layers" have a positive polarization referring to z-axis, while the green one, "B layers", have an opposite one. The electrical connection is then created referring all the upper nodes of the B layers to the master node of the upper face and all the upper nodes of the A layers to the one of the lower face. The SC and OC conditions are realized as for a single layer explained before. Since the PI actuators have been used as reference, the layers' thickness has been realized equal to 0.5 mm. The number of layers changes as the height of the PZTs increases or decreases.

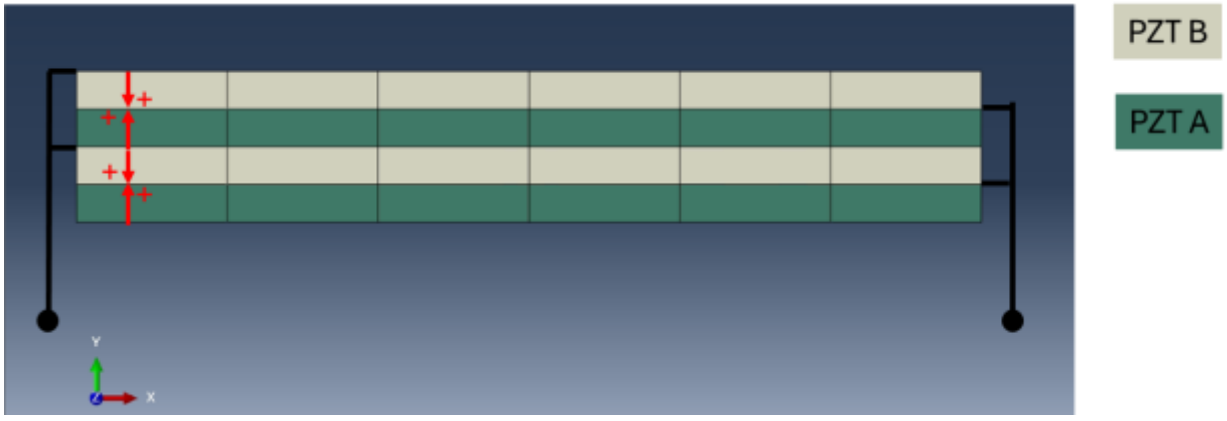

Figure 7: Piezoelectric stack scheme

2.4. Mechanical boundaries

One of the aspects which required special attention is the mechanical connection between the piezoelectric actuators and the structures. Indeed, in literature there are many examples of FE implementation of piezoelectric patches. These transducers are glued to the host structure, so the Abaqus function Tie is generally implemented, because it allows to make the translational and rotational motion equal for a pair of surfaces, in this case the patches' bases surfaces and the relative area of the host structure. Firstly, this type of constraint

was implemented. However, afterwards, it was substituted by the "PIN rigid body constraint", which allows the creation of a region which includes nodes that will have only translational degrees of freedom associated with the rigid body reference point. So, in this case, the upper and lower faces of the piezo stack are linked to the relative reference node of the structure as shown in Figure 8.

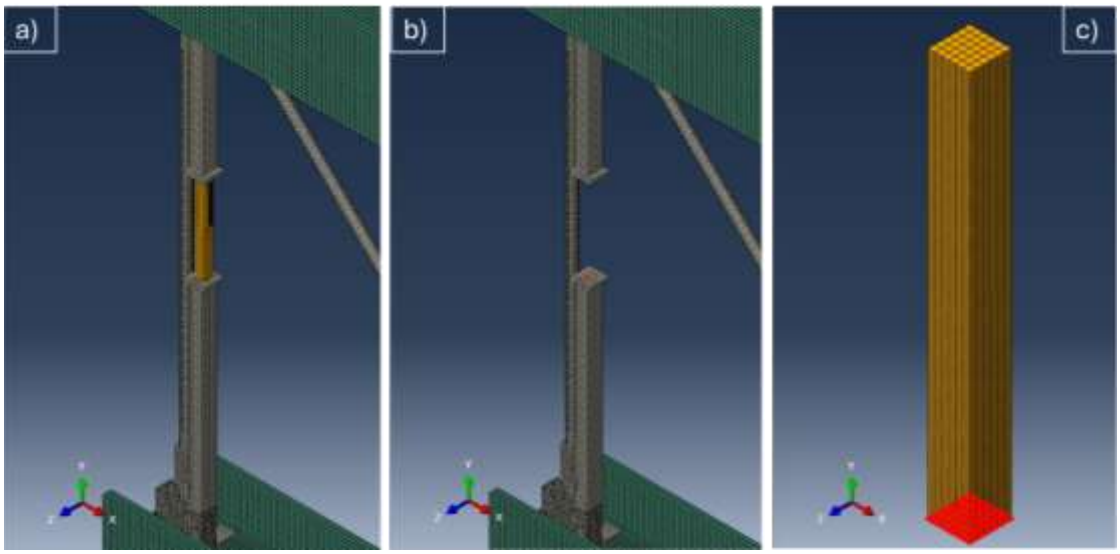

Figure 8: Pin-rigid body constraint elements used to link the PZT with the structure (a), focus on the master node (b), focus on the slave surface (c)

This solution was preferred to the tie constraint because it allows the simulation of the correct mounting of the piezo actuator, in which it has to be subjected only to longitudinal loads and displacements. Indeed, because of the complexity of the structure's geometry under investigation, it is possible to obtain some flexural-torsional mixed modes, which might have non-null coupling factors even if experimentally these modes would not induce any deformation in the stack. The implementation of the PIN constraint allows the reduction/deletion of torsional influence. In Figure 9 the vertical displacement u_2 of the piezo stack resulting from the two different constraints at a vibration mode in which it is compressed by the structure is reported. The piezo A is linked to the structure with the tie constraint, while the piezo B with the PIN constraint.

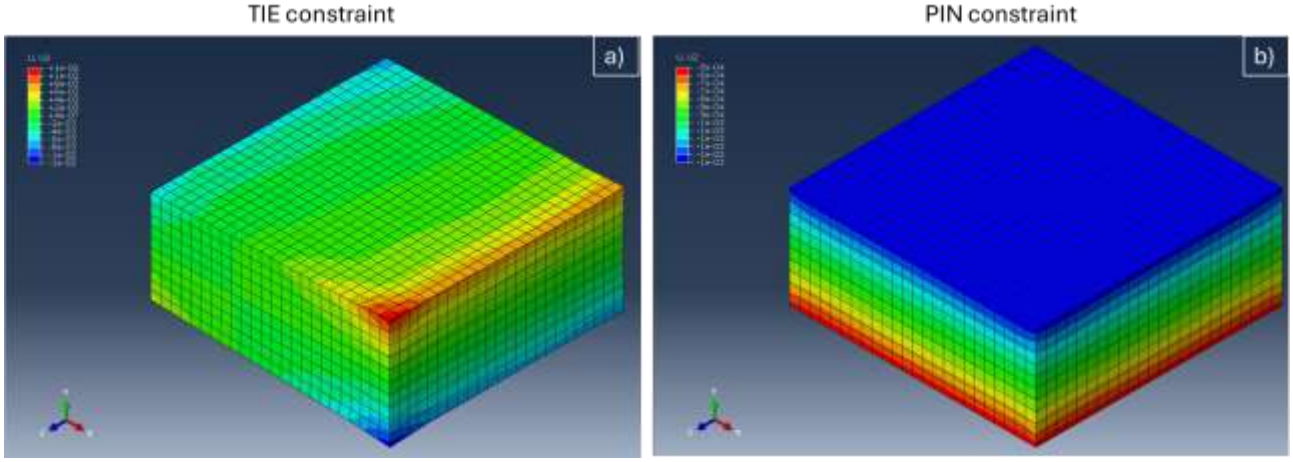

Figure 9: Comparison between vertical displacement obtained with TIE constraint (a) and PIN constraint (b)

When the piezo is coupled to the host structure with the tie constraints, it is also subjected to bending, indeed its horizontal surfaces do not exhibit equal vertical displacement, while with the PIN constraints only axial loads are transmitted.

This behaviour results also in the electric potential of the piezo stack. In Figure 10 a comparison of the resulting electric potential of the same vibration mode of two piezo stacks is depicted. The horizontal surfaces of the piezo (so the electrodes) with tie constraint do not have the same electric potential, nonetheless, the boundary conditions because the piezo is affected by bending. This does not occur in the PIN constraint case.

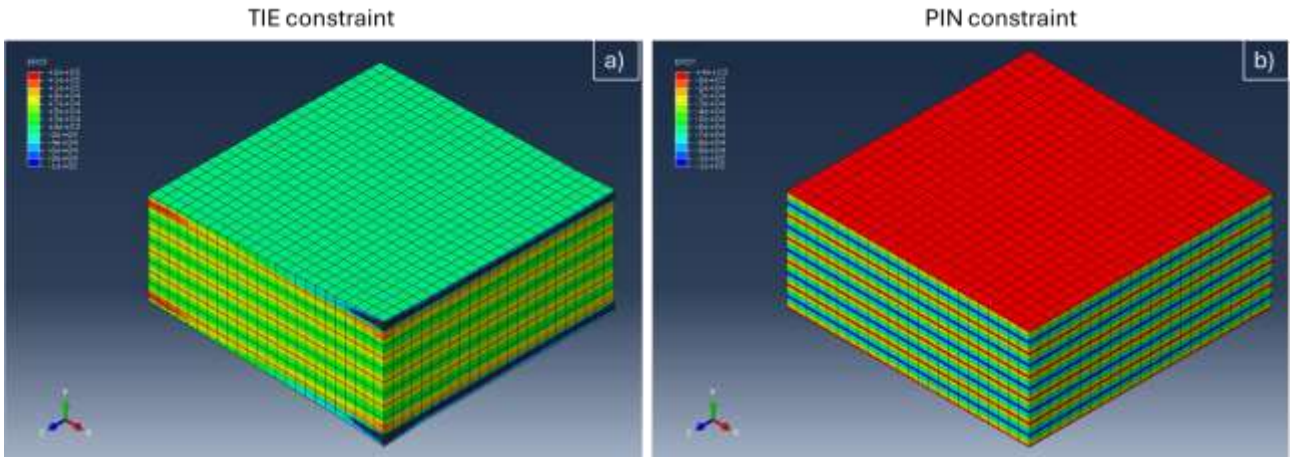

Figure 10: Comparison between electric potential obtained with TIE constraint (a) and PIN constraint (b)

Once the electrical and mechanical boundary conditions were established, the modal electromechanical coupling factors can be numerically evaluated as described in the next paragraph.

2.5. MEMCF evaluation in the FE model

MEMCF variations from an undamaged to a damaged condition could be used as a warning of the presence of damage. Starting from its definition, the variation of the MEMCF can be evaluated, for a ith mode as

$$\Delta k_i = \left| k_i^{und} - k_i^{dam} \right|$$

Eq. 16

where

$$k_i^{und} = \sqrt{\frac{\left(\omega_{i,und}^{OC}\right)^2 - \left(\omega_{i,und}^{SC}\right)^2}{\left(\omega_{i,und}^{SC}\right)^2}}$$

Eq. 17

$$k_i^{dam} = \sqrt{\frac{\left(\omega_{i,dam}^{OC}\right)^2 - \left(\omega_{i,dam}^{SC}\right)^2}{\left(\omega_{i,dam}^{SC}\right)^2}}$$

Eq. 18

Where the superscripts *und* and *dam* are, respectively, for the undamaged and damaged condition.

The FE model electromechanical system has been simulated, damaged and undamaged, in both the electrical conditions of the piezo actuators (short and open circuit).

In the next chapter, the description of the laboratory truss girder under investigation and its FE model are reported.

3. Laboratory truss girder

3.1. Girder truss design: theoretical background

Truss girder design is a commonly used design in many engineering applications and fields, such as mechanical, civil and aerospace. For example, they are used in buildings like bridges, roofs, trusses and support structures, as depicted in Figure 11. Their widespread use is due to their strength and stability while also reducing the weight of the structure itself while supporting large loads. Girder trusses are also highly customizable and so can fit a large range of applications. Truss structures are rigid assemblies made by a triangulated system of members such as beams connected by nodes. The elements are connected together where they join not exerting, individually, net moment on the node. Loads are applied at the nodes, and so each rod is subjected to either compression or tension force.

Figure 11: Examples of truss girder structures

The members of the trusses, nevertheless the configuration, are commonly identified as chords and webs. The chords (top and bottom) are the horizontal beams spanning the length of the truss while webs are the internal members. These are distinguished in diagonals and rods, called tension rods when they are stressed by tensile stress and struts when stressed by compressive stress.

Despite the theoretical analysis, truss elements can be influenced also by bending moments and shear stresses, which must be taken into account even if they are often negligible contributions in practice. The not perfectly ideal behaviour can be attributed to two main factors:

- External loads are not always applied on the nodes, but are often applied directly on the rods;
- The actual connection between the members exhibits some rotational stiffness.

Moreover, in existing structures joints are rarely realised as true hinges, but, as in steel trusses, they are almost bolted or welded. Thus, bending moments are transmitted through connections to the structure's elements. A more realistic model of the connection therefore could be connections with fixities that are elastically yielding. However, the geometry of the joints is designed to transmit quite limited moments, making the behaviour of the real structure comparable to that of the ideal model.

Given the main basics of the theory of truss girders, the structure analysed in this work will be presented.

3.2. Trusses layout

As said in the previous paragraph, several real existing constructions, buildings or components, are realised employing trusses. Despite this, if an ad-hoc design is not required, it is possible to reduce the most commonly used layouts to four main traditional ones. Their schematic layouts are reported in Figure 12.

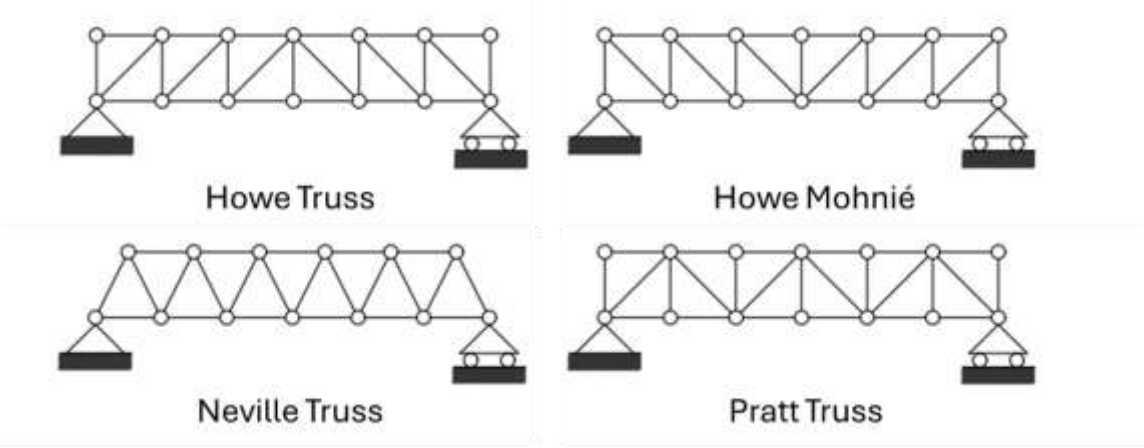

Figure 12: Truss layouts

The main differences between these layouts are the configuration of the rods, and thus the different load distribution. One configuration is preferred over the other based on the intended use, materials etc.

The laboratory truss analysed in this work suits the Mohniè scheme, so diagonal elements are subjected to tension and load are distributed as shown in Figure 13.

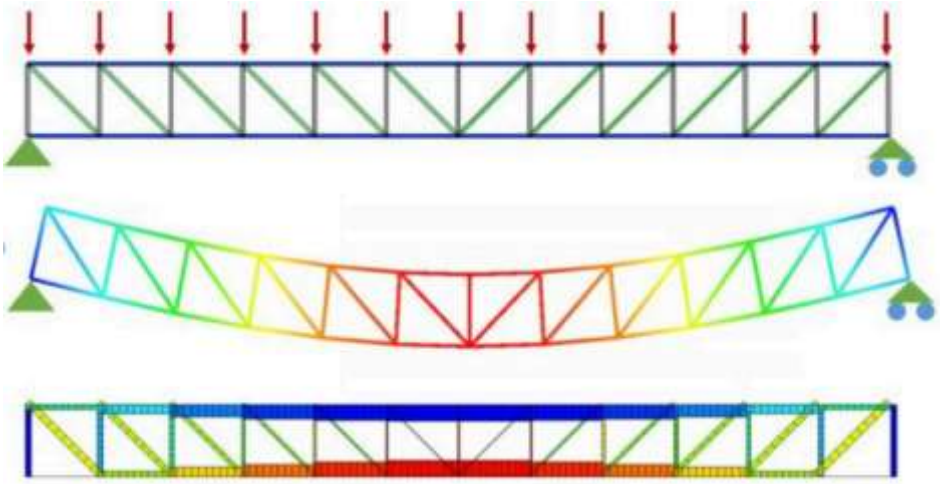

Figure 13: Load distribution on a Mohniè truss

3.3. Laboratory truss girder design

The structure under investigation in this work has been designed, suiting the Mohniè scheme in Figure 13, to be developed on a single vertical plane. The chords are composed of unique elements, while vertical and diagonal rods are supposed to be single elements jointed to them. These solutions have been made to favour the vertical displacements of the structure with respect to the other directions since only vertical vibrations were supposed to be evaluated. Connection elements have been designed ad-hoc to overcome problems such as non-linear dynamic behaviour due to friction between rolling elements or imperfect tightening. Joints have been designed to be directly bolted to the chords and specific nuts with a double fillet providing the connection between vertical/diagonal rods and nodes. Another interesting development of using bolts, rods and nodes elements is that the induction of damages and return to a healthy state can be done easily and repeatedly. The top and bottom beams are 2 H-beams with the middle section arranged horizontally, so the connection joints-beams are done with classic bolts.

The total length of the structure is 4.20 metres, and its height is about 0.80 metres. Diagonal and vertical truss elements are aluminium rods with a hexagonal section with a 1.2 cm diagonal and 50 (vertical) or 70 (diagonal) cm long, while the horizontal members are 2 steel H-beams 430 cm long with a thickness of 1.1 cm. Seven rectangular masses of 15 kg are placed at the bottom of the truss at each node to increase the structure stability.

Moreover, a series of aluminium masses are glued to vertical (50 g) and diagonal rods (160 g). This stratagem was used to shift the natural frequencies of the rods since preliminary tests [7] have shown that they superimposed two overall natural frequencies of the structure. The structure was designed to comprehend the first natural frequencies in the range between 0-200 Hz.

3.4. Truss girder constraints

The structure sits on two rigid supports bolted to the floor. This solution should mitigate potential issues from non-linearities in the dynamic behaviour of the structure itself. Moreover, the traditional hinge-roller constraint scheme has been substituted by a layout composed of two rollers based on clamp systems. This solution should remove possible clearances between elements. Therefore, both bottom ends of the structure have been linked to floor supports with rollers connection made by Teflon elements tight with a clamp system. The entire structure is held vertically with four struts placed at 1/3 and 2/3 of the overall span of the structure. The interaction between struts and the superior beam is provided by four stainless steel cylinders which work as rollers and allow only vertical movement.

A picture of the truss girder is reported in Figure 14.

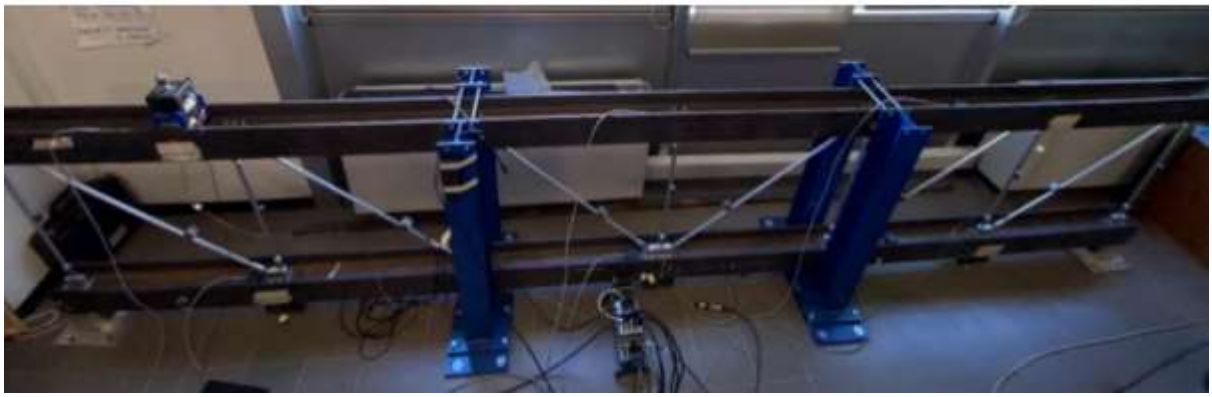

Figure 14: Laboratory truss girder

3.5. Finite element analysis

As mentioned above, a preliminary Finite Element Analysis (FEA) of the entire electromechanical system has been carried out. Specifically, the FE model has been used for studying several aspects, as choosing the best placement and geometrical layout of the piezoelectric stack, the effects of different kinds of damages... etc.

The model of the structure has been developed with the 3D CAD design software SolidWorks for the geometry and then the FEM has been set up with Altair Hypermesh software for adding structural characteristics and creating the mesh. The FE model is depicted in Figure 15.

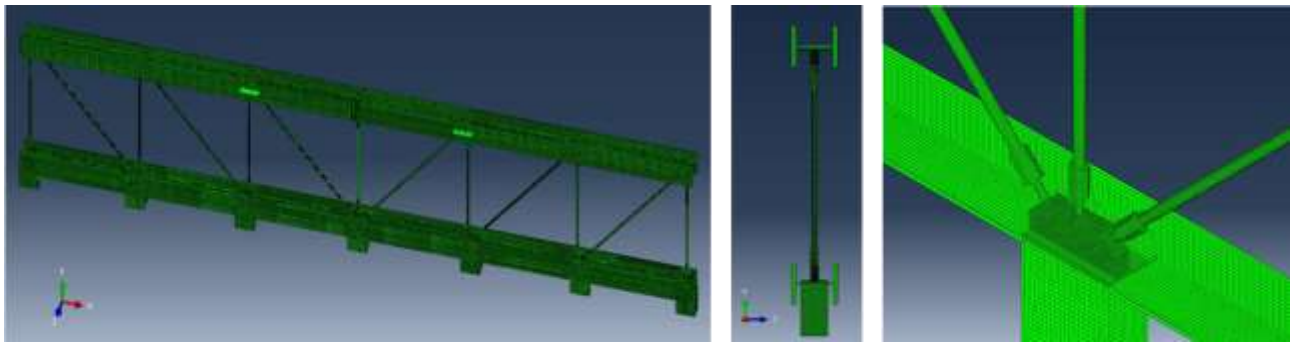

Figure 15: FE model of the structure

This model has been imported into the Abaqus software where the dynamic analyses have been performed. Even if it is not properly a part of the structure, the FE model considers the presence of the electro-dynamic PCB shaker placed on the upper chord, specifically on the upper second node starting from the left, which excites the structure in the vertical direction. The shaker, with other sensors such as thermocouples and accelerometers, makes up a monitoring system for the development of another technique of vibration-based modal analysis. However, only the shaker was added to the model since its mass (3.5 kg) affects the dynamic behaviour of the structure. This is not true for the other sensors, because their mass is too low, so their loading effect is negligible. A scheme of the truss girder layout is reported in Figure 16 above

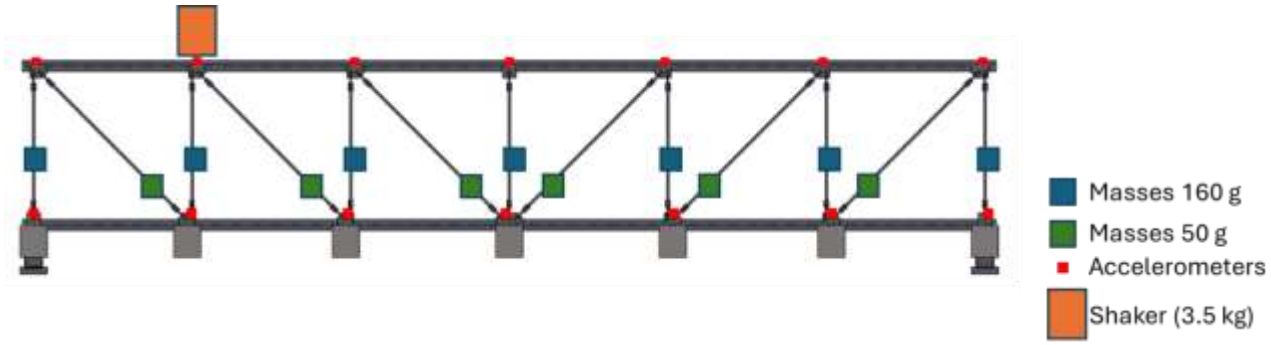

Figure 16: Truss girder layout and sensors mounted on it

3.6. Validation of the FE model

For the validation of the FE model modal parameters such as mode shapes and natural frequencies have been evaluated through both experimental and FE approaches. Indeed, the Modal Assurance Criterion (MAC) index was used to correlate the modes evaluated experimentally and numerically. The MAC index is a synthetic index used to establish the degree of correlation of two different mode shapes; it gives scalar value between 0 and 1, representing respectively no correlation and perfect correlation. It can be evaluated as

$$MAC\left(\varphi_j^{FEM}, \varphi_j^{EXP}\right) = \frac{\left|\varphi_j^{FEM^T} \varphi_j^{EXP}\right|^2}{\left(\varphi_j^{FEM^T} \varphi_j^{FEM}\right)\left(\varphi_j^{EXP^T} \varphi_j^{EXP}\right)}$$

Where $\varphi_j^{FEM}, \varphi_j^{EXP}$ are the mode shapes evaluated numerically and experimentally respectively (i.e. eigenvectors). For the experimental analysis, structure vibrations were measured with 6 low-cost triaxial MEMS accelerometers model TE4030, with a sensitivity of 1000 mV/g, a frequency range of 0-200 Hz and a measurement range of ±2g. Acquired signals were processed with an Operational Modal Analysis (OMA) algorithm to evaluate the main modal parameters such as natural frequencies and modes shapes.

The Power Spectral Density (PSD) of the accelerometers was evaluated and highlighted the first six resonances of the structure (Figure 17), while in Figure 18 the mode shapes for each mode are represented. The first three mode shapes align with the canonical bending modes, whereas, starting from the fourth mode onward, the structural behaviour appears to deviate.

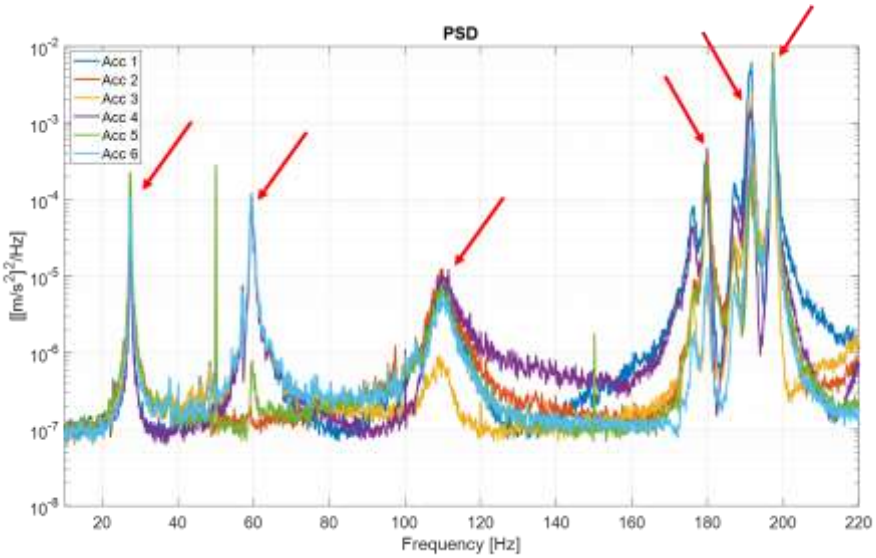

Figure 17: Power spectral densities and highlights of the first six resonances of the structure

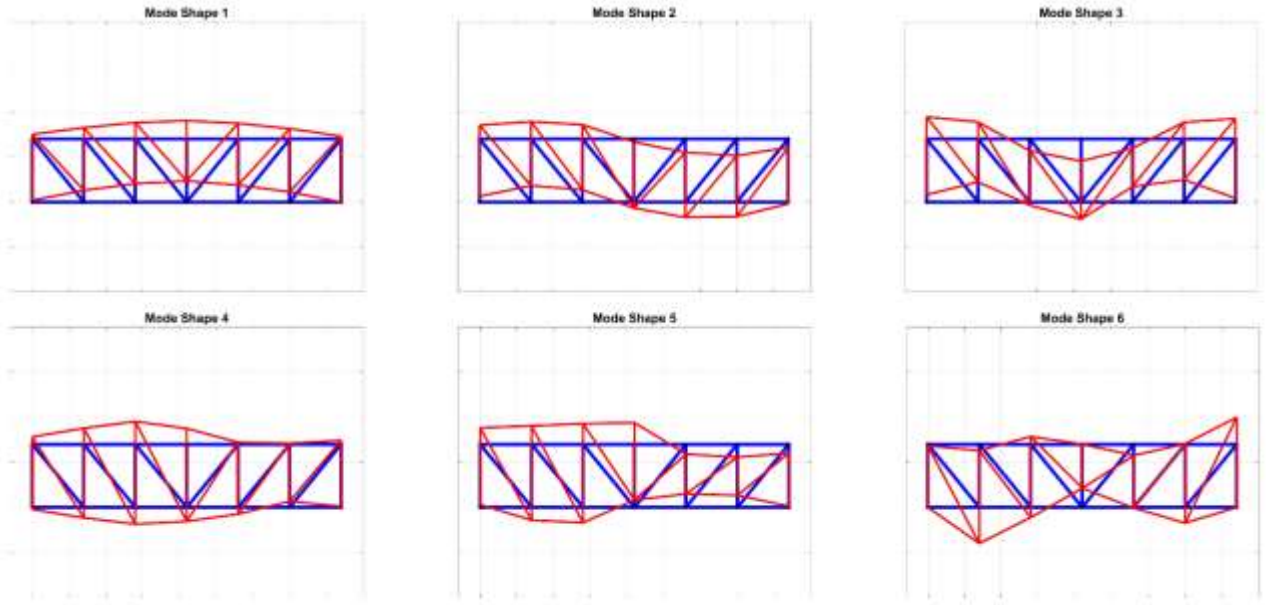

Figure 18: Mode shapes of the first six resonances

The MAC index can be represented through the so-called MAC matrix, in which each element represents the degree of correlation between the different mode shapes. The MAC matrix between the six main vertical modes evaluated experimentally and all the modes found by the FE simulations is reported in Figure 19 below.

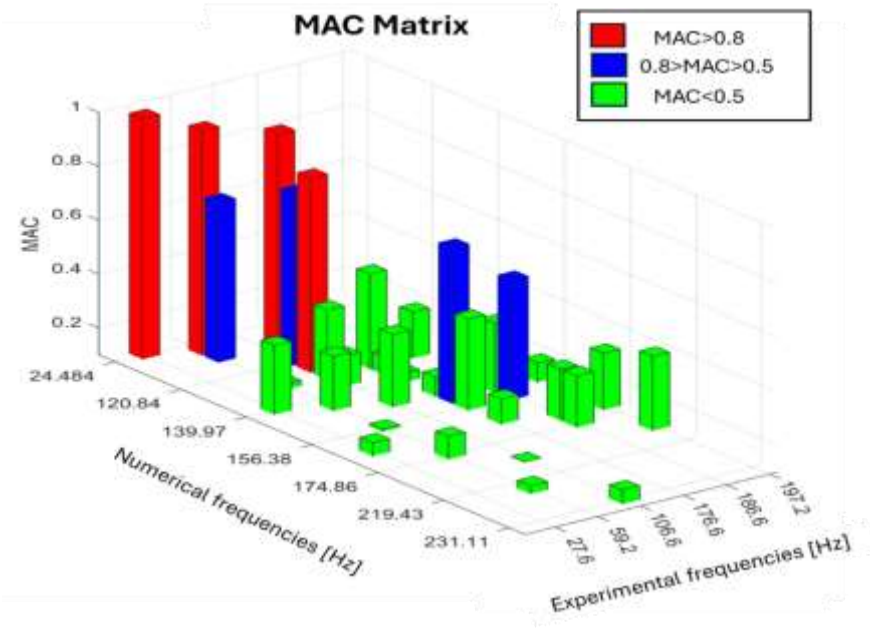

Figure 19: MAC Matrix

A comparison between the natural frequencies of the matching modes is reported in Table 2, where the MAC index values are also reported.

Mode number	Numerical natural frequency [Hz]	Experimental natural frequency [Hz]	MAC Index
1	24.4	27.6	0.99
2	59.7	59.2	0.92
3	106.6	106.6	0.92
4	149.8	176.6	0.68
5	156.6	186.6	0.55
6	185.8	197.2	0.38

Table 2: Comparison between FEM and experimental natural frequencies and related index

Finally, the comparison between the first three mode shapes, evaluated experimentally and numerically, are reported as example in Figure 20, Figure 21, Figure 22. The resulting FE model of the first vertical mode is also shown in Figure 23.

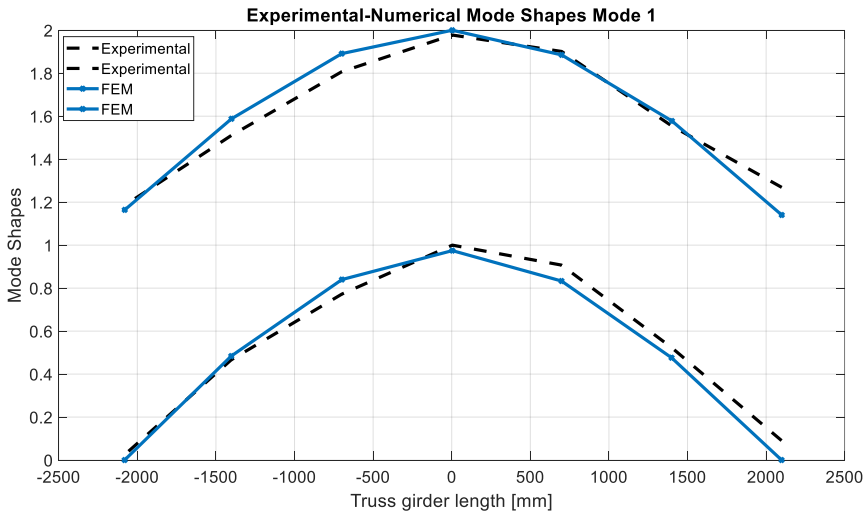

Figure 20: Mode shape comparison of the 1st vertical mode

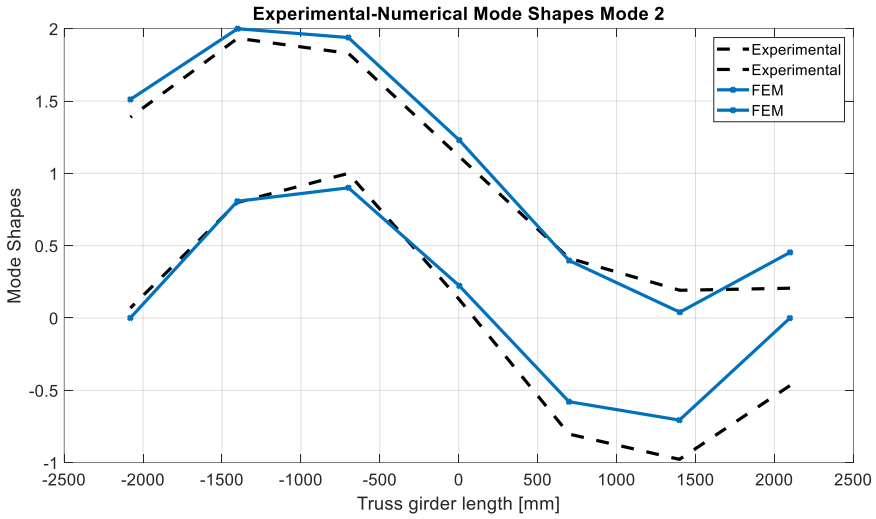

Figure 21: Mode shape comparison of the 2nd vertical mode

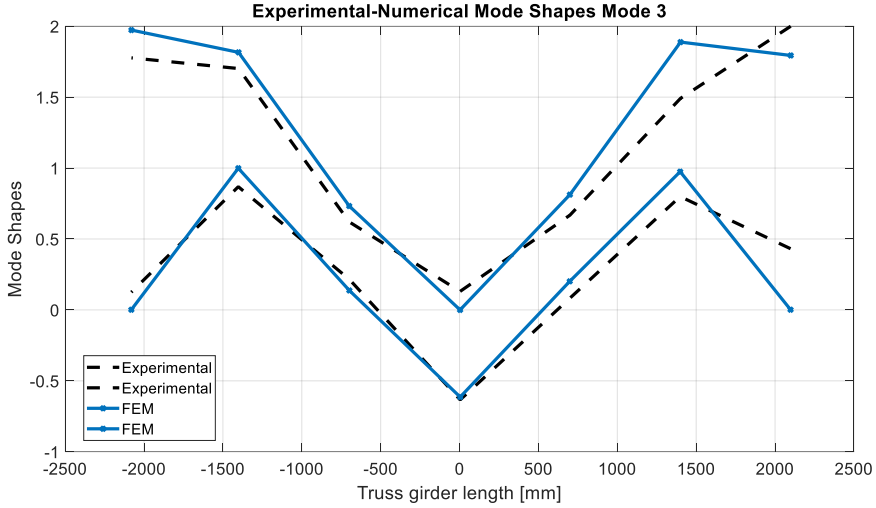

Figure 22: Mode shape comparison of the 3rd vertical mode

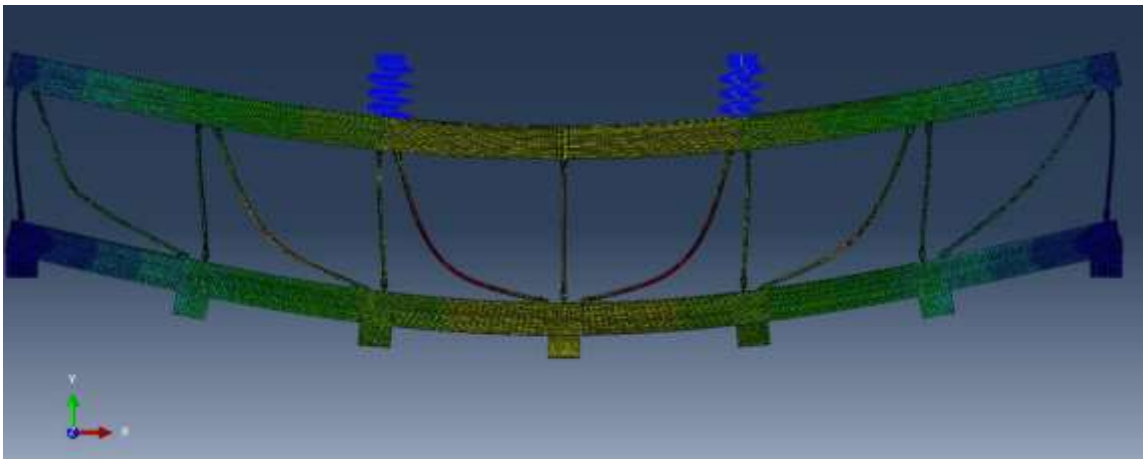

Figure 23: Mode shape of the 1st vertical mode at FE analysis

It is noticeable that experimental and numerical results are in good agreement for the first three modes, while there's a slight divergence for the others, in both natural frequencies and mode shapes (and, hence, in the MAC

index). The FE model identifies about 86 modes in the frequency range between 0-220 Hz, so the MAC index and a comparison with the experimental data is crucial for assessing which of these modes are effective.

The frequency ranges of the modes of the vertical and diagonal rods were identified too.

Specifically, it was found that:

- the first modes of the diagonal rods appear in the frequency range between 34-44 Hz;
- the first modes of the vertical rods appear in the frequency range between 84-100 Hz;
- the second modes of the diagonal rods appear in the frequency range between 137-146 Hz.

Once the undamaged model has been validated, several possible damage scenarios can be simulated.

4. Structure' s damages

As already said in the previous chapters, SHM techniques are developed to prevent and detect possible damages in structures/ mechanical components. So, it is necessary to have almost two different states of the structure, a healthy one and an unhealthy or damaged one. Damage can be defined as a change in the material and/or geometric properties of a system, which affects its current or future performances. It does not necessarily imply the total loss of functionality of the component, but rather that the system is no longer operating optimally. When the damage's level reaches a point that is not acceptable anymore it is referred to as failure.

The main causes of damages arising can be resumed in environmental and operational conditions and variations, such as humidity, mass loading, wind... etc. Truss girder structures can be affected by various types of damage since they are employed in very different engineering fields. Some examples of damages could be warping, cracking of components, joints failure, and insufficient bearing capacity. The main factors can be summarised as follows:

- Warping, or cracking of components due to temperature differences or gradients.
- Corrosion damages: it can be caused by a wide variety of environments, the most common for metallic structures is the corrosion in aqueous environments. Especially for steel structures, chemical or electrochemical corrosion causes the section of the structure to be weakened and to its breaking.
- Load changes, extended service, overload and fatigue.
- Loss of effectiveness in connections. In truss structures, the load distribution and transfer are ensured by connections and joints, as for example pins, bolts or welds. These connections can be affected by bolt loosening compromising the functionality of the structure.

Whatever the type of damage, its onset leads to an alteration of the system's dynamic behaviour, and consequently, to its modal characteristics such as mass, stiffness and damping, and thus to its modal parameters such as natural frequencies and mode shapes [1].

Starting from this, different damages have been simulated in the FE model of the structure.

4.1. Mass addition

The first damage simulated has been the addition of masses on the model in different positions of the structure. The reason for this choice is that this damage condition is very simple and quick to introduce both numerically and experimentally. In the FE model, the mass is added as a *point mass* to a node of the mesh specifying its magnitude, experimentally it is added or glued to the structure. Despite its simplicity, the mass addition can simulate a decrease of the stiffness in determined structure locations.

The placement of the mass is depicted in Figure 24. Its weight is equal to 1 kg.

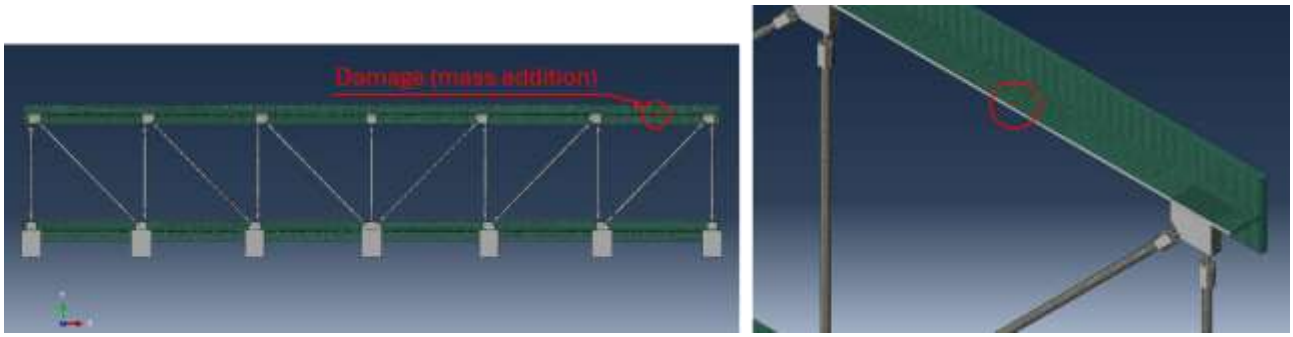

Figure 24: First damage, mass addition

4.2. Cracks

Another damage simulated has been the warping of some vertical and diagonal rods due to the occurrence of cracks. Cracks have been simulated in two different ways:

- With the reduction of Young's modulus (Y) by about 50% and 75%, for different deterioration levels.
- Removing some elements from the mesh where the crack had to be simulated.
- Comparing the results from the FEM, no significant differences were noticed, so the reduction of Young's modulus was preferred to the removal of the elements as it was easier to implement.

Damages were induced into the first and second diagonal rods as shown in Figure 25 below.

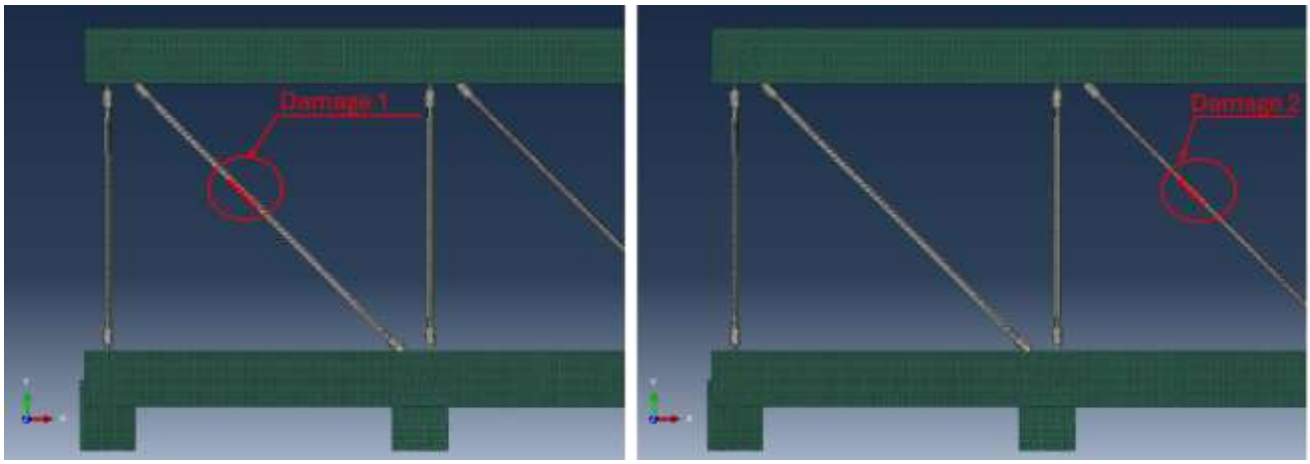

Figure 25: Second and third damages, cracks on the first two diagonal rods

4.3. Break

Finally, the total break of a rod was simulated. This is the heaviest damage tested since it signifies the failure of the structure. Specifically, the second vertical rod was broken removing an entire section of it and deleting the connection between the upper and lower chord in that region of the structure (Figure 26).

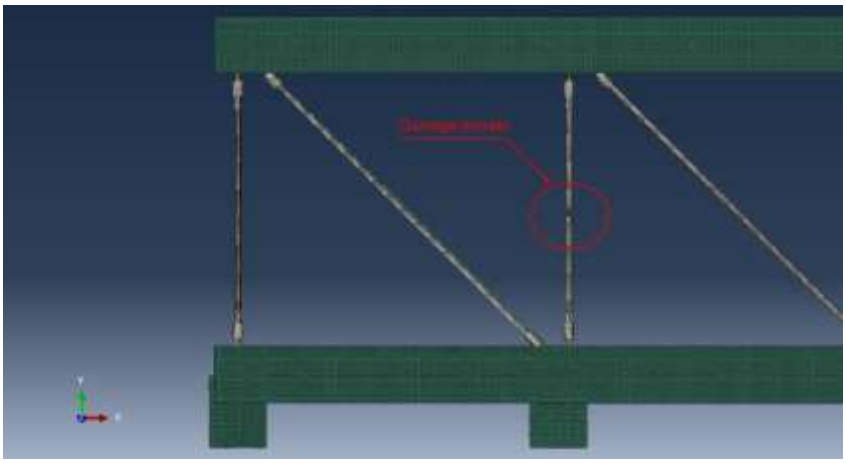

Figure 26: Fourth damage, break of the second vertical rod

All the damages were chosen to be simulated close to the area or directly on the rod where the piezo stacks would be placed. This is because it should have been easier for it to sense the variation of the mode shapes due to the damage's presence and its proximity.

4.4. Mac index between damage-undamaged condition

The use of the MAC Index to correlate two different mode shapes has been introduced in the previous section for the validation of the FE model. In that case, the comparison was between experimental and numerical mode shapes. However, now the MAC Index is used to compare only numerical mode shapes, specifically ones of the damaged and damaged conditions. This evaluation allows the modes to be paired between different simulations, and to make the comparison of different configurations possible.

It is important to remember that the FE model, even if it is very similar to the real structure, gives a series of possible modes of the element under investigation. Moreover, two modes might exchange their order, switching between the undamaged and damaged condition or between the SC and OC condition.

Damages change physically the structures, and so do their mode shapes. The heavier the damage, the higher the difference between the models, so a perfect correlation, and consequently MAC=1, could not be achieved.

Moreover, since the damage implies a modification of the model, it is possible that new mode shapes could arise. For example, the simulation of cracks, thus the reduction of the stiffness of the rods, resulted in a new mode shape of the rod itself (Figure 27) which did not exist in the healthy condition of the structure.

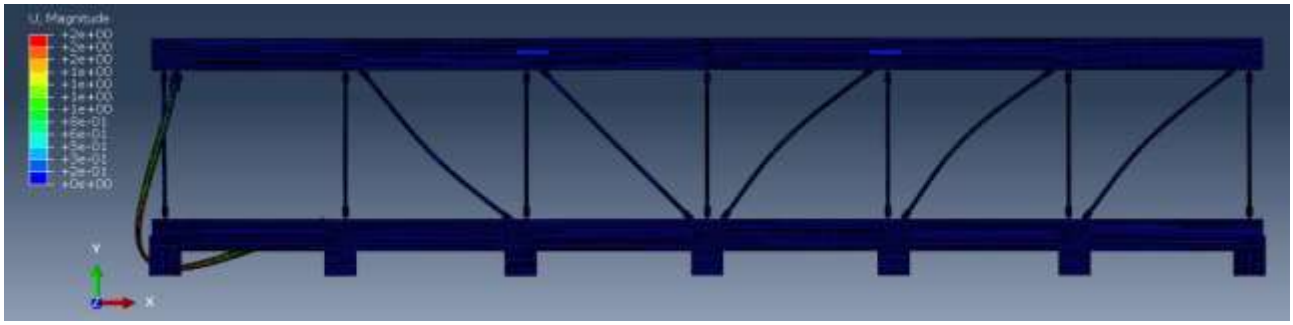

Figure 27: Example of new mode shapes arising in the FE model due to the damage to the diagonal rod

Eventually, for the correct evaluation of the MEMCF variation, the MEMCFs must match for each mode.

The MAC has been evaluated between the undamaged model with PZT stack short-circuited and open-circuited, the undamaged model with PZT stack short-circuited and the damaged model with PZT stack short-

circuited and open-circuited. However, simulations showed that the variation between electrical conditions does not affect the structure behaviour so that modes exchange. Thus, there was no observable variation in the MAC matrix, as in the example reported below in Figure 28. For this reason, only the comparison between damaged and undamaged conditions is reported and analysed.

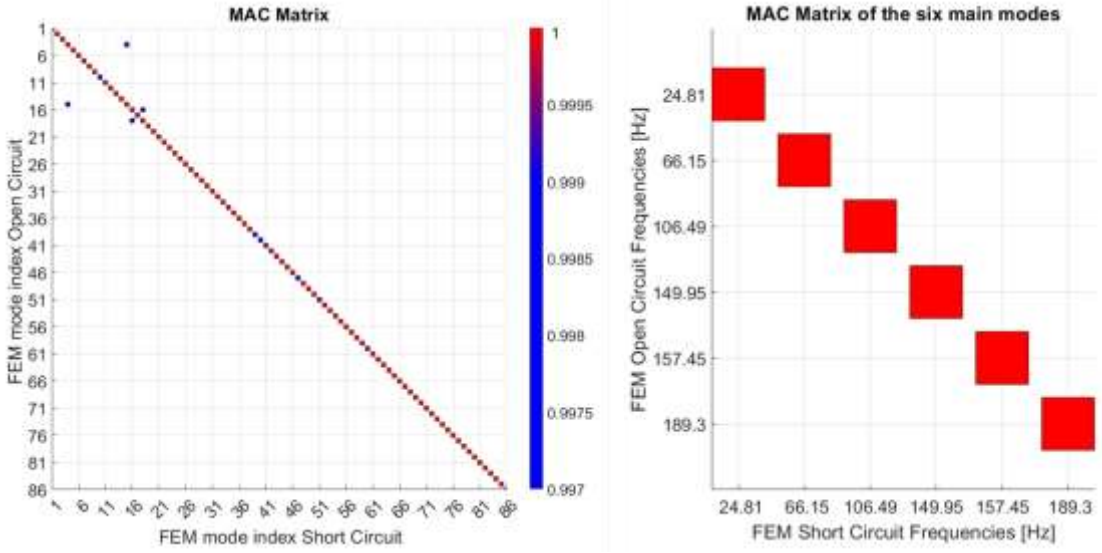

Figure 28: MAC matrix of all the modes evaluated at the FEM (a), focus on the MAC values of the six main vertical resonances (b)

4.5. Preliminary study of PZT stack placement

A preliminary evaluation of the different behaviour of the structure from damaged and undamaged conditions has been done. Starting from the six main vertical modes reported in Table 2 the displacements of some reference nodes of the structure have been evaluated. The focus was to assess where the mode shapes differed the most between the two situations and place the piezo stack there to be compressed. Since a global approach was first suited, the damaged condition in which a 1 kg mass is added to the chord was simulated, vertical elongations/contractions were evaluated. Displacements in correspondence of the vertical rods were evaluated since they represent the connection elements between the two load-bearing components, the chords.

Results are reported in Figure 29 below, for both conditions.

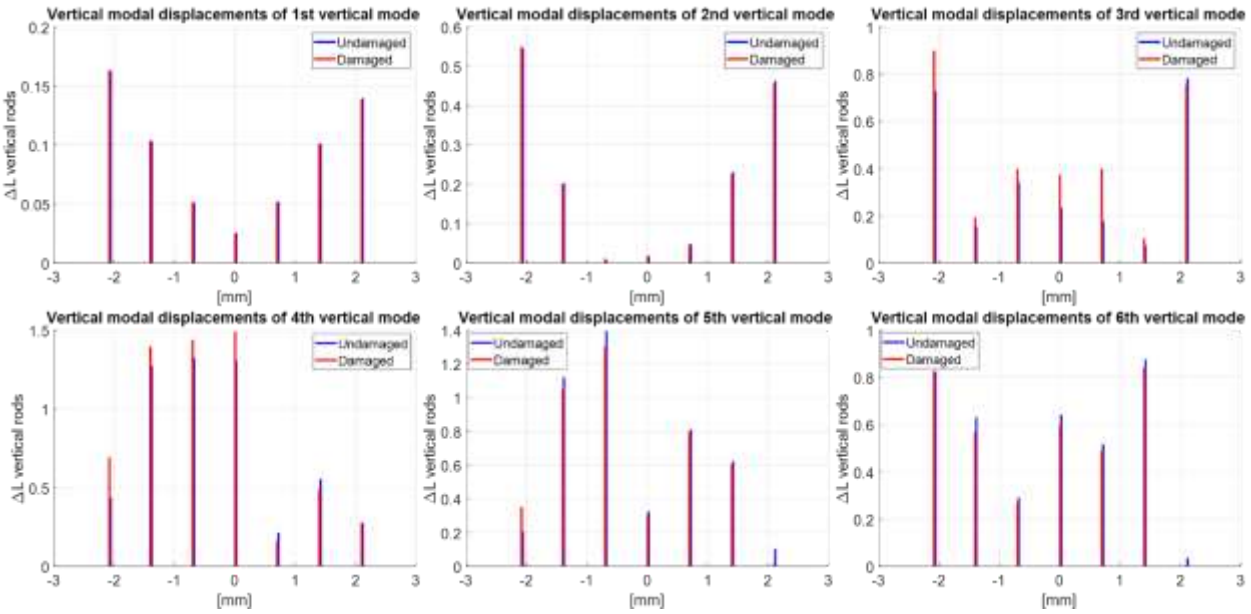

Figure 29: Elongation/contraction of vertical rods in both damaged and undamaged condition

It can be observed that there is no significant difference between the two healthy conditions, especially in the first two vertical modes. At the same time, a different behaviour can be noted around the first three/four rods from the left. Because of these results, it was decided to implement the piezoelectric stacks in this area. The three possible solutions were evaluated and simulated are described in the next chapter.

5. Placement of the PZT stack

The effectiveness of piezo transducers hinges not only on their inherent properties but also on the proper choice of placement within the structure. Strategic positioning plays a crucial role in optimising the transducers' tuning to specific frequencies and modes of vibration, and so it has to be properly investigated. In the literature, it is possible to find various studies examining this topic, such as in [41] or [42].

Moreover, in structural health monitoring applications, the correct positioning of sensors is critical for effective data acquisition and damage detection. Some considerations that should be considered for the best placement are:

- **Mode shapes analysis**: placing the PZTs in the areas where vibrations and correlated displacement are most pronounced enhances sensitivity to damages since it allows higher deformation of the PZTs themselves.
- **Critical location identification**: a good placement could be in areas subjected to stress concentration, such as joints, welds, and supporting elements because structural failure and damages are more likely to develop here.
- **Exploiting symmetry and redundancy**: a symmetric distribution of PZTs across the structure should ensure comprehensive monitoring, and on the other hand, a symmetric design of the structure under investigation could allow the reduction of the number of sensors to be implemented.
- **Surface preparation and correct mounting**: optimal adhesion for patches and correct mounting for the stacks ensure good signal transmission and integrity of the sensors themselves. Especially for the piezo actuators it is mandatory to avoid stresses and forces for which they were not designed. As in this case, where actuators are designed to contract/elongate along their longitudinal direction, torques and lateral forces must be avoided when mounting and operating the actuator by using suitable structures or guides.
- **Orientation**: the alignment of the orientation of the PZT with the expected vibration modes should be considered to improve its effectiveness.

Starting from these key considerations different placements and layouts have been analysed and then simulated in the FE software Abaqus. As mentioned before, placements were chosen to start from the resulted mode shapes of the six main vertical modes, evaluated in the damaged and undamaged condition of the structure. Indeed, placing the PZTs stacks in the areas where they differ the most, should ensure different MEMCFs and thus a higher Δ_{MEMCF} index.

5.1. PZT stack inserted in the rods

The first solution implemented has been the substitution of the central part of the first vertical rod with a piezo stack as depicted in Figure 30.

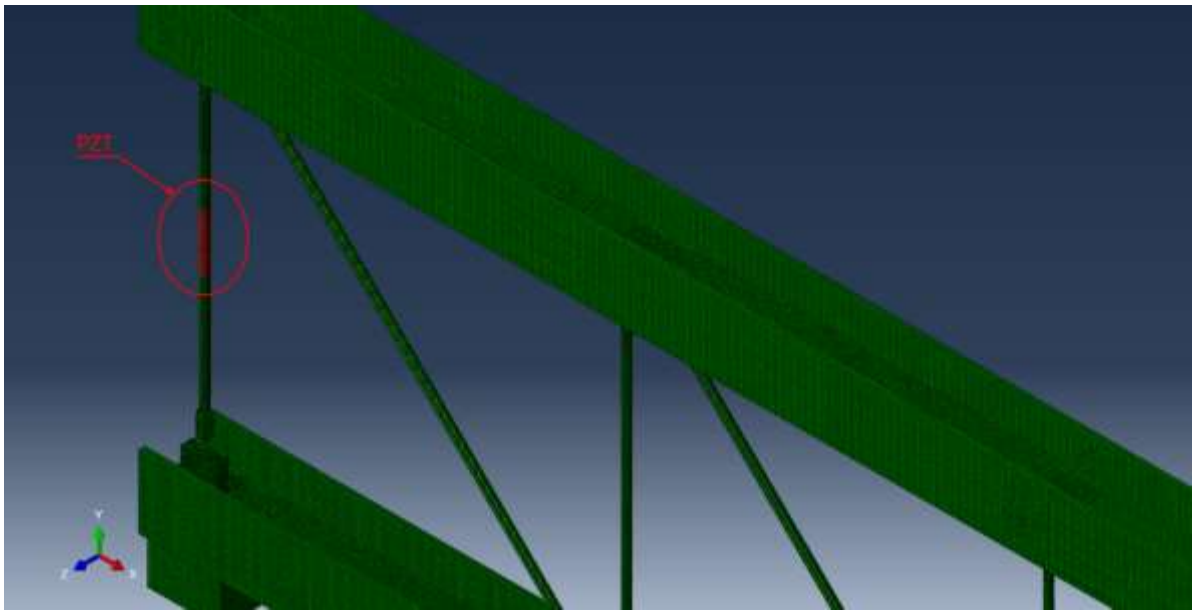

Figure 30: PZT stack inserted in the first vertical rod

Vertical and diagonal rods are indeed the elements of the structure which connect the two chords, contracting and expanding differently depending on the mode analysed. The higher difference between damaged (mass addition on the higher chords) and undamaged mode shapes are obtained at the first vertical rod, so the PZTs were implemented here.

The implementation resulted in the cut of the rod and the addition of the stack, constrained with the structure with the PIN as already discussed. The height of the cut was equal to that of the PZT simulated, no mounting structure was simulated and the PZT was directly connected to the structure. The piezo actuator implemented in this analysis has a circular base with a diameter equal to that of the vertical rods (i.e. 13 mm) and a height equal to 98 mm.

The analysis was performed both in short-circuit and open circuit conditions. All the modes found in the frequency range of 0-200 Hz were analysed. The first goal was to understand if the coupling factor k is readable experimentally and its order of magnitude. The threshold value that separates the valuable k from the worthless ones was set equal to 0.01.

5.1.1. Preliminary results

The resulting MEMCFs and their variation between damaged and undamaged configuration at the main vertical modes are depicted in Figure 31, while numerical values are reported in 11.1.1. Only the eigenmodes of the structure with non-zero coupling factors are reported and those with k or Δk higher than 0.01 are highlighted.

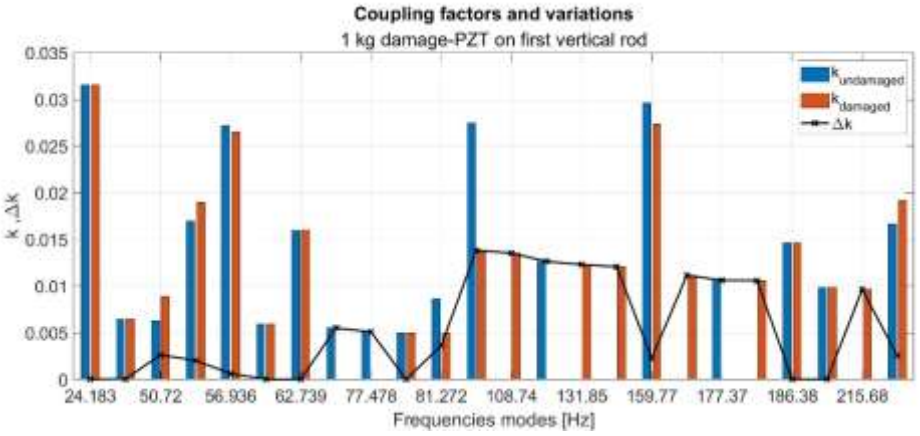

Figure 31: Damaged and undamaged coupling factors and their variation (Δk)

Twenty-four out of eighty-five modes identified by the FE simulations exhibit a non-zero coupling factor, in most cases higher than 0.01 both in damaged and undamaged conditions. However, the variation between these conditions is often lower than the threshold value. Given these results, different solutions had to be implemented. Thus, in order to maintain the layout with the PZT inserted in the rods, other PZTs were added in other vertical rods, to exploit the different deformation along the structure. By doing this, a global overview of the modes of the structure should be realised, and the different mode shapes should be exploited to maximise the elongation of the actuators in various frequency ranges.

Two different configurations have been evaluated: the first one provides the implementation of two actuators, specifically in the first and third vertical rods, since their dynamic behaviour showed the most significant alteration due to the damage's insurance; in the second one a PZT stack in every vertical rod.

For the evaluation of the MEMCFs, the eigenfrequencies of the structure were evaluated for the SC condition with all the PZTs shorted and then activating one actuator at a time for the OC ones. The configuration in which all the PZT are open-circuited (PZT all) is evaluated too. Piezo stacks are identified as PZT1, PZT2, ..., and PZT7 depending on which vertical rod they are mounted on, and the electrical configuration is identified depending on which actuator is active. For example, PZT1 OC means that the open circuit frequency is evaluated when the actuator on the first rod from the left is open-circuited while all the others are short-circuited.

Results are reported in the next paragraphs.

5.2. Piezo actuators inserted in the first and third vertical rods

Results, in terms of MEMCFs and their variation, from undamaged to damaged configuration are depicted in Figure 32 below. Complete numerical results are reported in 11.1.2.

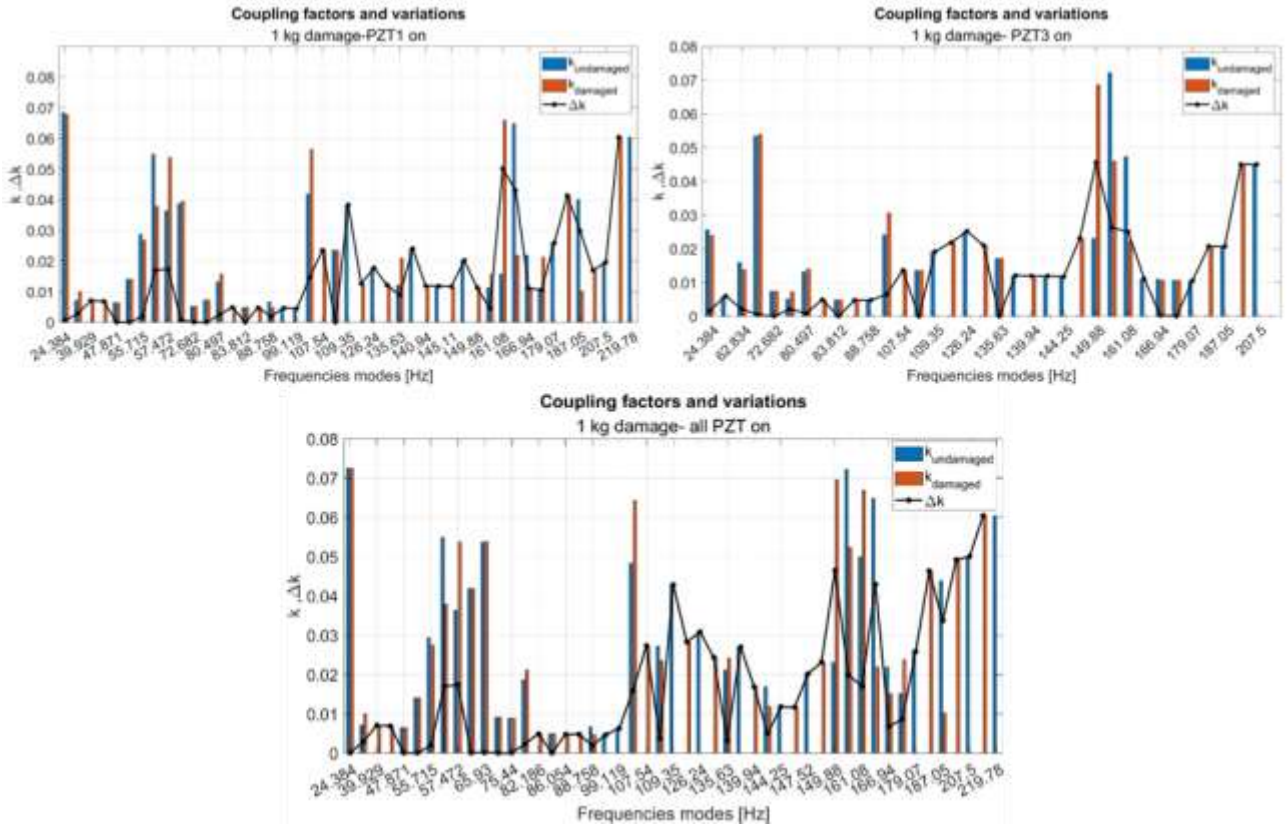

Figure 32: Undamaged MEMCF vs damaged MEMCF and variation in different activation configurations

It is observable that better results than those obtained with the implementation of only one piezo actuator are reached. For example, in Table 3 the comparison between the coupling factor and their variation evaluated at first vertical mode at 24 Hz are shown.

Comparison of coupling factor evaluated at the first vertical mode			
Configuration	**K undamaged**	**K damaged**	**ΔK**
1 PZT on rod 1	0.03151	0.03151	0.00001
2 PZT, PZT1 on	0.06842	0.06780	0.00062
2 PZT, PZT3 on	0.02562	0.02396	0.00166
2 PZT, all PZT on	0.06842	0.06780	0.00062

Table 3: Undamaged MEMCF vs damaged MEMCF and variation in different activation configurations at first mode

Since the advantages taken by the addiction of the PZT in the third vertical rod are observable but not significant, the configuration in which a PZT is added in every vertical rod of the structure is tested.

5.3. Piezo actuators inserted in each vertical rod

As in the previous case, the coupling factors are depicted in Figure 33, while in Table 4 results evaluated at the six main vertical modes are reported as examples. Complete numerical results are reported in 11.1.3,

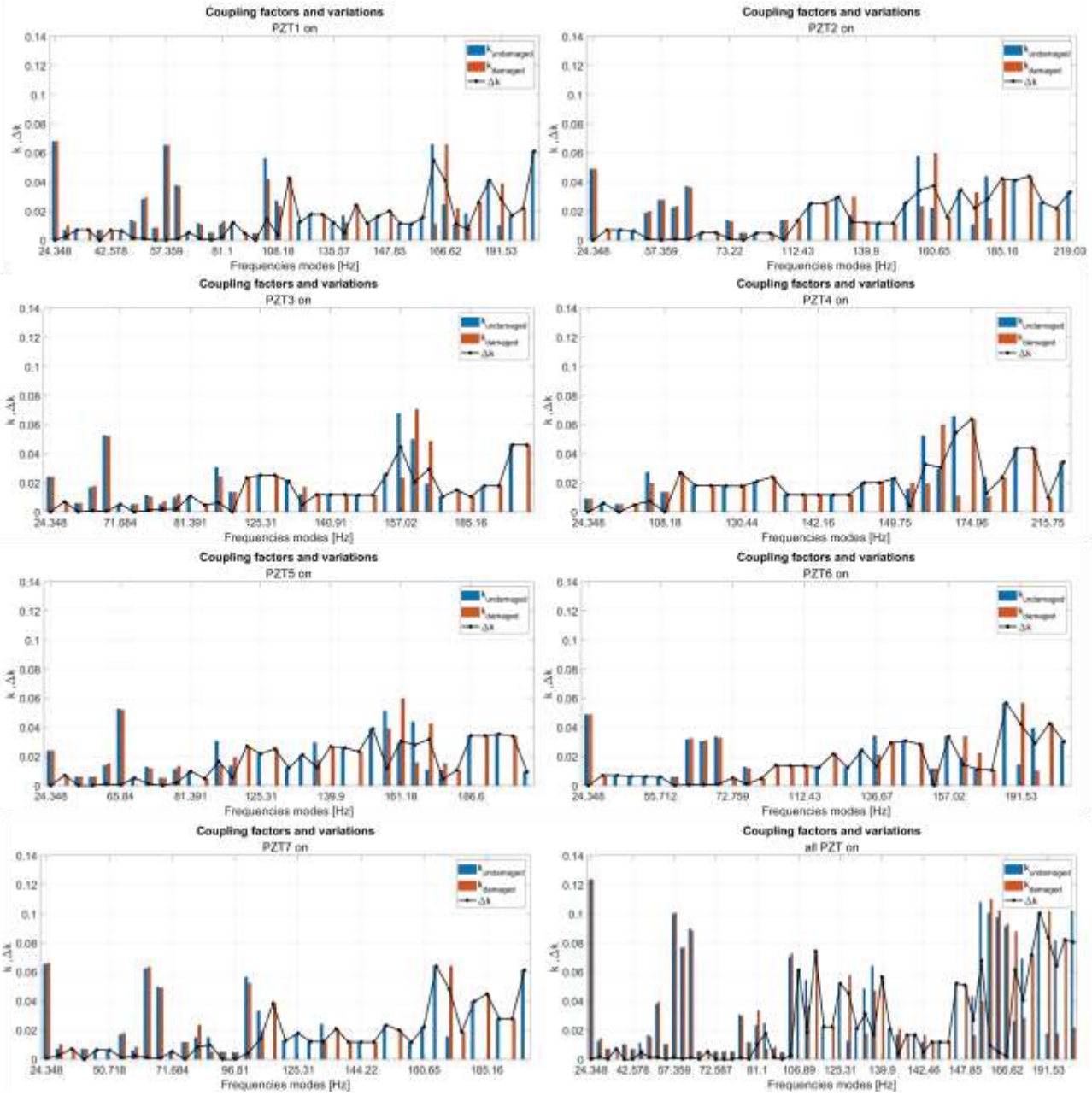

Figure 33: Undamaged MEMCF vs damaged MEMCF and variation in different activation configurations

	Mode 1			Mode 2			Mode 3		
	K undamaged	**K damaged**	**ΔK**	**K undamaged**	**K damaged**	**ΔK**	**K undamaged**	**K damaged**	**ΔK**
All PZT OC	0.12350	0.12350	0.00000	0.07660	0.07690	0.00030	0.09300	0.07260	0.02040
PZT 1 OC	0.06790	0.06790	0.00000	0.03390	0.03700	0.00310	0.06990	0.04190	0.02800
PZT 2 OC	0.04880	0.04880	0.00000	0.02260	0.02330	0.00070	0.06990	0.01400	0.05590
PZT 3 OC	0.02400	0.02400	0.00000	0.01690	0.01790	0.00100	0.06990	0.02420	0.04570
PZT 4 OC	0.00910	0.00910	0.00000	0.00000	0.00000	0.00000	0.06990	0.01980	0.05010
PZT 5 OC	0.02400	0.02400	0.00000	0.01380	0.01490	0.00110	0.06990	0.01400	0.05590
PZT 6 OC	0.04880	0.04880	0.00000	0.03040	0.03090	0.00050	0.06990	0.01400	0.05590
PZT 7 OC	0.06540	0.06600	0.00060	0.04950	0.04890	0.00060	0.06990	0.05230	0.01760
	Mode 4			**Mode 5**			**Mode 6**		
	K undamaged	**K damaged**	**ΔK**	**K undamaged**	**K damaged**	**ΔK**	**K undamaged**	**K damaged**	**ΔK**
All PZT OC	0.04330	0.04000	0.00330	0.10780	0.11010	0.00230	0.10210	0.10150	0.00060
PZT 1 OC	0.01160	0.00000	0.01160	0.01130	0.00000	0.01130	0.04140	0.03870	0.00270
PZT 2 OC	0.02580	0.02310	0.00270	0.05760	0.05970	0.00210	0.04140	0.04390	0.00250
PZT 3 OC	0.02580	0.02310	0.00270	0.06780	0.07050	0.00270	0.01790	0.01790	0.00000
PZT 4 OC	0.02310	0.02000	0.00310	0.01600	0.01950	0.00350	0.04390	0.04390	0.00000

PZT 5 OC	0.00000	0.00000	0.00000	0.03910	0.03910	0.00000	0.03430	0.03430	0.00000
PZT 6 OC	0.01160	0.00000	0.01160	0.03390	0.03380	0.00010	0.05670	0.05670	0.00000
PZT 7 OC	0.01160	0.00000	0.01160	0.00000	0.00000	0.00000	0.00000	0.00000	0.00000

Table 4: Resulting MEMCF for different activation configurations at the six main modes

Starting from these results, different considerations should be made. First, it can be seen that the k and Δk values change by up to an order of magnitude in the same way depending on which actuator is activated, due to the different behaviour along the structure. However, only in some Open/ Short Circuit configurations acceptable MEMCF values are reached. Despite the k values in most cases are above the threshold value, the variations between healthy and damaged conditions are very low. Furthermore, installing PZT actuators in each vertical rod would mean significantly modifying the structure and its components and would also represent a high cost.

For these reasons, it was decided to evaluate a similar alternative solution, which would still take advantage of the vertical displacement of the structure, but which provided for the possibility of adding PZTs without modifying the load-bearing components. Therefore, instead of placing the PZT stacks in the vertical rods already present in the structure, it was decided to add a rod in parallel to the vertical ones of the structure to act as a support structure for the PZT. The rod added is designed to be in aluminium as the ones already installed and connected to the chords through the same connection elements used by the vertical rods.

In the next sections, the layout, simulations and results of this configuration will be discussed.

5.4. PZT stack and mounting structure: Conf 1

As depicted in Figure 34 new vertical rod has been added next to the first vertical rod from the left, and the PZT has been placed in the middle of it. To minimise the influence of this addition on the overall stiffness of the structure the rod is designed to be in aluminium as those already installed.

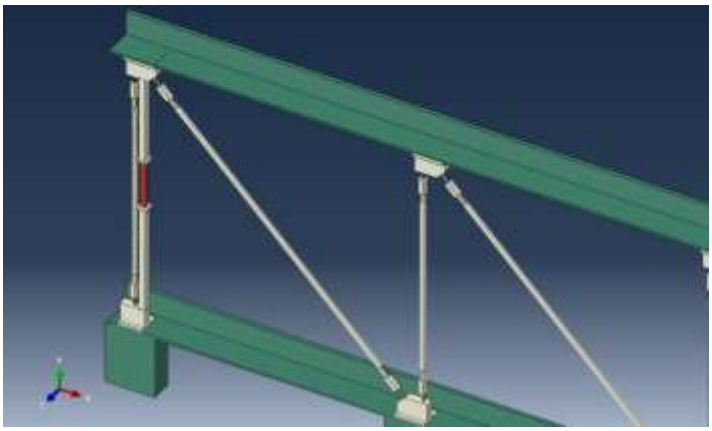

Figure 34: Example of PZT placed on a mounting structure

Previous results and placements have been exploited; so, the PZTs and their mounting rod have been implemented:

- Next to the first vertical rod (1 PZT actuator)
- Next to the first and third vertical rod (2 PZT actuators)

The mounting rods have been created directly in Abaqus software as the PZTs, and they are constrained to the structure with the Tie Constrained, which enforces the nodes of a slave surface (in this case, the base of the rod) to have translational and rotational motion equal to the ones of a master surface (here, the corresponding area of the structure). The constraint between PZT bases and the corresponding area of the rod is realised

through the PIN Constraint. The section and the length of the rod changed depending on the height of the PZT tested.

5.4.2. Preliminary results

In this section preliminary results for the layout described before are reported.

In the frequency range analysed, between 0-200 Hz, the FE model finds 85 vibration modes. Each configuration layout has been studied in both healthy states (damaged-undamaged), in short-open circuit electric conditions. The MAC index has been evaluated to check the correspondence between the vibration modes. So, the MEMCFs and their variation have been evaluated. The first piezo actuator tested takes as reference the P025-90P model produced by PowerPI [26], whose main characteristics are reported in Table 5.

PZT	Displacement [µm]	Diameter OD [mm]	Length L [mm]	Blocking force [N]	Stiffness [N/µm]	Capacitance [nF]	Resonant frequency [kHz]
P-025 .90P	180	25	165	14000	80	4000	7

Table 5: PICA Power P02590P characteristics

Many vibration modes resulted in a zero-coupling factor, so they are not reported here. Results are reported in 11.2.1 and they are depicted in Figure 35 below in terms of natural frequencies (Short Circuit in the undamaged state), coupling factor k and Δk.

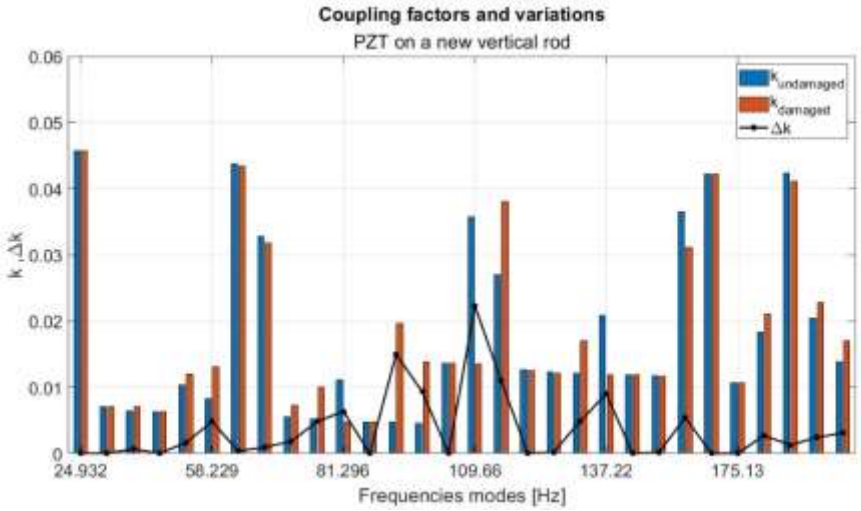

Figure 35: Undamaged MEMCF vs damaged MEMCF and variation Δk evaluated with P02590P installed next to the first vertical rod

Compared to the results of the previous configuration, there is a higher number of modes with k index higher than the threshold value of 0.1, but the coupling factor's variation is generally very low.

To try to increase these values, other PZT stacks were added to the simulation, specifically next to the third vertical rod. Results are reported in 11.2.2 and are depicted in figures below. The MEMCFs were evaluated considering the short circuit frequency as the one in which both PZT are short-circuited, and the open circuit frequencies were evaluated considering the cases in which one PZT is open-circuited and the other one is short-circuited and the case in which they are both open circuited. These results are reported as:

- **k PZT1 on undamaged, k PZT1 on damaged**: MEMCF evaluated considering the PZT next to the first vertical rod on, and the PZT next to the third rod short-circuited, in damaged and undamaged condition Figure 36;

- **k PZT2 on undamaged, k PZT2 on damaged**: MEMCF evaluated considering the PZT next to the third vertical rod on, and the PZT next to the first rod short-circuited in damaged and undamaged condition Figure 37;
- **k PZT1, PZT2 on undamaged, k PZT1, PZT2 on damaged**: MEMCF evaluated considering both PZT short-circuited and open-circuited in damaged and undamaged condition Figure 38.

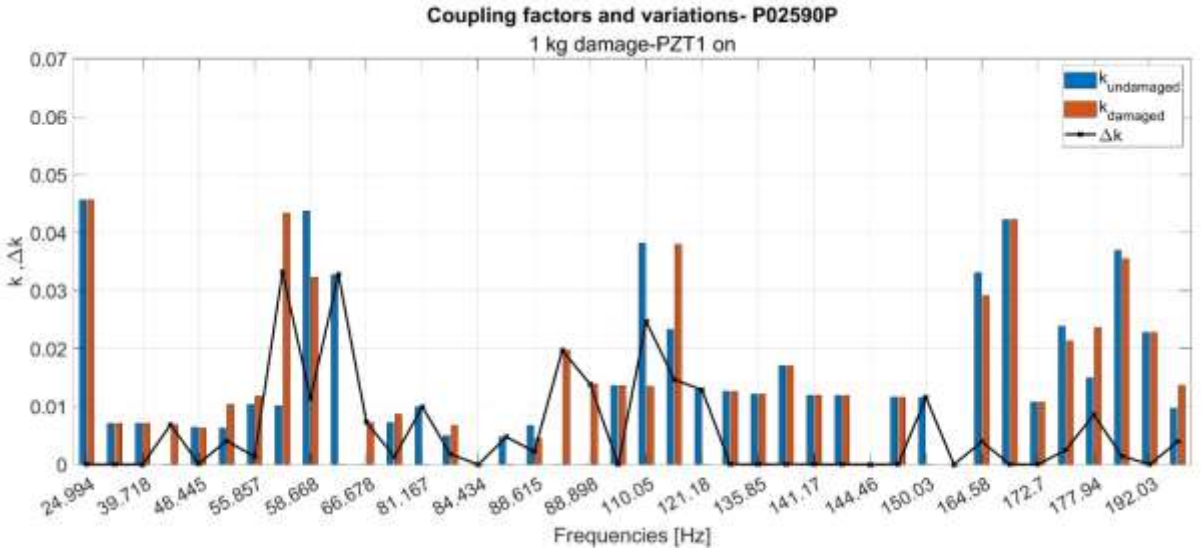

Figure 36: Undamaged MEMCF vs damaged MEMCF and variation Δk evaluated with P012590P installed next to the first and third vertical rod, PZT1 on

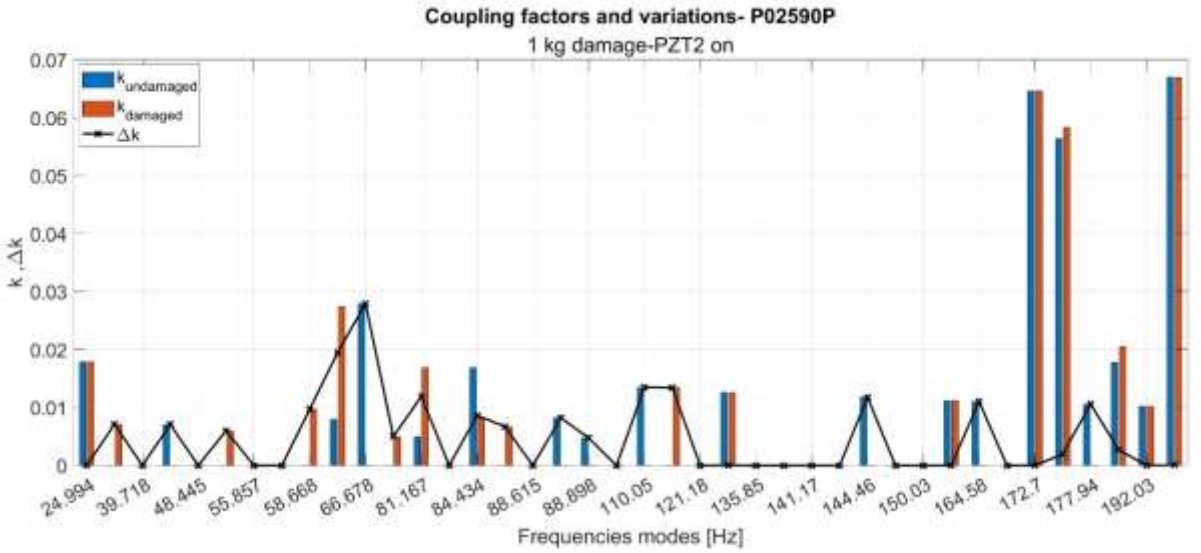

Figure 37: Undamaged MEMCF vs damaged MEMCF and variation Δk evaluated with P012590P installed next to the first and third vertical rod, PZT2 on

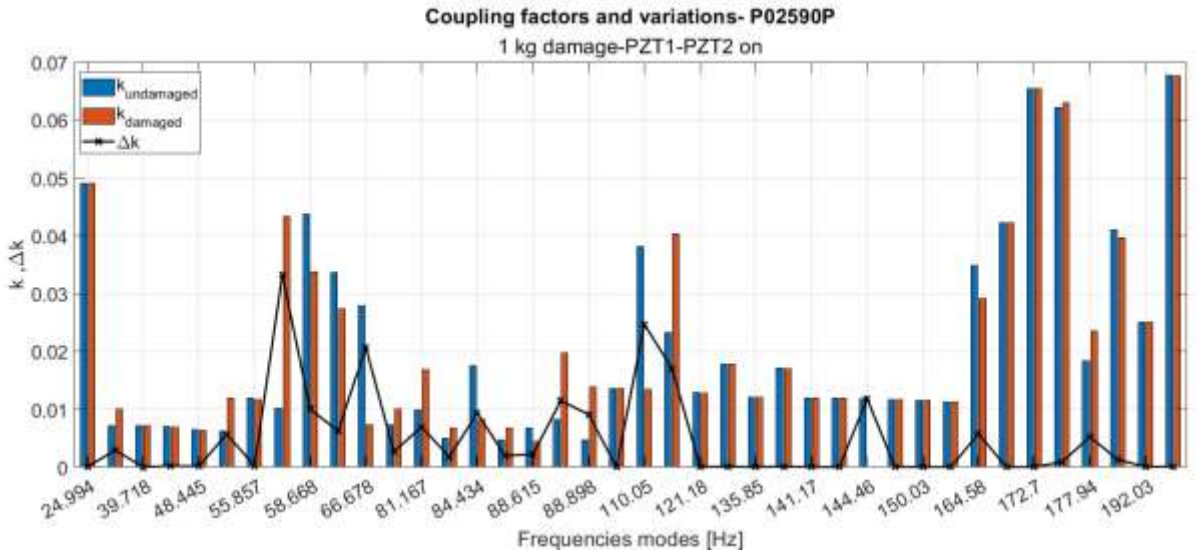

Figure 38: Undamaged MEMCF vs damaged MEMCF and variation Δk evaluated with P012590P installed next to the first and third vertical rod, all PZT on

Despite the higher number of modes which show non-zero coupling factors and with a higher magnitude than those obtained in the configuration with only one actuator, there is no observable variation between damaged and undamaged configuration.

Mode shapes do not change significantly with the onset of this type of damage. Indeed the total mass of the structure is equal to 300 kg, thus the variation of 1 kg could be too low to affect its dynamic behaviour, and thus the electromechanics coupling with the piezo actuator.

For this reason, this damage configuration was discarded, and we focused on the damaged configuration 2, where the diagonal rods are weakened by a reduction of the Young Modulus by about 50%. Studying these damages should increase the magnitude of k and Δk since they are next to where the PZT are placed and being a damage to a connecting element between the chords it should affect the behaviour of the structure the most. The MEMCFs evaluated in the damage configuration are denoted "k_dam_rod1" and "k_dam_rod2" for the index evaluated in the damaged configurations in which the first diagonal rod or the second diagonal rod are weakened respectively.

Using the PI catalogue as a reference [26] PZT actuators with different characteristics were simulated. Their geometrical, mechanical and electrical characteristics are reported in Table 6.

Piezo actuators	Displacement	Diameter	Length	Blocking force	Stiffness	Capacitance	Resonant frequency
	[µm]	[mm]	[mm]	[N]	[N/µm]	[nF]	[kHz]
P-010 .40P	60	10	58	2200	37	180	20
P-010 .80P	120	10	111	2300	19	370	10
P-016 .80P	120	16	111	5900	49	1000	10
P-016 .90P	180	16	163	6000	33	1600	7
P-025 .40P	60	25	60	13000	220	1300	19
P-025 .90P	180	25	165	14000	80	4000	7
P-035 .20P	30	35	34	23000	760	1200	34

Table 6: Geometrical, mechanical and electrical properties of PICA Power actuators

It is necessary to find a compromise between blocking force and actuator stiffness. On one hand, given the magnitude of the forces exerted and transmitted within the structure, it was assumed that a high-blocking force actuator must be used. On the other hand, the greater the blocking force that the piezoelectric actuator can exert, the higher its stiffness will be, and, consequently, the smaller its elongation will be.

A comparison between the different MEMCFs obtained at the first vertical mode with different PZT is reported in Table 7.

Piezo actuators	Blocking force [N]	Stiffness [N/µm]	K undamaged	K damaged rod2	ΔK rod2	K damaged rod1	ΔK rod1
P035 20P	23000	760	0.015413	0.015514	0.000100	0.015514	0.000100
P025 40P	13000	220	0.019908	0.017921	0.001986	0.017922	0.001985
P025 90P	14000	80	0.030836	0.031036	0.000200	0.029716	0.001120
P016 80P	5900	49	0.036733	0.036972	0.000238	0.035869	0.000864
P010 40P	2200	37	0.040850	0.041115	0.000265	0.040125	0.000725
P016 90P	6000	33	0.045430	0.045725	0.000295	0.044839	0.000592
P010 80P	2300	19	0.054996	0.056078	0.001082	0.055356	0.000360

Table 7: Resulting MEMCF and variation for different PZT tested, evaluated at the first main mode

Piezo actuators with high blocking force such as the P03520P are too stiff and result in the lowest MEMCF among all the simulated actuators. In contrast, PZTs with less stiffness and low blocking force result in higher MEMCFs. A global overview of the MEMCFs and their variation obtained with the different PZTs among all the modes identified in the FE model is shown in Figure 39 and Figure 40 for the damage of the first and second diagonal rod respectively. Only the modes with at least one non-zero coupling factor, evaluated in damaged or undamaged configuration, are shown. Numerical results are reported in 11.2.

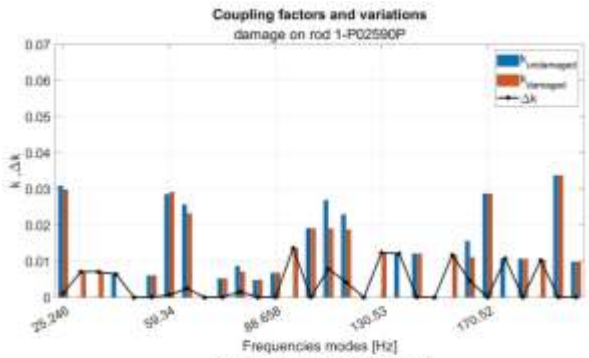

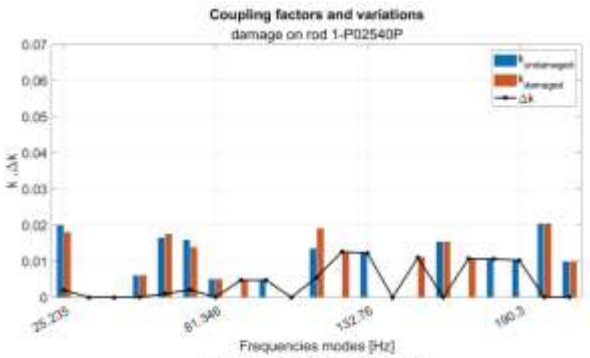

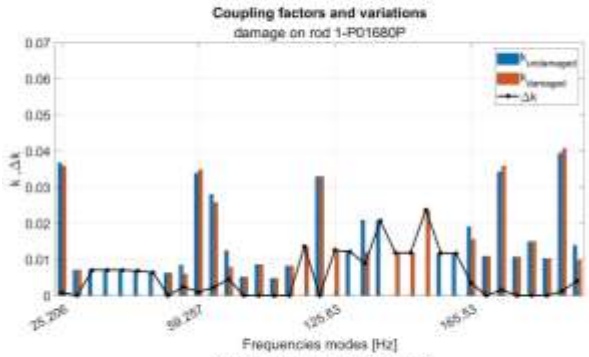

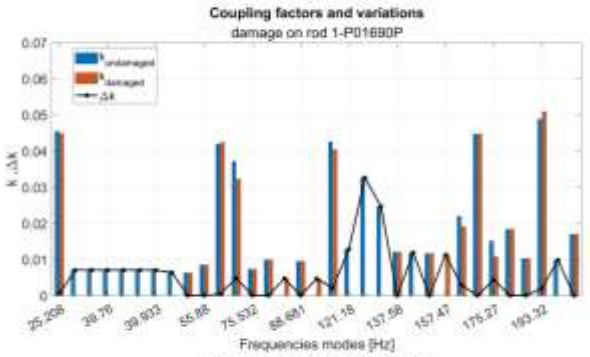

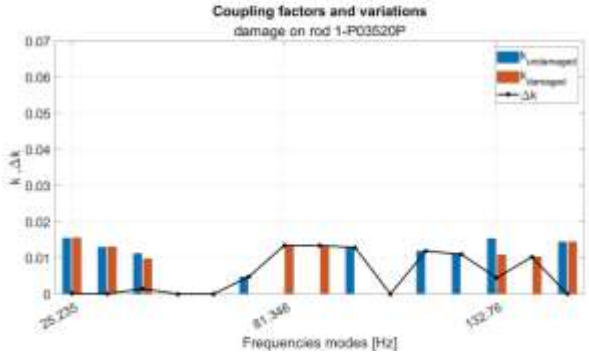

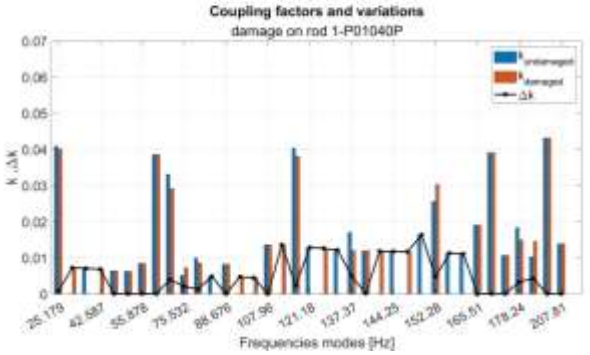

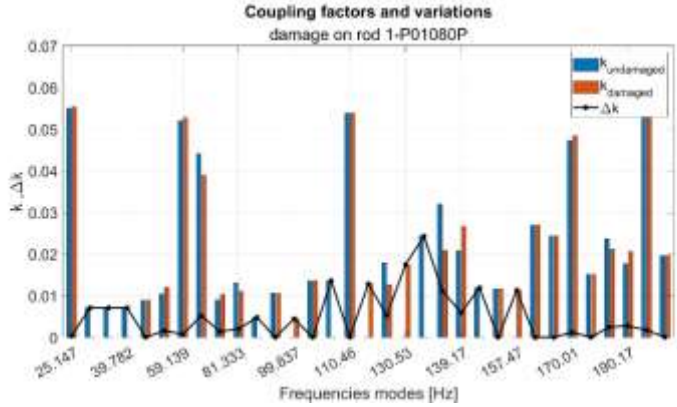

Figure 39: Undamaged MEMCF vs damaged MEMCF and Δk with different PZT tested - damage on first diagonal rod

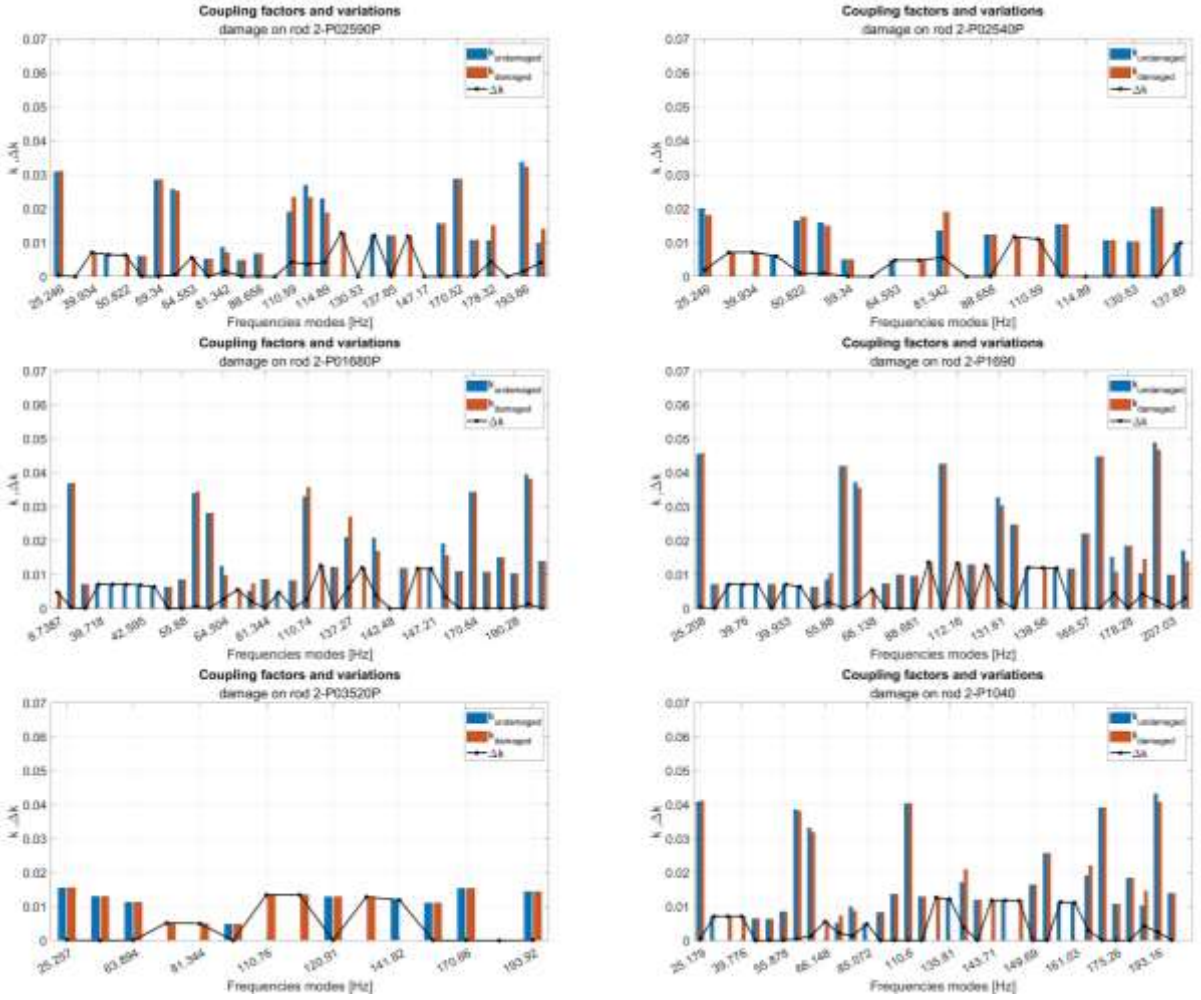

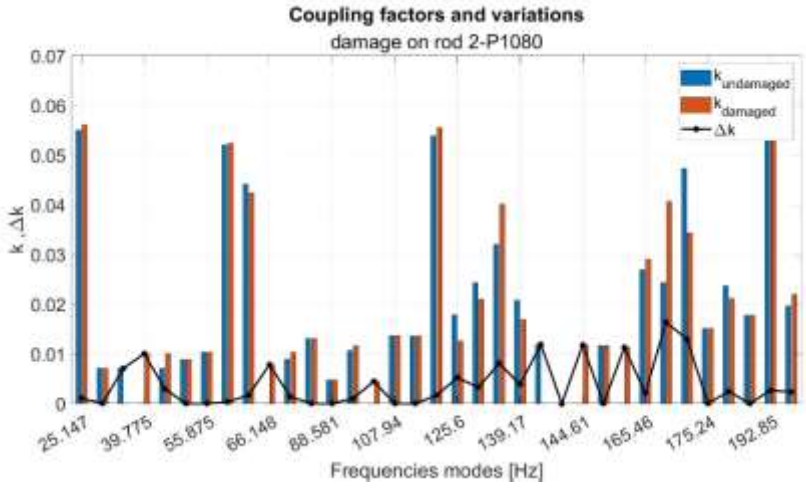

Figure 40: Undamaged MEMCF vs damaged MEMCF and Δk with different PZT tested - damage on 2nd diagonal rod

Starting from these results, some considerations should be made. Piezo actuators characterized by larger strokes, such as P01080P and P01690P, generally exhibit higher MEMCF values compared to the stiffer ones, but the levels remain significantly low. Also, the variation between damaged and undamaged states is low. This can be attributed to the fact that, relative to the overall dimensions of the structure, those of the piezo actuators are not comparable, resulting in very low coupling coefficients. Additionally, the modal shapes negligibly differ between the healthy and damaged states, so even where the coefficients are higher (as at 24.15 Hz), they do not change significantly upon damage, leading to an almost negligible variation in the coefficient.

Given these results, since even the use of multiple PZTs does not seem to provide any benefit, the decision to focus on the modes of the vertical and diagonal rods rather than the global modes of the structure was made. The beams indeed have smaller cross-sections compared to the chords, making them comparable to those of the piezo actuators. For this reason, it was decided to connect the piezo actuators directly to the beams using aluminium connection elements. The two layouts tested are described in the next sections.

5.5. PZT stack connecting rods and rods-chords

As for the previous scenarios first of all the mode shapes, in the undamaged and damaged condition, have been evaluated, this time focusing the attention on the vertical and diagonal rods. Modal displacement along the vertical (*uy*) and horizontal direction (*ux*) have been evaluated in several nodes of the rods and compared with each other. An example is reported in (Figure 41) where the mode shapes of the fourth vertical mode evaluated in undamaged condition are compared with those from the structure damaged (1 kg added). The area where the mode shapes differ more is the one between the two first vertical rods, so it is reasonable to consider placing the PZTs here.

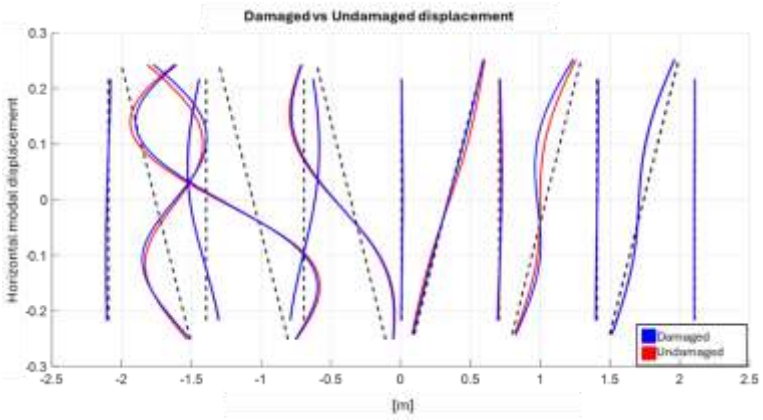

Figure 41: Damaged vs undamaged horizontal displacement of the rods

Two different solutions have been tested:

- PZT inserted between the first diagonal rod and the upper/lower chord.
- PZT inserted between the first diagonal rod and the second vertical rod.

The connection between the PZTs and the rods is realized through connection elements in aluminium similar to those between the chords and the rods. As for the previous cases, each configuration layout has been studied in each healthy state (damaged-undamaged) and in both electric conditions (short-open circuit). The MAC index has been evaluated to check the correspondence between the vibration modes. Finally, the MEMCFs and their variation have been evaluated.

Many vibration modes resulted in a zero-coupling factor, so they are not reported here. Results are reported in the next paragraphs in terms of natural frequencies (short-open circuit), MEMCFs, Δk, for each piezo and damage tested.

5.6. Conf 2: PZT stack between diagonal rods and chords

As shown in (Figure 42) PZT stack are connected from one side to the first diagonal rod through a connection element, and on the other side directly to the upper chord. The connection element is added to the structure through the Tie constraint, while the connection with the chord is realized via the Pin constraint. This solution has been implemented because the idea was to exploit the higher stiffness of the chord, compared to the rod's one, to obtain a higher elongation of the PZT.

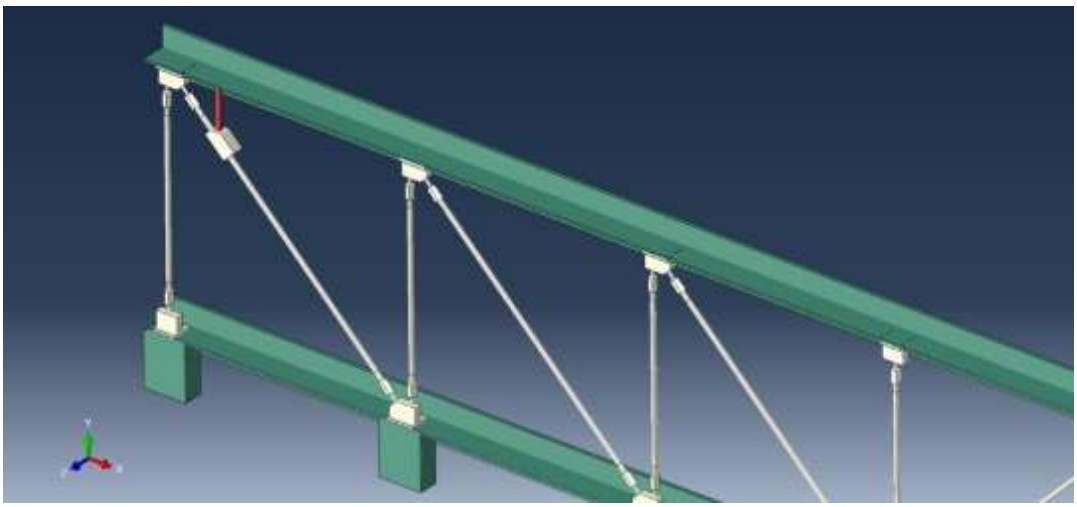

Figure 42: Placement 2: PZT connecting the upper chord and the diagonal rod

For this reason and on the basis of the results obtained in the previous layout, PZTs simulated were chosen to have the lowest stiffness available in the PI catalogue. Specifically, the P101080P and P01680P, whose characteristics are reported in Table 6, were employed.

Unfortunately, as it can be seen from the results presented in Table 8 and Table 9, this solution did not yield any improvement in terms of k or Δk. The results obtained are worse, both in terms of quantity and magnitude, compared to those previously achieved. The reason for this behaviour can be attributed to the fact that, while oscillating, the chord drags the diagonal rod via the piezo, which therefore acts as a connecting element and does not deform. Since it does not deform, the piezo does not cause any variation in the mode of the structure, resulting in a zero coefficient, even if the damage is induced on the rod to which the piezo is mounted on.

P01080P							
Damage on diagonal rod 1				Damage on diagonal rod 2			
Frequency (SC) [Hz]	K undamaged	K damaged	ΔK rod1	Frequency (SC) [Hz]	K undamaged	K damaged	ΔK rod2
50.48	0.00629	0.00630	0.00000	50.48	0.00629	0.00629	0.00000
54.75	0.02180	0.02096	0.00083	54.75	0.02180	0.02181	0.00001
55.87	0.00598	0.00598	0.00000	55.87	0.00598	0.00846	0.00248
57.58	0.00589	0.00000	0.00589	57.58	0.00589	0.00000	0.00589
135.01	0.01217	0.01218	0.00001	135.01	0.01217	0.01215	0.00002
141.20	0.00000	0.01685	0.01685	136.47	0.00000	0.01211	0.01211
142.07	0.01187	0.01188	0.00001	142.07	0.01187	0.01187	0.00000
142.60	0.01184	0.00000	0.01184	142.60	0.01184	0.00000	0.01184
145.14	0.01660	0.01664	0.00004	145.14	0.01660	0.01664	0.00003
147.43	0.00000	0.00000	0.00000	147.43	0.00000	0.01165	0.01165
148.57	0.01641	0.01162	0.00479	148.57	0.01641	0.01164	0.00477
				158.10	0.00000	0.01126	0.01126
163.13	0.01107	0.00000	0.01107	163.13	0.01107	0.00000	0.01107
168.13	0.01091	0.01093	0.00002	168.13	0.01091	0.01091	0.00001
				177.99	0.00000	0.01061	0.01061
189.49	0.00000	0.01032	0.01032	189.49	0.00000	0.01028	0.01028

Table 8: Resulting MEMCFs, variations, for P01080P PZT, damage on diagonal rod 1 and 2

P01680P					
Frequency (SC) [Hz]	K undamaged	K damaged rod2	ΔK rod2	K damaged rod1	ΔK rod1
57.07	0.00837	0.00837	0.00000	0.00593	0.00245
58.26	0.01015	0.00829	0.00186	0.01015	0.00001
134.38	0.01220	0.00000	0.01220	0.01221	0.00001
136.38	0.00000	0.01217	0.01217	0.00000	0.00000
141.30	0.01190	0.00000	0.01190	0.01191	0.00002
144.50	0.01176	0.01177	0.00000	0.00000	0.01176
147.59	0.01164	0.01165	0.00001	0.00000	0.01164
148.18	0.01162	0.01162	0.00000	0.00000	0.01162
163.43	0.00000	0.00000	0.00000	0.01108	0.01108
190.15	0.00000	0.00000	0.00000	0.01029	0.01029

Table 9: MEMCFs, variations, for P01680P PZT, damage on diagonal rods 1 and 2

Given these results, the configuration in which the piezo is inserted between the first diagonal rod and the second vertical rod was simulated.

5.7. Conf 3: PZT between diagonal and vertical rod

As shown in (Figure 43) PZT stack is connected to the first diagonal rod and the second vertical rod through connection elements in aluminium.

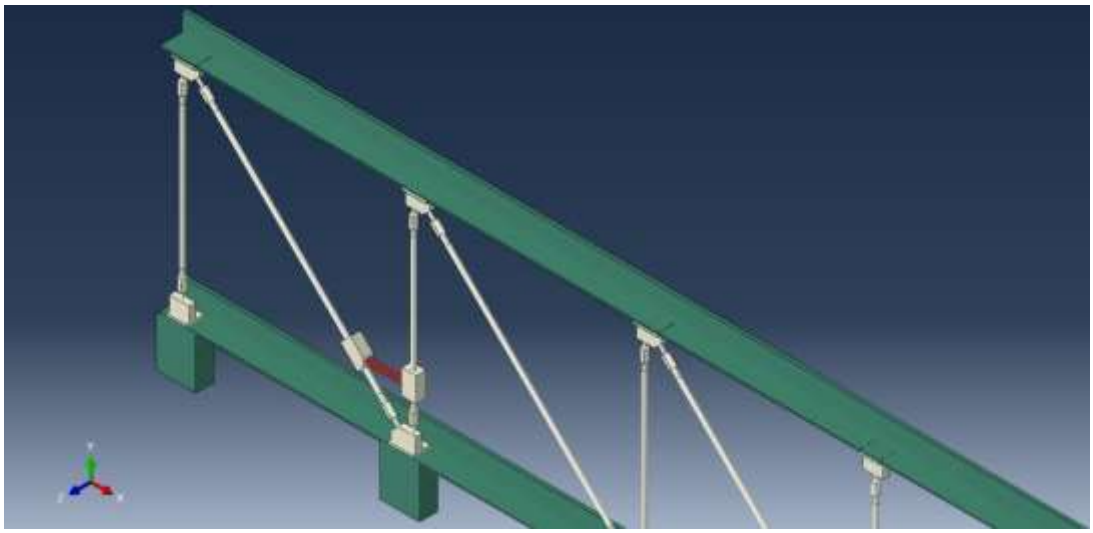

Figure 43: Placement 3: PZT connecting the vertical and the diagonal rod

Constraints with the structure and connection elements are analogues to the previous one, so the Tie constraint for the structure-connection element, and the Pin constraint for the PZT-connection element were used. This solution has been implemented because the idea was to exploit the lower stiffness of the rods compared to the chord's one, and so their possible higher displacements to obtain a higher elongation of the PZT. Moreover, the section of the roads is comparable to the one of the PZT, so the electromechanical coupling could be better than before.

For this reason and based on the results obtained in the previous layout, PZTs simulated were chosen to have the lowest stiffness available in the PI catalogue. Specifically, the P01080P and P016980P were simulated.

Results are reported in Table 10 and Table 11 below.

P01080P			
Frequency (SC) [Hz]	**K undamaged**	**K damaged**	**ΔK**
50.73	0.00628	0.00628	0.00000
51.02	0.01878	0.01878	0.00000
57.58	0.00589	0.00000	0.00589
57.79	0.00000	0.00588	0.00588
150.37	0.01153	0.00000	0.01153

Table 10: MEMCFs, variations, for P01680P PZT, damage on diagonal rod 1

P01640P			
Frequency (SC) [Hz]	**K undamaged**	**K damaged**	**ΔK**
43.01	0.01804	0.01929	0.00125

Table 11: MEMCFs, variations, for P01480P PZT, damage on diagonal rod 1

Unfortunately, this solution provides comparable results to the one with the PZTs connecting the diagonal rod and the chord; indeed, only few modes result in non-zero MEMCFs, but with a value lower than the threshold one. Because of this, only the indices in case the damaged rod is the same one on which the piezo is mounted are shown.

5.8. Preliminary conclusions

Considering these results, the configuration in which the piezo actuators are mounted on a vertical rod next to the first vertical one from the left is the best solution among those tested. Indeed, it provides a higher number of modes with non-zero coupling factors and variation between damaged and undamaged conditions. Moreover, also the magnitude of these indices is generally greater than those obtained in other configurations. Similar results have been obtained in the configuration in which the PZTs were implemented directly in the structure's vertical rods, but this solution was discarded because it entailed too high costs and significant modification of the structure itself.

MEMCFs variation higher than 0.01 obtained with the PZT mounted next to the first vertical rod at plausible modes of the structure are compared in Figure 44 below. The unhealthy condition is the damaging of the second diagonal rod.

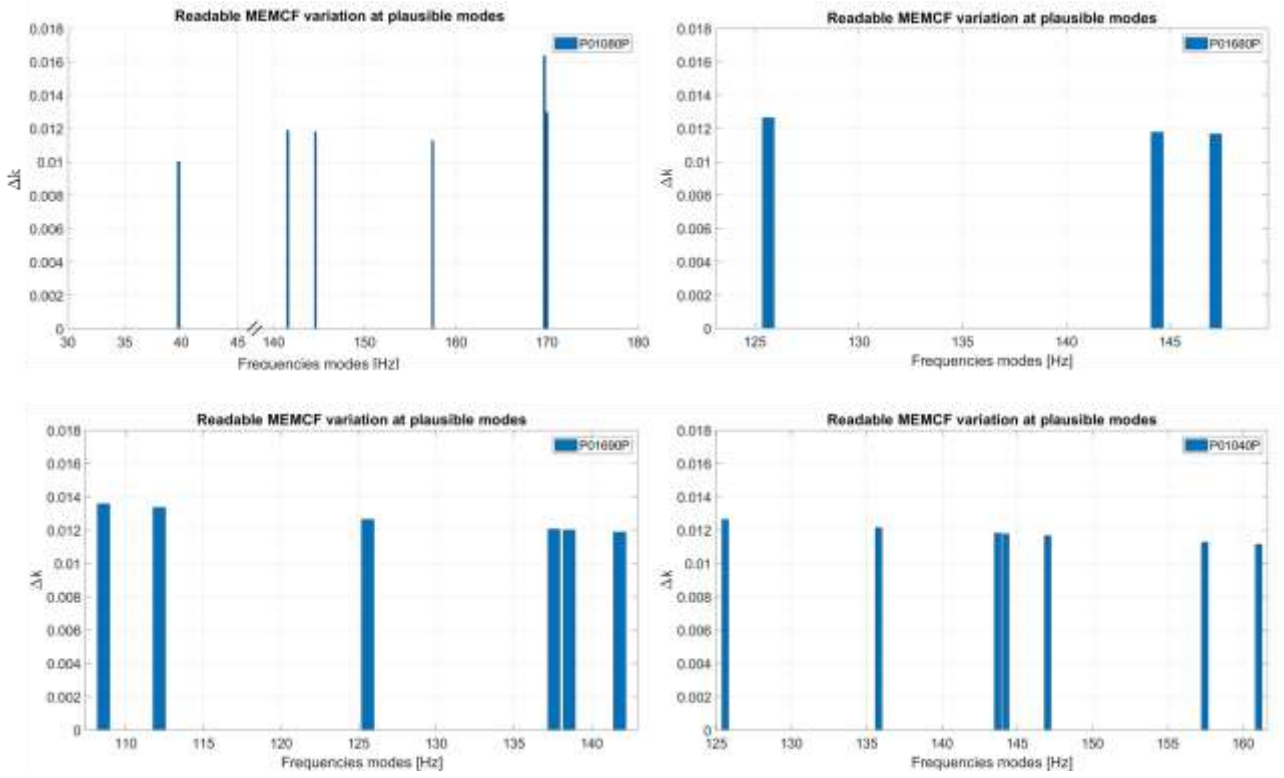

Figure 44: MEMCFs variations obtained with different PZT tested- damage on 2nd diagonal rod-placed next to the first diagonal rod

P01080P actuator is identified as the best solution in terms of compromise between obtainable MEMCFs and the cost of the sensor itself. This actuator provides the best results with both mounting configurations (next to the first vertical rod and between the diagonal and vertical rod) and it can therefore be tested in both setups. For these reasons, it was chosen to be implemented for the experimental tests.

6. Preloaded piezo actuators

The results of the FE model have demonstrated that piezo actuator P01080P, positioned either parallel to the first vertical rod or between the diagonal and vertical one, appears to be the best solution among the various tested actuators. It can identify a good number of modes with coupling coefficients greater than 0.1 and its variation between the damaged and undamaged state is, for a couple of modes, greater than 0.1.

However, this kind of actuator is sold by Power Pi only in the form of a simple stack of piezo layers glued together as show in Figure 45. They are not supplied with any mounting case which could ensure the correct installation. Moreover, piezo actuators need to be mechanically preloaded for several reasons, as for example:

- Dynamic forces compensation: preloading the actuators suppresses dynamically induced tensile forces in brittle ceramic material, allowing response times in the microsecond range and improving its mechanical performance
- stability increment: Preloading indeed reduces hysteresis, improving the linearity of the piezo actuator's response and ensuring more stable performance;
- prevention of breakage: it helps avoid the saturation of the actuator or excessive loads which could damage the actuator

Figure 45: PICA Power piezo stacks

The preload should be selected as low as possible. According to the manufacturer's reports, 15 MPa is sufficient.

Based on these considerations and the difficulty of creating a mounting structure capable of ensuring the correct preload on the piezo and achieving effective coupling with the structure, it was decided to move on to the implementation of preloaded piezo actuators produced by Pica Power PI (Figure 46). These actuators consist of piezo stack actuators with similar geometrical and electrical characteristics as the ones mentioned so far but encapsulated in a mounting case which facilitates their installation and ensures the correct preload needed.

Figure 46: Preloaded piezo actuators

Unfortunately, the preloaded version of the P01080P actuator was not available, so a similar one had to be chosen. A comparison between that sensor and the various versions available by Power PI, denoted P840 and P844 are reported in Table 12 and Table 13 respectively.

Characteristic	Unit	PICA POWER ACTUATORS	PICA POWER PRELOADED P-840				
		P010.80P	P-840.10	P-840.20	P-840.30	P-840.40	P-840.60
Displacement	µm	120	15	30	45	60	90
Diameter	mm	10	12	12	12	12	12
Length	mm	111	32	50	68	86	122
Blocking force	N	2300					
Permissible push force in Z	N		1000	1000	1000	1000	1000
Permissible pull force in Z	N		50	50	50	50	50
Stiffness	N/ µm	19	57	27	19	15	10
Electrical capacitance	nF	370	1500	3000	4500	6000	9000
Resonant frequency	kHz	10	18	14	10	8.5	6
Operating Voltage	V	0-1000	0-100	0-100	0-100	0-100	0-100

Table 12: P01080P vs preloaded P840-models

Characteristic	Unit	PICA POWER ACTUATORS	PICA POWER PRELOADED P-844				
		P-010.80P	P-844.10	P-844.20	P-844.30	P-844.40	P-844.60
Displacement	µm	120	15	30	45	60	90
Diameter	mm	10	20	20	20	20	20
Length	mm	111	47	65	83	101	137
Blocking force	N	2300					
Permissible push force in Z	N		3000	3000	3000	3000	3000
Permissible pull force in Z	N		700	700	700	700	700
Stiffness	N/ µm	19	225	107	75	57	38
Electrical capacitance	nF	370	6000	12000	18000	24000	36000
Resonant frequency	kHz	10	16	12	9	7.5	5.5
Operating Voltage	V	0-1000	0-100	0-100	0-100	0-100	0-100

Table 13: P01080P vs preloaded P844-models

The preloaded actuators with the most comparable geometrical, mechanical and electrical characteristics are the P840-30 and P840-60.

In order to verify their efficiency, new FE simulations were carried out. In this case, wishing only to validate the similarity of piezo behaviour, only the layout in which the piezo mounted in a rod next to the first vertical one is replicated. For the same reason, the damaged conditions simulated are the ones in which the first and second diagonal rods are weakened by a reduction of the Young Modulus by about 50%. Results are reported in the following section.

6.1. Results

The MEMCFs and their variation are reported in Table 14 and Table 15 below, for the P840-30 and P840-60 respectively.

Damage on diagonal rod 2			
P840 30			
Freq. SC [Hz]	K undamaged	K damaged rod2	ΔK rod2
63.72	0.01585	0.02507	0.00923
63.86	0.02565	0.01584	0.00981
125.63	0.00000	0.01263	0.01263

130.53	0.00000	0.01238	0.01238
135.81	0.00000	0.01212	0.01212
P840-60			
Freq. SC [Hz]	**K undamaged**	**K damaged rod2**	**ΔK rod2**
107.97	0.00000	0.01361	0.01361
121.18	0.01285	0.00000	0.01285
142.12	0.00000	0.01689	0.01689
142.56	0.01184	0.00000	0.01184
146.84	0.00000	0.01167	0.01167
147.17	0.01166	0.00000	0.01166
157.47	0.00000	0.01128	0.01128

Table 14: Damaged-undamaged, MEMCFs Δk obtained with P84030 and P84060- damage on diagonal rod 2

Damage on diagonal rod 1			
P840 30			
Freq. SC [Hz]	**K undamaged**	**K damaged rod1**	**ΔK rod1**
63.72	0.01585	0.02574	0.00990
63.86	0.02565	0.00560	0.02005
125.63	0.00000	0.01262	0.01262
135.81	0.00000	0.01262	0.01262
P840-60			
Freq. SC [Hz]	**K undamaged**	**K damaged rod1**	**ΔK rod1**
59.203	0.04615	0.04618	0.00004
108.61	0.00000	0.01357	0.01357
121.18	0.01285	0.00000	0.01285
135.63	0.02103	0.00000	0.02103
136.97	0.02960	0.01705	0.01256

Table 15: Damaged-undamaged, MEMCFs Δk obtained with P84030 and P84060- damage on diagonal rod 1

Comparing these results with those obtained with the P01080P it is noticeable that the P840-60 is the one which should ensure similar results and efficiency. For this reason, this actuator has been identified as the best solution for this application.

Despite the good results, the magnitude of the variation of the MEMCF index is low. To evaluate the response to a more drastic damage situation, it is decided to test the piezo under severe damage, such as that caused by the breaking of one of the rods in the structure, specifically the second vertical rod from the left. A more severe damage should indeed alter the dynamic behaviour of the structure more significantly, and consequently its mode shapes, and thus also the MEMCFs from undamaged to damaged configuration. Results are reported and discussed in the next chapter.

7. P840-60 actuator and broken rod configuration

The last damaged configuration simulated in the FE model is the one described in Section 4 in which the rod to which the piezo is connected is broken. This heavy damage configuration can be assumed as a failure configuration of the element of the structure. Defined the damaged configuration, the piezo element has been added to the structure according to the three layouts simulated for the previous ones. Results are shown in Figure 47, Figure 48 and Figure 49, divided according to the piezo layout suited. Numerical reports are reported in 11.3.

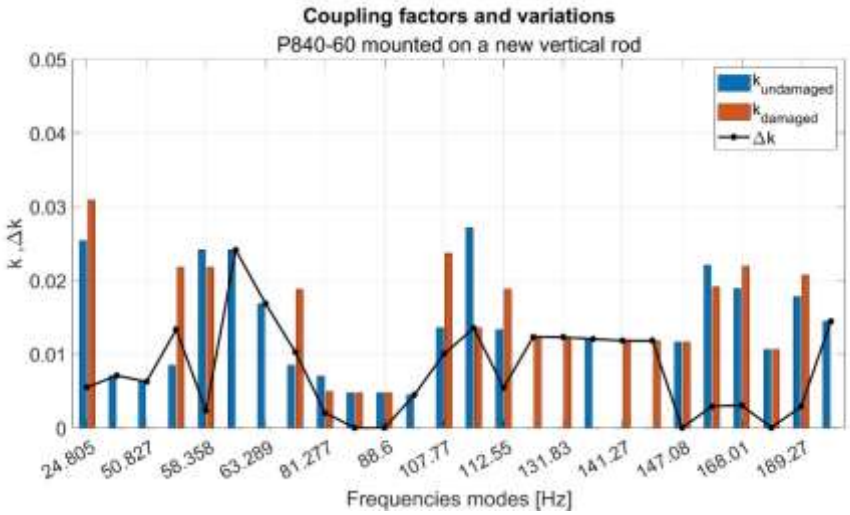

Figure 47: Damaged-undamaged, MEMCFs Δk - P84060- damage on vertical-rod -PZT next to the 1st vertical rod

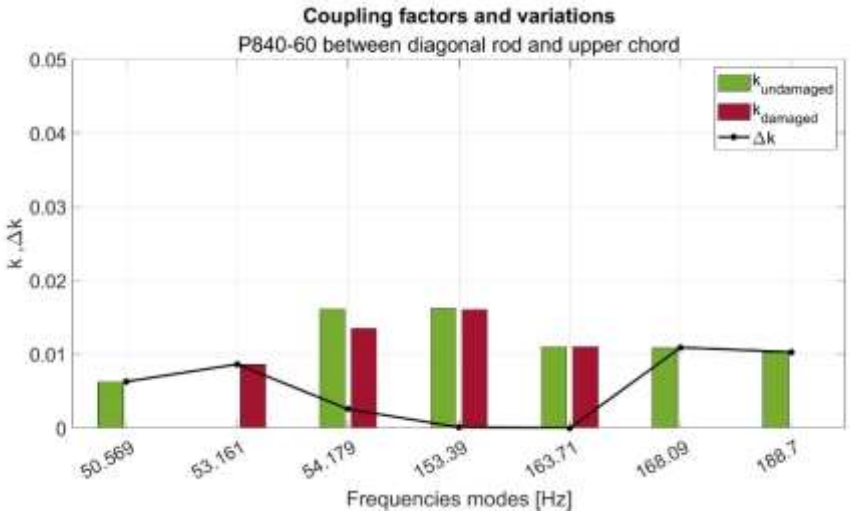

Figure 48: Damaged-undamaged, MEMCFs Δk - P84060- damage on vertical-rod -PZT between diagonal rod and upper chord

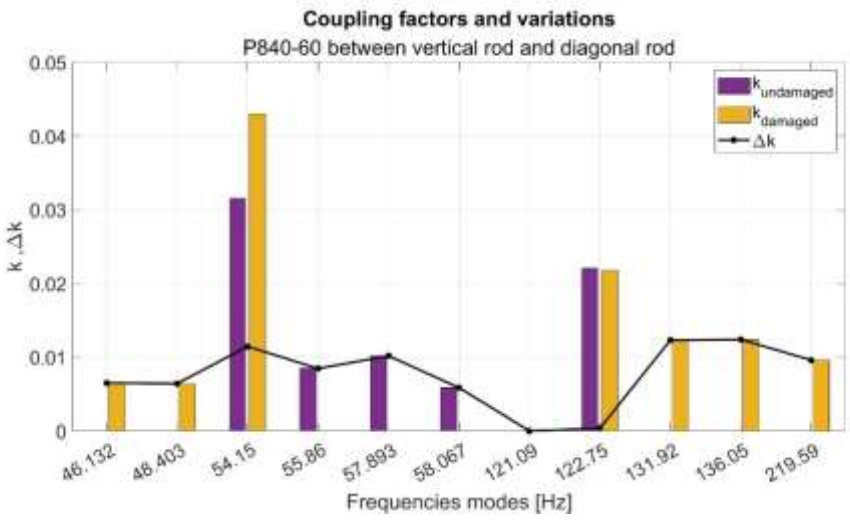

Figure 49: Damaged-undamaged, MEMCFs Δk - P84060- damage on vertical-rod -PZT between diagonal-vertical rod

Results show that the configurations with the PZT connecting the chord and the diagonal rod do not offer observable results. The solution with the PZT between the diagonal and vertical rod results in MEMCF and its variation is evaluated at the eigenmode of the first diagonal rod higher than the previous case in which the rod was affected by a lighter damage. This shows the dependency of the index to the damage and its magnitude. Finally, the solution in which the PZT is mounted next to the first vertical rod results in a higher number of modes with non-zero coupling factors, generally with a greater magnitude than the previous damaged cases simulated.

7.1. Preliminary conclusions

The possibility of implementing piezoelectric actuators and exploiting the variation of the Modal electromechanical Coupling Factor (MEMCF) due to the insurgence of damages to develop new SHM techniques on complex truss girder structures has been analysed. A model-based approach has been suited to do that.

First, the FE model of the structure was developed and validated by comparing modal parameters such as natural frequencies and mode shapes evaluated numerically and experimentally. For the experimental results, Operational Modal Analysis (OMA) algorithm has been applied to the acquired signals. The MAC index was evaluated too.

Once the FE model had been validated, the electromechanical system composed of the structure and the piezoelectric actuators was analysed. The most suitable piezoelectric actuators between those available from the main producers and the best placements of them had to be estimated. To do that, the MEMCFs were evaluated in undamaged and damaged conditions of the structure. The best placements and actuators are those that ensure the greatest values of MEMCFs and of their variation between different healthy states.

The best solution provides the implementation of the P840.60P actuator produced by Physical Instruments, placed on an additional rod next to the first vertical rod or connecting the first diagonal rod and the second vertical rod of the structure. Experimental tests have to be performed to validate the numerical results.

8. Experimental tests

8.1. Dynamic analysis of the rods

FE numerical results should be validated through experimental tests. As already described in 3.6 the FEM was validated by comparing the eigenfrequencies and mode shapes evaluated by studying the global behaviour of the structure. Since the PZT actuator placement could be either next to the first vertical rod or between the diagonal and vertical rod, these rods' local dynamic behaviour should be evaluated.

The experimental test setup is described referring to Figure 50. A PCB tri-axial accelerometer Model 356B21 (Figure 50a) has been mounted on the rod to analyse, while a dynamic hammer was used to excite the structure. Different impact tests were performed, hitting the chord or the rod.

As depicted in Figure 50b, where the excitation's directions are represented by green arrows the dynamic behaviour of the first diagonal rod was analysed either by exciting the chord along the direction of vertical development of the structure or the rod directly along the direction orthogonal to the rod's axis (z-axis). These FRFs are reported in Figure 51 and Figure 52, respectively.

For the study of the dynamic behaviour of the first and second vertical rods, the excitation was given directly to the chord along the direction of vertical development of the structure or along the direction orthogonal to the rod's axis (z-axis). The FRFs of vertical rod 1 are reported as examples in Figure 52 and Figure 53, respectively

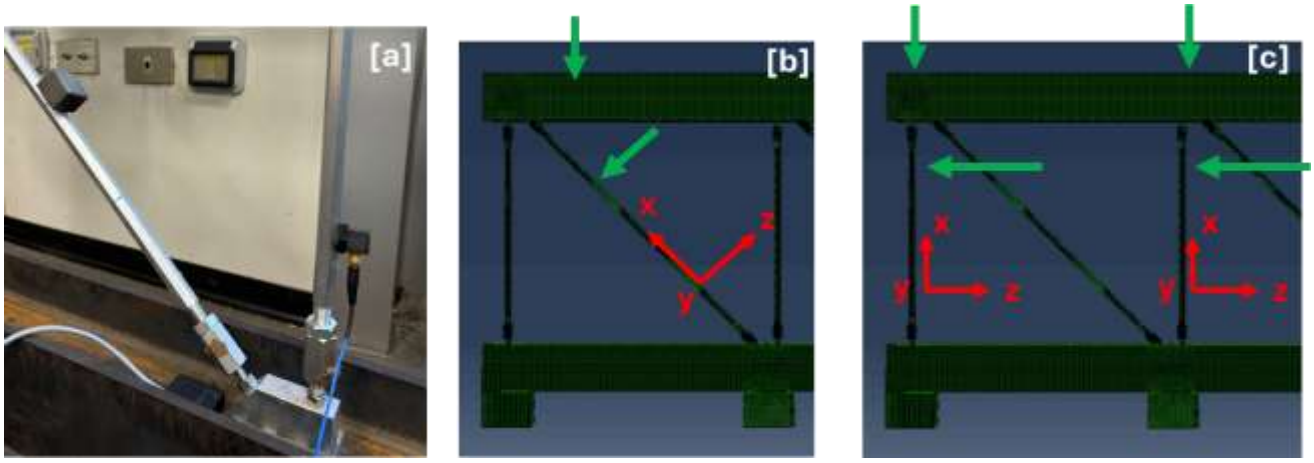

Figure 50:a) Experimental test setup, excitation and measurement directions for testing the first diagonal rod (b) and vertical rod (c)

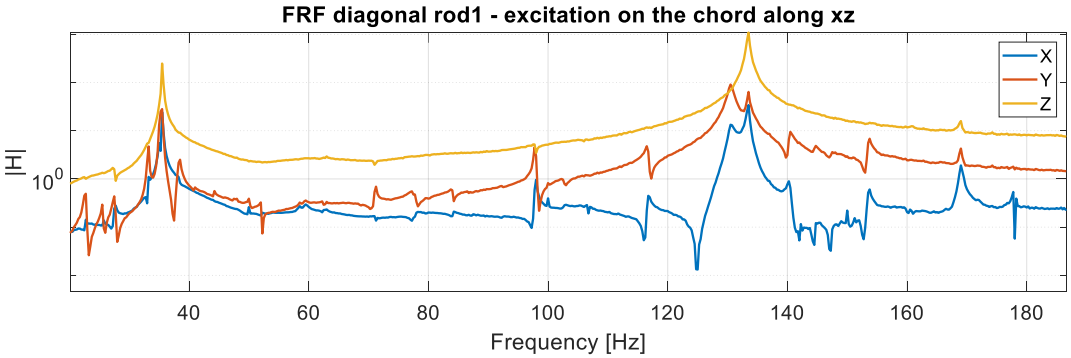

Figure 51:FRFs of the first diagonal rod exciting the chord

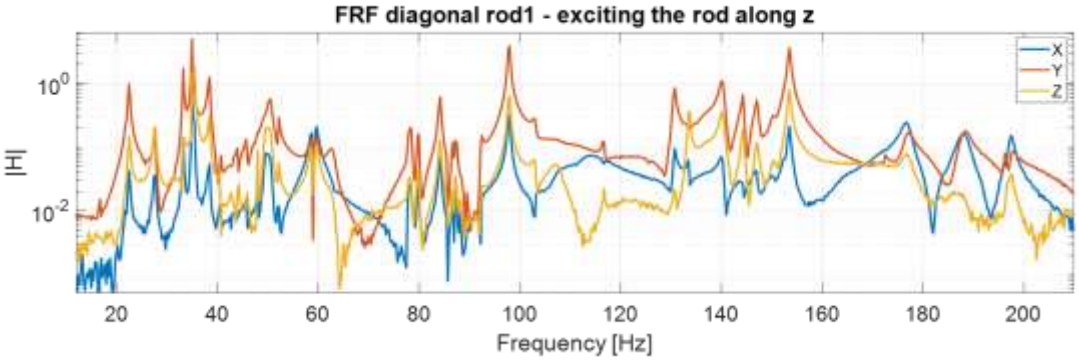

Figure 52: FRFs of the first diagonal rod exciting directly the rod

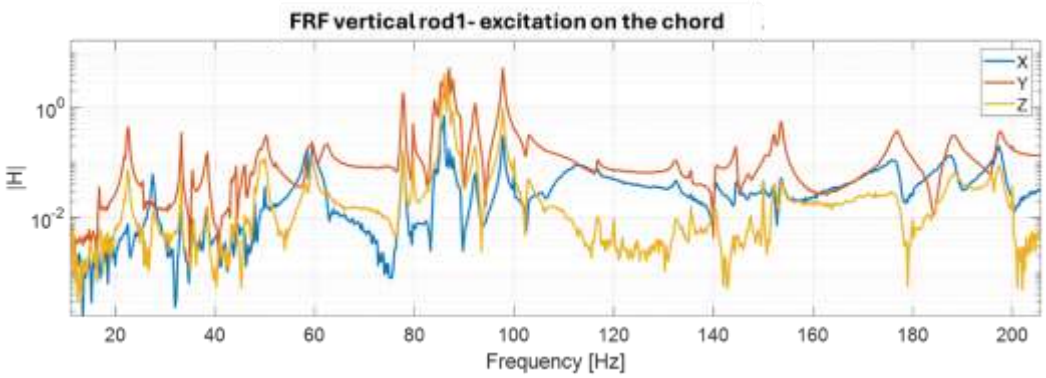

Figure 53:FRFs of the first vertical rod exciting the chord

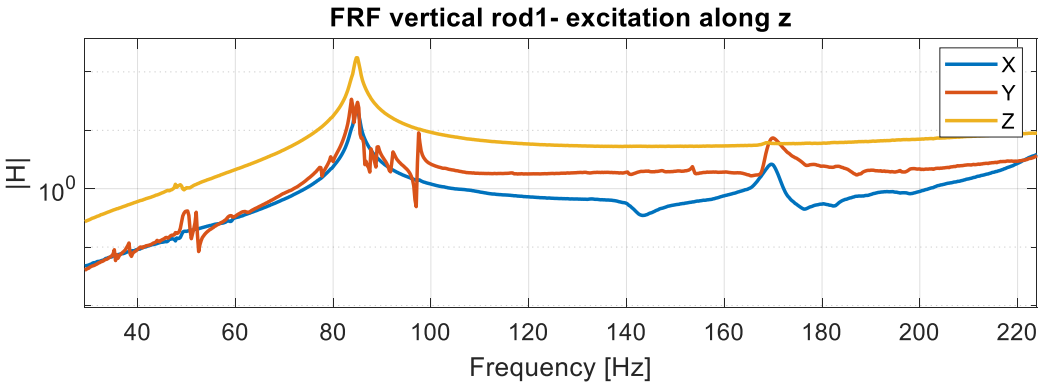

Figure 54: FRFs of the first vertical rod exciting directly the rod

As can be observed, when the excitation is given directly to the rod the FRFs show only two peaks, while when the excitation is given to the chord the number of peaks is greater. Thus, by hitting the rod, only its two eigenmodes can be estimated, while by hitting the chord, some global modes can also be analysed. The reason for this difference can be attributed to the connection rod-chord, which does not allow the energy given to the rod to excite the entire structure.

The next step was to compare the resonance estimated experimentally with those from the FE model of the electromechanical system PZT-structure. Specifically, the focus was to correlate the resonances which resulted in the greatest electromechanical coupling factors and in the greatest Δks. The two systems to be compared are actually different because of the presence, in the FE model of the piezoelectric transducer. The configuration in which the piezo is mounted between the diagonal and vertical rod modifies more the stiffness of the structure than the other configuration, so, the comparison with the experimental results has been done with that. Nonetheless, a perfect correlation is not expected. Results are reported in Table 16, where the experimental

and numerical frequencies and their respective Δk are compared. There is a good agreement in these results, so the model can be considered validated.

Description	$F_{SC\ FEM}$ [Hz]	F_{EXP} [Hz]	K_{und}	Δk
1st vertical global mode	24.81	27.75	0.02540	0.00550
Rods	39.63	35.5-38.5	0.00710	0.00710
Rods	55.83	50.5-52.25	0.00846	**0.01334**
2nd vertical global mode	58.36	59.75	0.02414	**0.02414**
	63.29	59.75	0.01687	**0.01687**
Rods	55.83	50.5-52.25	0.00846	**0.01030**
Rods	130.52	131-133	0.00000	**0.01236**
	131.83		0.00000	**0.01230**
Flexural modes	137.26		0.01207	**0.01207**
	141.27	140-147	0.00000	**0.01182**
	144.37		0.00000	**0.01182**
	147.08		0.01166	0.00001

Table 16: Comparison between numerical and experimental natural frequencies

Even if the mode at 39.63 Hz does not result in a great Δk, it is reported in Table 16 as the matching mode of the experimental mode at 35.5 Hz. In the following Figure 55 some numerical FE mode shapes are represented to show how they could match the experimental ones.

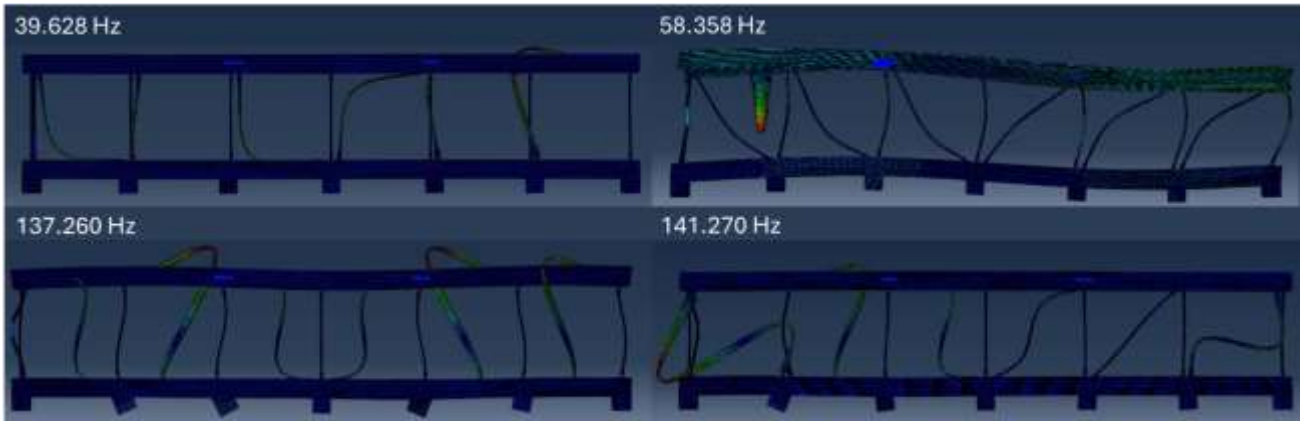

Figure 55: FEM modes representation with the piezo next to the 1st vertical rod

Even if a comparison is not possible, for the completeness of the analysis, also the representation of the FEM modes with the greatest Δk in the configuration in which the piezo is mounted between the diagonal and vertical rod is reported in Figure 56 below.

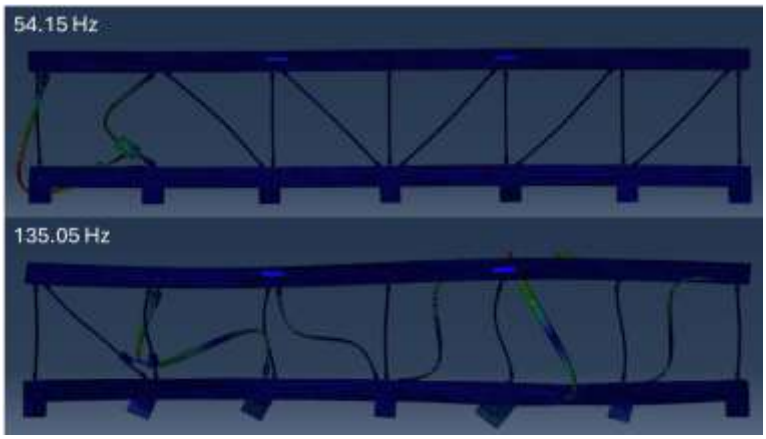

Figure 56:FEM modes representation with the piezo connecting the 1st diagonal rod and the 2nd vertical one

Given these good results, experimental tests were performed on the electromechanical system composed of the structure and the piezo. The mounting solution of the piezo and the tests' setup of the experimental test is described in the following section.

8.2. Mechanical assembly of the piezo support

As already discussed in the previous chapters, two possible mounting configurations of the piezo actuator were evaluated. The first configuration tested is the one in which the piezo is mounted in parallel to the first vertical rod because it was the easiest to implement and in the FE analysis gave better results in terms of coupling factor than the other mounting configuration.

In order to not damage the piezo and ensure its good performance the guidelines from PI [43] were followed. They are briefly summarised in the following points:

- The piezo stack's ends do not have to be both rigidly connected;
- Torques, bending, lateral and pull forces have to be avoided;
- A preload has to be created either externally in the mechanical structure or internally in a case.

The piezo stack chosen for this application is the Preload Piezo Actuator P-840.60. Its scheme and dimensions are reported in Figure 57; no additional preload has to be added. For more information about the stack, refer to its datasheet on [44].

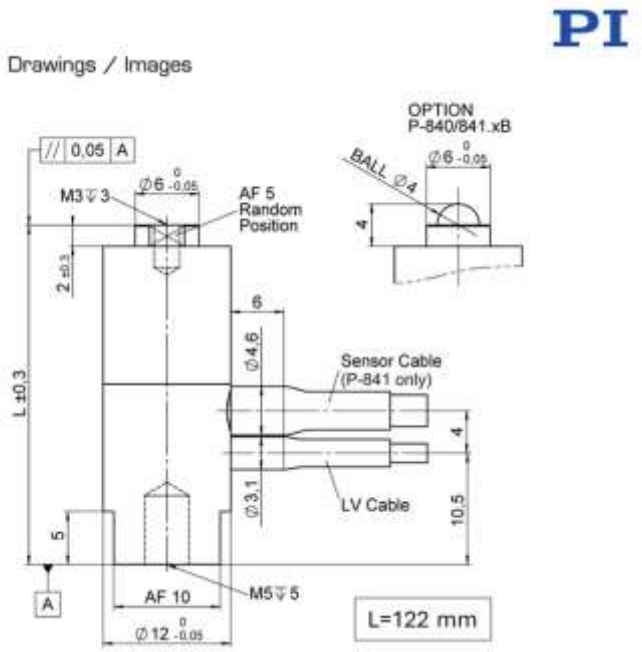

Figure 57:P840-60 piezo actuator drawing

To avoid lateral forces and ensure a connection in which only one end of the actuator is rigidly connected a stinger (typically employed for shaker application) was used. It is directly inserted into the threaded hole in the upper part of the piezo since they both have an M5 thread. The mounting rod of the piezo was designed to allow the regulation of its length and a simple installation of the piezo into the structure.

The rigid connection with the structure is realised with an M5 bolt which connects the piezo with a base glued to the joint element which connects the vertical rod to the lower chord. The piezo support is obtained with a rod with the same section and made from the same material as the vertical rods of the structure, in which a threaded hole was made so that a screw connected to the stinger could slide to obtain the desired length and ensure the correct mounting of the piezo. The stinger was included in a shaker kit.

In Figure 58, the piezo mounted as described.

Figure 58: Piezo stack and its mounting assembly on the structure

8.3. Electrical connection

The Piezo actuator P840.60 is provided with a pre-mounted electrical cable with a LEMO connector. To set it in short circuit condition a LEMO connector ERN.00.250.CTL with two wires is used, connecting the piezo actuator to a breadboard, while this connection is removed to use the piezo-stack in open circuit condition. The piezo actuator is discharged with a resistance of 10 kΩ before each short circuit connection. Since the first tests were done in order to verify the validity and reliability of the FEM analysis no additional electrical circuit was developed.

8.4. Experimental setup

A general description of the experimental setup is now reported.

Despite the focus of this thesis being to develop a damage detection technique using piezoelectric actuators exploiting ambient-type vibrations, the excitation of the structure is provided by an electro-dynamic PCB model 2007E shaker. This solution was mandatory since previous analysis demonstrated that in the laboratory in which the truss structure is placed the ambient excitation is not enough to provide proper vibrations for modal parameter extraction.

The shaker is placed on the truss, specifically on the upper chord in correspondence with the second vertical rod, on the upper second node starting from the left of the structure. The force transmitted is measured with a force transducer ((Brüel & Kjær type 8200 model) placed between the shaker and the structure. A mass of 100 g is placed on the top of the shaker to increase the excitation force. Since the excitation should represent an environmental forcing term, the shaker is driven with the employment of a band-limited white noise input signal up to 200 Hz.

Structure vibrations are measured with 6 low-cost triaxial MEMS accelerometers model TE4030, with a sensitivity of 1000 mV/g, a frequency range of 0-200 Hz and a measured range of ± 2g placed on the chords as depicted in Figure 59; moreover, a triaxial capacitance accelerometer model CA-DR-1001 is placed on the first diagonal rod from the left. All signals are generated and acquired with a National Instruments data acquisition system which consists of:

- 1 voltage output NI9263 module for shaker signal generation;
- 2 voltage input NI9234 modules for acceleration, force and shaker signal measurement.

All modules have been included in an analog-to-digital converter NIcompact-DAQ that can be connected to a PC through a USB cable.

In Figure 59 and Figure 60 respectively, the data acquisition system with accelerometers, shaker and load and the transducers employed in the data acquisition system are presented.

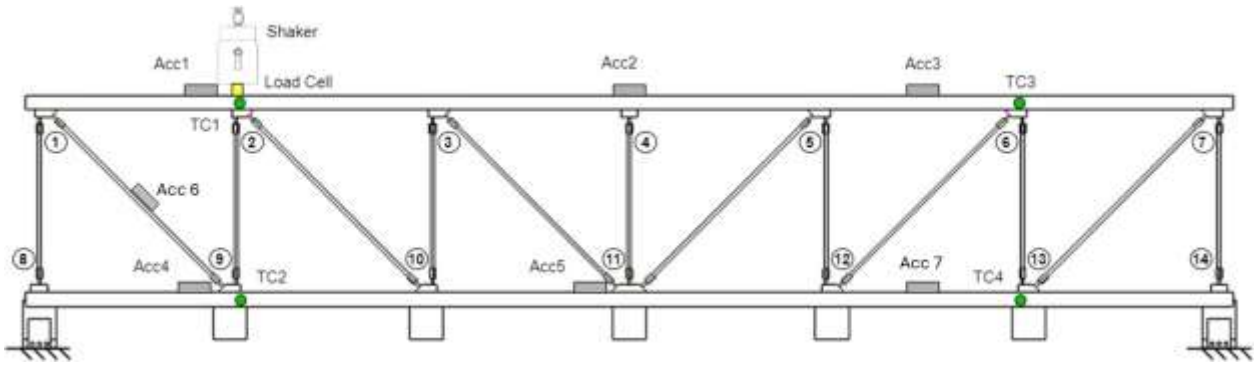

Figure 59: Measurement setup

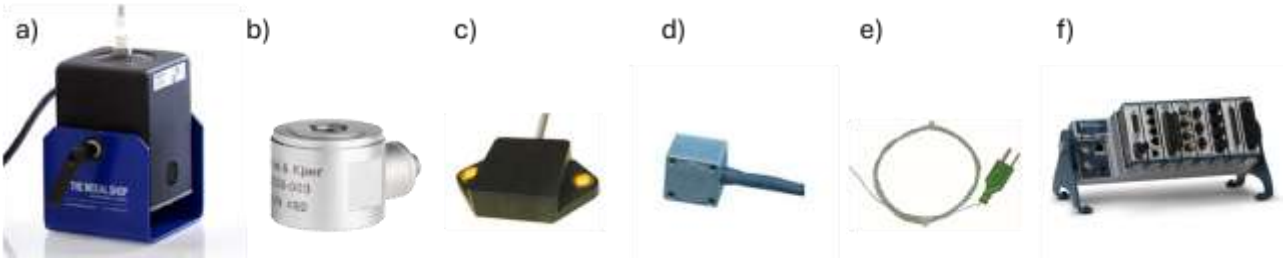

Figure 60: Transducers employed in the measurement system. a) Shaker PCB model 2007E, b)Force transducer Brüel & Kjær type 8200 model, c) Accelerometer TE4030, d) Accelerometer CA-DR-1001, e)Thermocouple type K, f) NiCompact-DAQ with NI 9234, 9219,9263

To evaluate the dynamic behaviour of the electromechanical system composed of the structure and the piezo actuator different tests were performed. Each test lasts 10 minutes: one minute to perform the control strategy and 9 minutes for the dynamic test. The frequency range considered for the first 6 modes of the structure spans from 20 to 200 Hz, so a sampling frequency of 2048 Hz is necessary for the measurements. The aliasing phenomenon is avoided by the module's built-in anti-aliasing filters. Data measured from each test are stored in binary files that can be imported into the Matlab environment, where the automated OMA is performed.

Finally, each configuration test is performed with the piezo actuator in short circuit and open circuit conditions in order to evaluate the MEMCFs.

The extraction of modal parameters has been performed by processing acceleration signals from dynamic tests on the electromechanical system using an operational modal analysis (OMA) method based on a poly-reference least-squares complex exponential method. In the next section, a brief theoretical introduction to this technique (based on Peeters' work [45]) is reported.

8.5. Modal parameters extraction

OMA methods applied in the frequency domain rely on output spectra as primary data; under the assumption that the excitation is a white noise input these spectra can be modelled as FRFs.

The OMA method used in this work to extract modal parameters is the so-called "PolyMAX" or polyreference least-squares complex frequency-domain method (LSCF), based on a weighted least-squares approach and uses multiple-input-multiple-output frequency response functions (FRFs) as primary data, identifying a right matrix-fraction model:

$$[H(\omega)] = [B(\omega)][A(\omega)]^{-1}$$

Eq. 19

where $[H(\omega)] \in \mathbb{C}^{lxm}$ is the FRF matrix containing the FRFs between all m inputs and all l outputs; $[B(\omega)] \in \mathbb{C}^{lxm}$ is the numerator matrix polynomial and $[A(\omega)] \in \mathbb{C}^{mxm}$ is the denominator matrix polynomial. $[B(\omega)]$ and $[A(\omega)]$ are constructed respectively with β_i and α_i coefficients which can be obtained by minimizing a set of equations to reduce the error between the modal model and experimental measurements as described in [RIF poly]. These coefficients provide the necessary information to construct the stability diagram. Theoretically, a complete right matrix-fraction model could be obtained by computing the numerator coefficient β_i otherwise an approach similar to the least-squares complex exponential (LSCE) method can be implemented [46].

First of all, a stabilisation diagram is obtained with modal parameters such as frequency, damping and participation factors. In order to have a high accuracy of the modal parameters estimated it is typically recommended to over-specify the model order considerably, so to try to fit high-order models that contain much more modes than those which really exist. True physical modes are separated from the spurious numerical ones by interpreting a so-called stabilisation diagram [47]. The poles associated with a specific model order are compared to those of the model with one lower order. If the differences between them fall within predefined limits, the pole is considered stable. Spurious numerical poles, which do not stabilize at all during this process, can be easily excluded from the modal parameter data set. The stabilisation diagram effectively addresses a common challenge in system identification: determining the appropriate model order.

The analysis of the stabilisation diagram results in a set of poles and their corresponding participation factors. The mode shapes can subsequently be determined by examining the pole-residue model:

$$[H(\omega)] = \sum_{i=1}^{n} \frac{\{v_i\}\langle l_i{}^T\rangle}{j\omega - \lambda_i} + \frac{\{v_i^*\}\langle l_i{}^H\rangle}{j\omega - \lambda_i^*} - \frac{LR}{\omega^2} + UR$$

Eq. 20

which is the partial fraction description of the Laplace-domain version of RIF eq prima. n is the number of modes, $\lambda_i{}^*$ is the complex conjugate of a matrix; $\{v_i\} \in \mathbb{C}^l$ are the mode shapes; $\langle l_i{}^T\rangle \in \mathbb{C}^m$are the modal participation factors and λ_i are the poles, which are occurring in complex-conjugated pairs and are related to the eigenfrequencies ω_i and damping ratios ζ_i as follows:

$$\lambda_i, \lambda_i^* = -\zeta_i\omega_i \pm j\sqrt{1-\zeta_i^2}\omega_i$$

Eq. 21

$LR, UR \in \mathbb{R}^m$ are respectively the lower and upper residuals modelling the influence of the out-of-band modes in the considered frequency band. The participation factors $\langle l_i{}^T\rangle$ and the poles λ_i are estimated based on the α polynomial and the stabilisation diagram. The only unknowns in Eq. 20 are the mode shapes $\{v_i\}$ and the lower and upper residuals. Mode shapes can be estimated in a second least-squares step commonly called least-squares frequency-domain (LSFD) method [46], [48],based on the stable poles selected by the user.

In Figure 61 a zoom of the stabilization diagram for an experimental test is shown, highlighting two columns of stable poles representing two physical modes of the truss girder. Adding to this plot of the FRF from accelerometer 1, it can be observed that stable poles are distributed in columns above the resonances of the truss girder. Since most of the modes with non-zero coupling factors are not global modes of the structure, but rather modes specific to the diagonal rods, the PolyMAX algorithm has been applied multiple times over narrow frequency ranges to improve the accuracy of mode identification.

The modal parameters of interest are in this case the eigenfrequencies, evaluated with the piezo in short and open circuit conditions, to evaluate the coupling factor at each mode of interest.

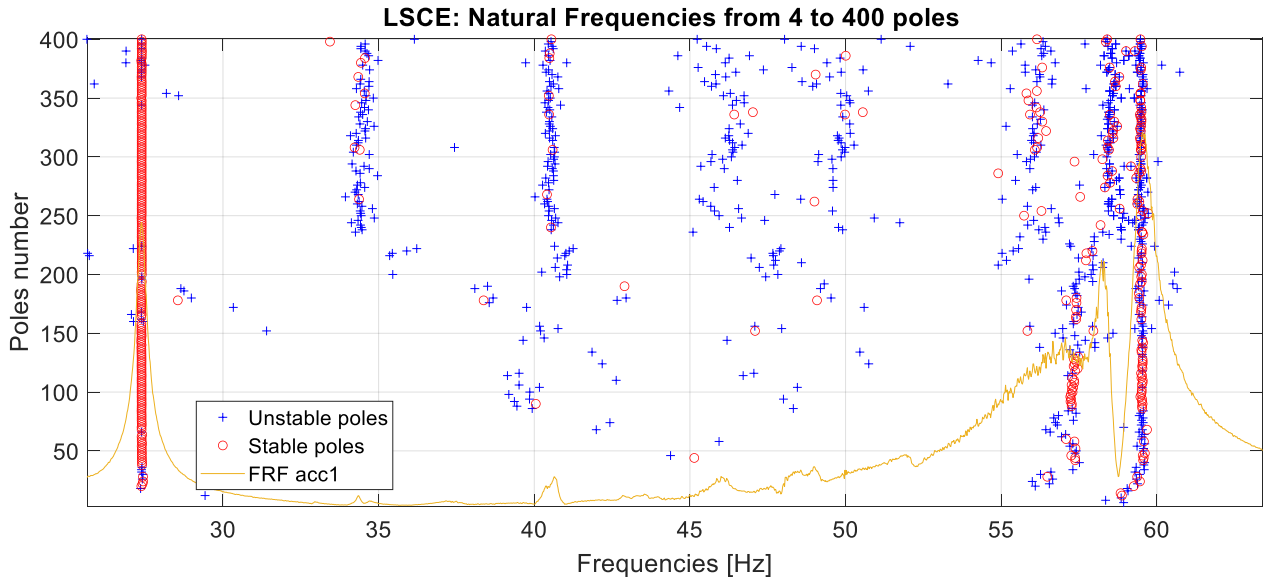

Figure 61:Stability diagram example

9. Experimental tests

In this section, experimental tests and results obtained with the piezo actuator installed on the truss structure will be reported. As already said in the previous chapter the configuration tested is the one with the piezo actuator mounted next to the first vertical rod. Dynamic tests are performed in different damaged configurations of the structure, and each test has been performed in short and open circuit conditions of the piezo, to evaluate the coupling coefficients and their variation from undamaged to damaged status. The tests carried out are briefly reported as follows:

- Undamaged configuration: test 101 and test 102, short circuit and open circuit;
- Damaged configuration: addition of commercial masses of 5 and 10 kg weight.

The structure has an overall mass of 300 kg, so the mass variation has been 3.2% for the 10 kg mass and 1.6% for the 5 kg mass. The masses have been placed in two different spots of the truss girder structure (nodes 3 and 6) as depicted in Figure 62:

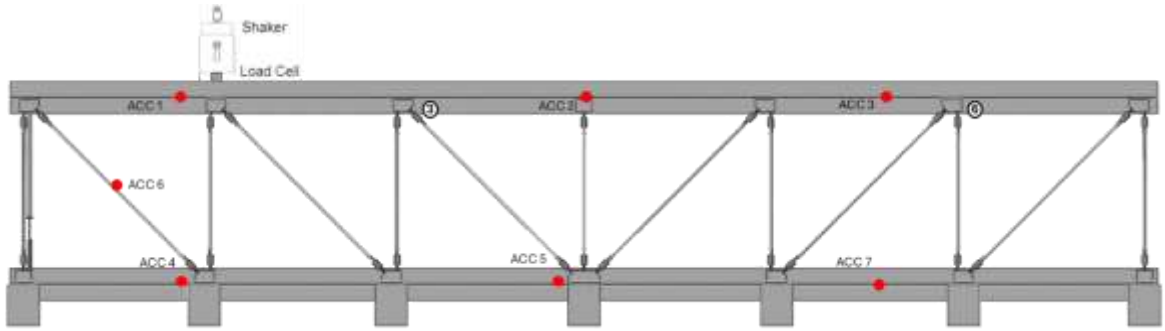

Figure 62: Schematic representation of the structure with damages locations

Two considerations need to be made. First, the choice to introduce this kind of damage despite the FEM simulations considered damages such as cracks due to corrosion or a rod's break. This occurred because this kind of damage is easy to implement and does not change irremediably the structure unlike the damages simulated. Moreover, damages have been introduced in different spots of the structure to test if the distance from the measurement point could affect the resulting MEMCFs and Δks.

For both undamaged/damaged and short/open conditions the excitation bandwidth is set to be 20-200 Hz, the sampling frequency is 2048 Hz and the histories are acquired for 10 minutes. FRFs were evaluated by dividing signals into sub-histories of 50 s with an overlap of 60% in order to provide clear peaks that are easier to identify. FRFs were evaluated through the estimator H1.

Signals were acquired from all the accelerometers reported in Figure 59 but only signals from accelerometers n.1 and n.6 were used to estimate FRFs and for the identifications of modes through the PolyMAX algorithm. These accelerometers were chosen over the others because they are the closest to the piezo actuator and could better identify the modes that, according to the FE model, would have brought higher values of k and Δk.

Results are reported and discussed in the following sections.

9.1. Undamaged configurations

The reference status of the study is the undamaged condition of the structure, so these tests were the first carried out. Two tests were performed, in SC and OC conditions, to verify their repeatability. They are identified in the following section as test 101 and test 102. FRFs evaluated in the frequency band of interest 20-200 Hz are reported in Figure 63 and Figure 64 for accelerometer 1 and accelerometer 6 respectively.

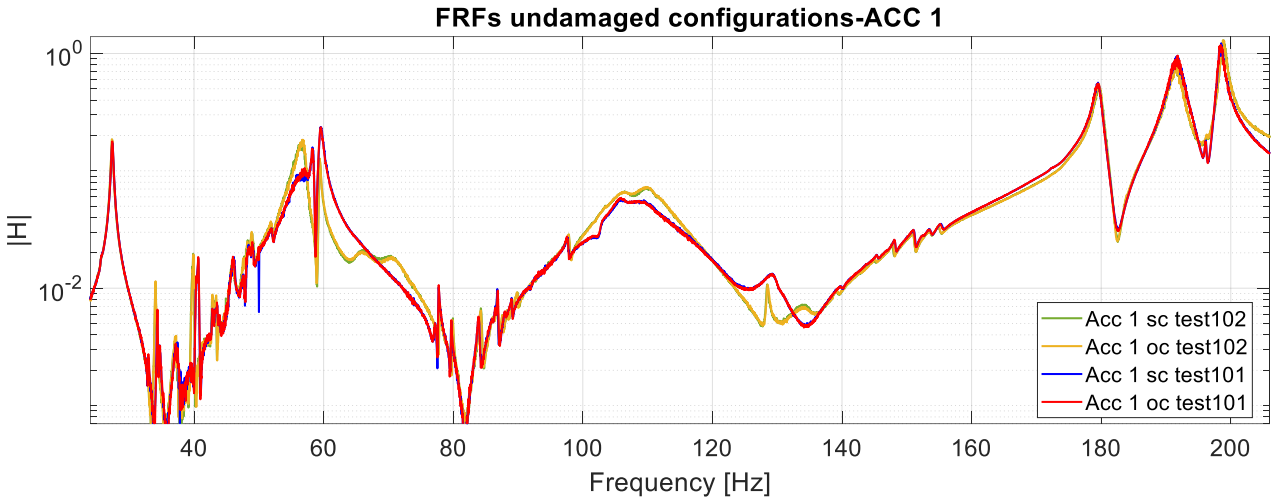

Figure 63:FRFs from signals of accelerometer 1

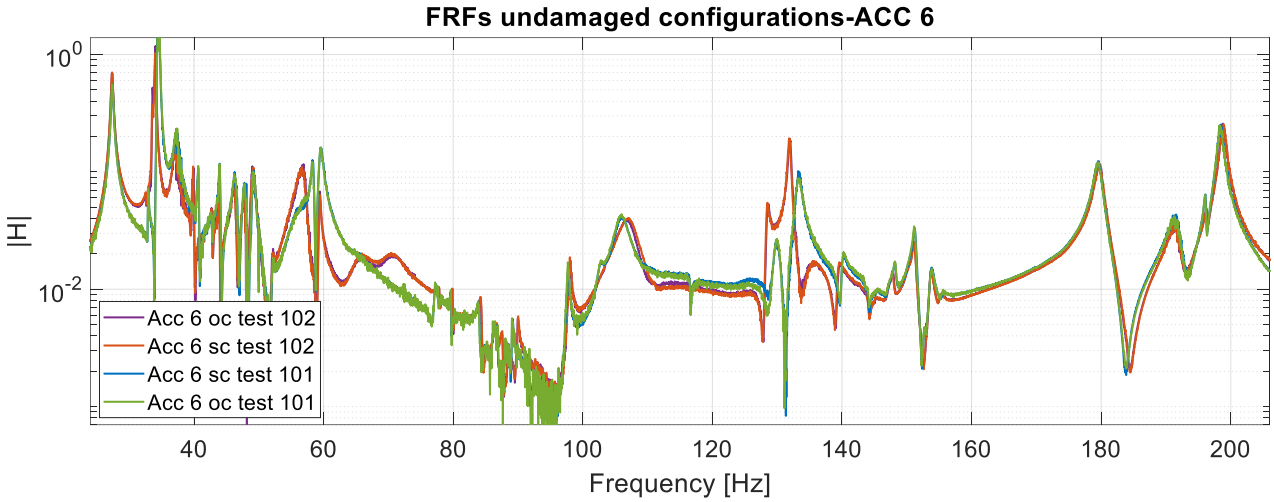

Figure 64:FRFs from signals of accelerometer 6

Natural frequencies and coupling factors evaluated with Eq. 12 are reported in Table 17 and represented in Figure 65. The differences between the coupling factors evaluated in each test was also estimated numerically.

Undamaged test 101			Undamaged test 102			
SC [Hz]	OC [Hz]	K	SC [Hz]	OC [Hz]	K	ΔK
27.4	27.4	0	27.34	27.34	0	0
34.33	34.36	0.041815	34.56	34.58	0.034026	0.00779
34.67	34.7	0.04161	34.03	34.05	0.03429	0.00732
40.65	40.68	0.038426	39.9	39.93	0.038786	0.00036
43.98	43.99	0.021326	43.84	43.88	0.042728	0.021401
58.43	58.36	0.048935	56.9	56.94	0.037503	0.011432
59.52	59.5	0.025922	59.4	59.39	0.018349	0.007573
77.73	77.75	0.022686	77.89	77.91	0.022663	2.33E-05
79.66	79.73	0.041931	79.92	79.94	0.022373	0.019558
83.98	83.97	0.015432	84.33	84.29	0.030797	0.015365
151.28	151.22	0.028162	151.17	151.18	0.011502	0.016659
153.73	153.73	0	153.73	153.73	0	0

Table 17:Experimental frequencies, coupling factors and variations

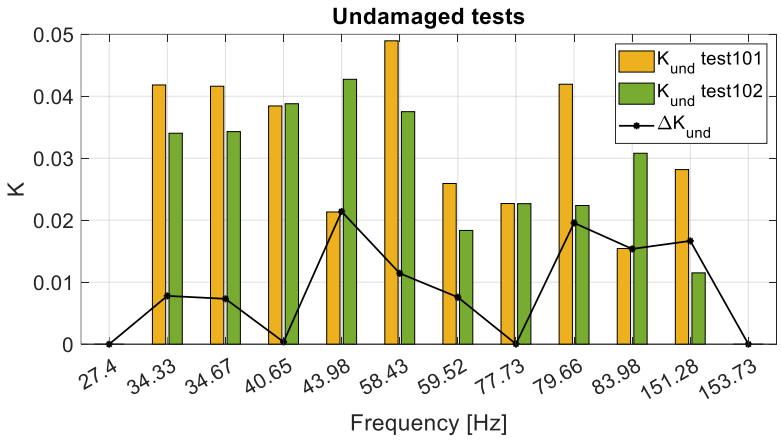

Figure 65: Undamaged tests coupling factors and variation comparison

First of all, it can be noticed that there is a frequency shift between the two tests, even if no damages occurred. This can be probably attributed to the different temperatures of the laboratory when the two tests were performed. In any case, this does not represent a problem since for the evaluation of k it is necessary to evaluate the variation in frequency between short and open circuit conditions.

Once the undamaged condition of the structure has been analysed, the damaged one can be studied. Since there is no remarkable difference between the two tests, results from test 101 will be used as a reference for the unmanaged tests.

9.2. Damaged configuration: 10 kg mass in node 3

The first damaged condition studied is the one in which a 10 kg mass is added to the structure in correspondence with node 3, as showed in Figure 66. Resulting FRFs from accelerometer 1 are reported in Figure 67.

Figure 66:10 kg mass addition on node 3 of the truss

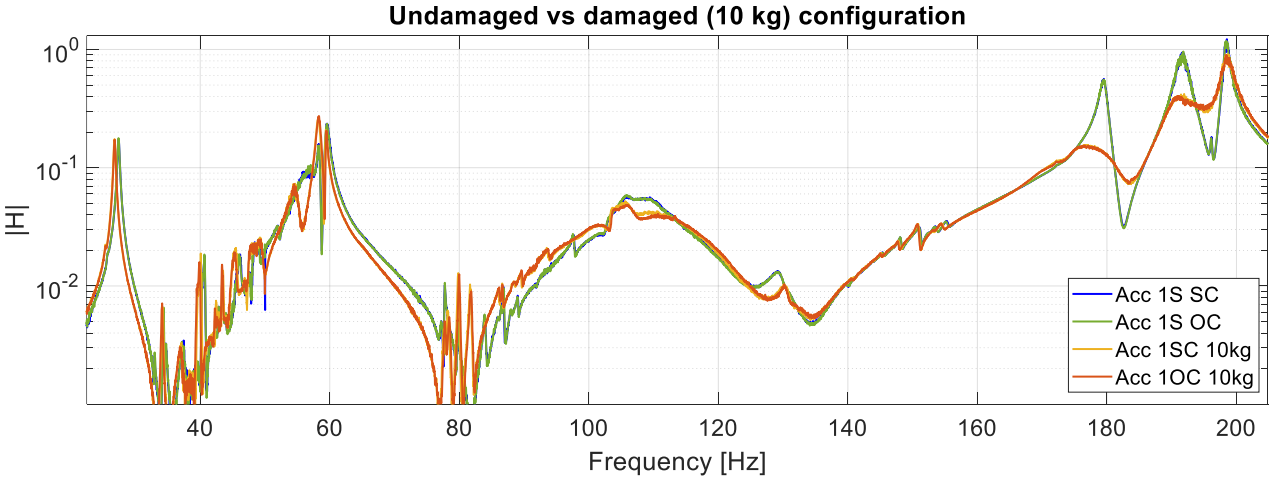

Figure 67: FRFs of data from acc.1 evaluated in the undamaged and damaged configurations (10 kg)

Coupling factors were evaluated and compared with those evaluated, at the same modes, in the undamaged configuration in order to evaluate their variation Δk. Since no evident frequency shift can be seen looking at the frequency range 20-200 Hz, the mode at about 40 Hz is reported in Figure 68 as an example of the different dynamic behaviour of the structure when the piezo actuator is in SC-OC condition and also of the response between the undamaged and damaged condition of the structure.

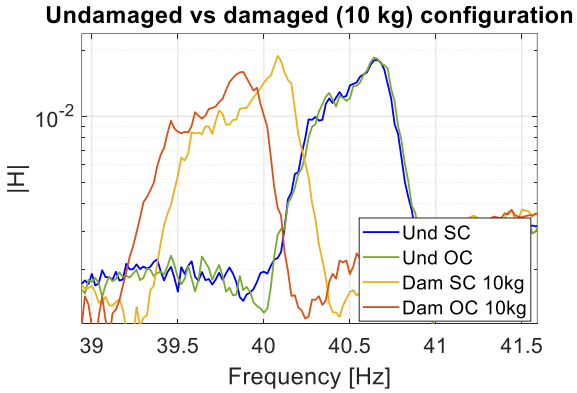

Figure 68: Zoom of the mode at about 40 Hz estimated in the undamaged and damaged configuration, with the piezo in SC and OC

All these results are reported in Table 18 and depicted in Figure 69.

Undamaged			Damaged 10 kg A3			Δk und-dam 10 kg
SC [Hz]	OC [Hz]	K	SC [Hz]	OC [Hz]	K	ΔK
27.4	27.4	0.00000	26.75	26.78	0.04737	0.04737
34.33	34.36	0.04182	33.96	33.72	0.11868	0.07686
34.67	34.7	0.04161	34.22	34.09	0.08708	0.04547
40.65	40.68	0.03843	40.12	39.91	0.10218	0.06376
43.98	43.99	0.02133	43.48	43.49	0.02145	0.00012
58.43	58.36	0.04893	58.24	58.31	0.04904	0.00011
59.52	59.5	0.02592	59.35	59.44	0.05509	0.02917
77.73	77.75	0.02269	78.24	78.44	0.07155	0.04886
79.66	79.73	0.04193	79.83	79.99	0.06334	0.02141
83.98	83.97	0.01543	81.72	81.84	0.05421	0.03878
151.28	151.22	0.02816	151	150.94	0.02819	0.00003
153.73	153.73	0.00000	153.19	153.34	0.04426	0.04426

Table 18: Resulting coupling factors and variations undamaged vs damaged 10 kg mass addition

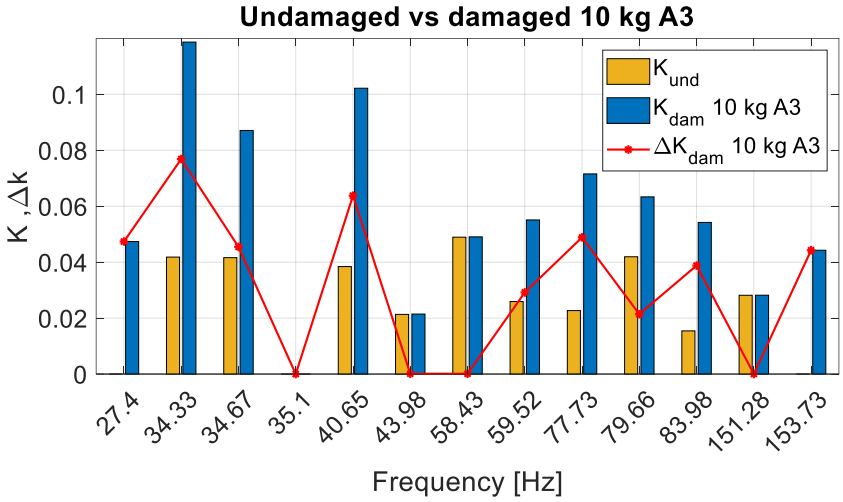

Figure 69: Undamaged vs 10 kg damaged coupling factors and variation comparison

It can be noticed that the coupling factors generally increase from undamaged to damaged conditions, according to the FEM analysis. Although the damages are different, and for this reason, it is not correct to compare the methods accurately, a comparison between experimental and numerical results is made. FEM results obtained with the structure in the damaged condition with the broken vertical rod are compared with those obtained experimentally with 10 kg mass addition since they both represent the most serious injured configurations.

Comparing the results reported in Appendix 11.3 with those in Table 18, the results obtained experimentally are generally better than those obtained through FE analysis. Even if the FE analysis showed a higher number of modes with a non-zero coupling factor, the coupling coefficients and their variation from undamaged to damaged cases are higher in the experimental case. The resulting k and Δk evaluated at the first vertical global mode at 27 Hz are reported as an example in Table 19 below.

	Undamaged		Damaged		Undamaged	Damaged	Δ und-dam
	SC [Hz]	OC [Hz]	SC [Hz]	OC [Hz]	K	K	ΔK
FEM	24.81	24.81	23.04	23.05	0	0.02947	0.02947
POLYMAX	27.40	27.40	26.75	26.78	0	0.04737	0.04737

Table 19: Numerical and experimental coupling factors evaluated at 1st vertical global mode

9.3. Damaged configuration: 5 kg mass in node 3

The second damaged condition studied is the one in which a 5 kg mass is added to the structure in correspondence with node 3 (see Figure 62), as in the case of the 10 kg mass. As in the previous case resulting FRFs from acc.1 are reported in Figure 70 for both undamaged and damaged configurations.

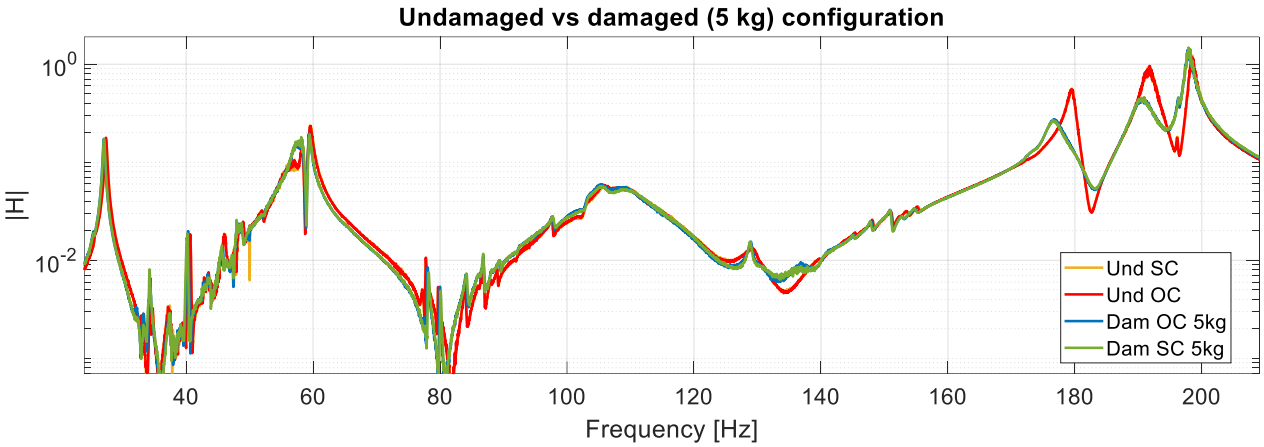

Figure 70: FRFs of data from acc.1 evaluated in the undamaged and damaged configurations (5 kg)

Coupling factors were evaluated and compared with those evaluated, at the same modes, in the undamaged configuration to assess their variation Δk. All these results are reported in Table 20 and depicted in Figure 71.

Undamaged			Damaged 5 kg A3			Δ und-dam 5 kg
SC [Hz]	OC [Hz]	K	SC [Hz]	OC [Hz]	K	ΔK
27.4	27.4	0.00000	27.08	27.07	0.02717	0.02717
34.33	34.36	0.04182	33.96	33.72	0.11868	0.07686
34.67	34.7	0.04161	34.26	34.35	0.07253	0.03092
40.65	40.68	0.03843	40.24	40.32	0.06309	0.02466
43.98	43.99	0.02133	43.48	43.49	0.02145	0.00012
58.43	58.36	0.04893	58.24	58.31	0.04904	0.00011
59.52	59.5	0.02592	59.35	59.44	0.05509	0.02917
77.73	77.75	0.02269	78.16	78.22	0.03919	0.01650
79.66	79.73	0.04193	80.12	80.01	0.05238	0.01045
83.98	83.97	0.01543	84.23	84.14	0.04622	0.03078
151.28	151.22	0.02816	151	150.94	0.02819	0.00003
153.73	153.73	0.00000	152.68	152.72	0.02289	0.02289

Table 20: Resulting coupling factors and variations undamaged vs damaged 5 kg mass addition

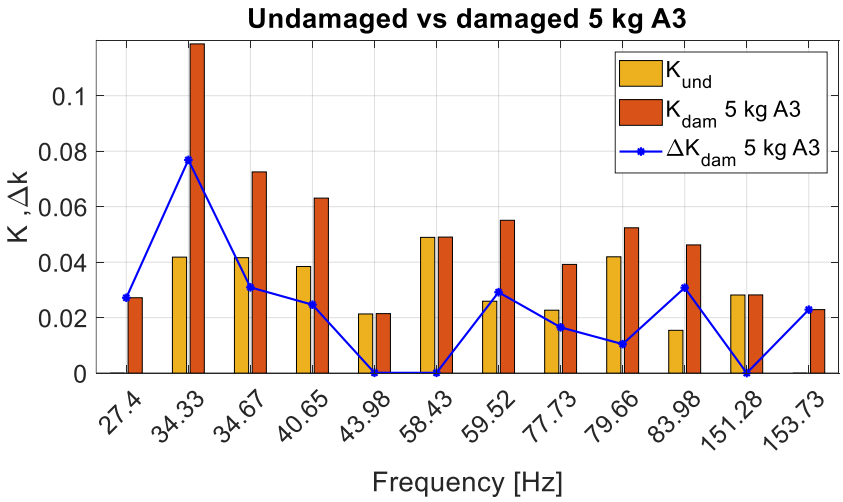

Figure 71: Undamaged vs 5kg damaged coupling factors and variation comparison

As in the case of the 10 kg mass, there is an increment in the coupling factors from undamaged to damaged condition.

Moreover, it is possible to compare the resulting k and Δk between the two damaged configurations to estimate if the different damage entity affects these factors. This comparison is reported in Figure 72, where it is possible to see that generally, the highest coupling factors and variation result in the case where more serious damage is applied (i.e. 10 kg). Numerical results represented in Figure 72 are also reported in Table 21.

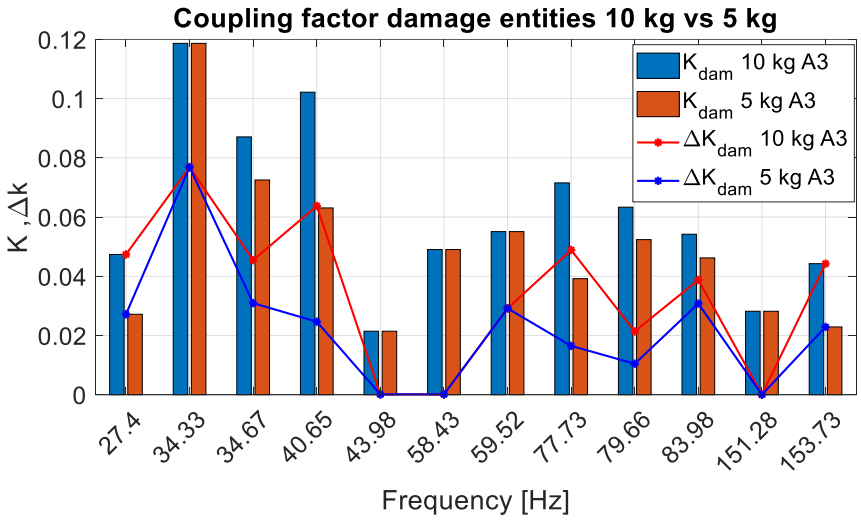

Figure 72: 10 kg vs 5kg damaged coupling factors and variation comparison

Damaged 10 kg A3			Damaged 5 kg A3			Δ und-dam 10 kg	Δ und-dam 5 kg
SC [Hz]	OC [Hz]	K	SC [Hz]	OC [Hz]	K	ΔK	ΔK
26.75	26.78	0.04737	27.08	27.07	0.02717	0.04737	0.02717
33.96	33.72	0.11868	33.96	33.72	0.11868	0.07686	0.07686
34.22	34.09	0.08708	34.26	34.35	0.07253	0.04547	0.03092
40.12	39.91	0.10218	40.24	40.32	0.06309	0.06376	0.02466
43.48	43.49	0.02145	43.48	43.49	0.02145	0.00012	0.00012
58.24	58.31	0.04904	58.24	58.31	0.04904	0.00011	0.00011
59.35	59.44	0.05509	59.35	59.44	0.05509	0.02917	0.02917
78.24	78.44	0.07155	78.16	78.22	0.03919	0.04886	0.01650
79.83	79.99	0.06334	80.12	80.01	0.05238	0.02141	0.01045
81.72	81.84	0.05421	84.23	84.14	0.04622	0.03878	0.03078
151	150.94	0.02819	151	150.94	0.02819	0.00003	0.00003
153.19	153.34	0.04426	152.68	152.72	0.02289	0.04426	0.02289

Table 21: Resulting coupling factors and variations 10 kg vs 5 kg damage comparison

9.4. Damaged configuration: 10 kg mass in node 6

The third damaged condition studied is the one in which a 10 kg mass is added to the structure in correspondence with node 6 indicated in Figure 62. The resulting FRFs of signals from acc.1 are reported in Figure 73, for both undamaged and damaged configurations.

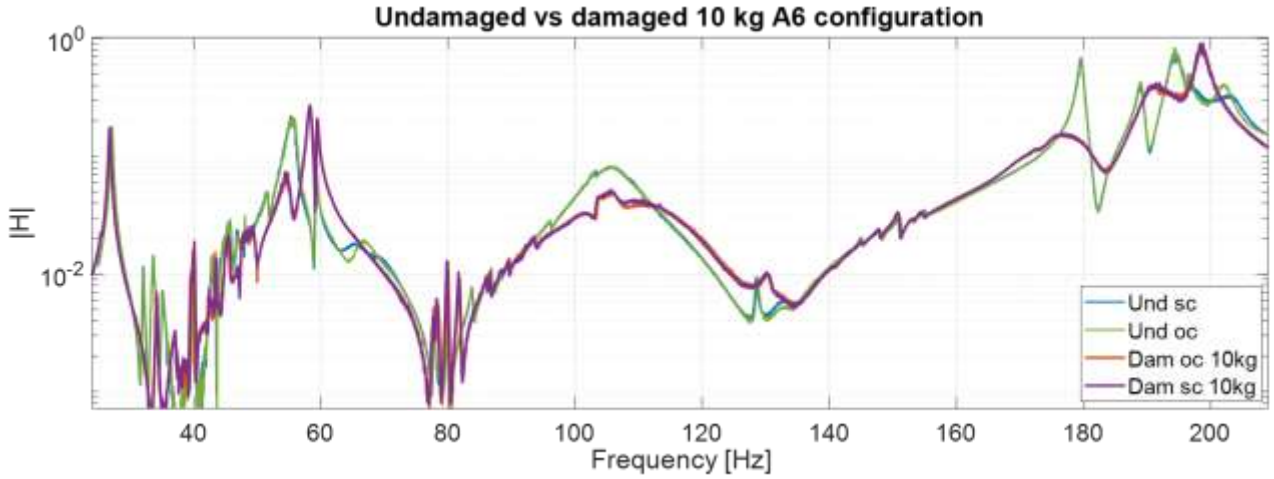

Figure 73: FRFs of data from acc.1 evaluated in the undamaged and damaged configurations (10 kg positioned at node 6)

Coupling factors were evaluated and compared with those evaluated, at the same modes, in the undamaged configuration in order to evaluate their variation Δk. All these results are reported in Table 22 and depicted in Figure 74.

Undamaged			Damaged 10 kg A6			Δ und-dam 10 kg A6
SC [Hz]	OC [Hz]	K	SC [Hz]	OC [Hz]	K	ΔK
27.4	27.4	0.00000	27.1	27.1	0.00000	0.00000
34.33	34.36	0.04182	32.03	32.12	0.07502	0.03320
34.67	34.7	0.04161	33.63	33.59	0.04876	0.00715
			35.1	35.12	0.03376	0.03376
40.65	40.68	0.03843	40.03	40.17	0.08371	0.04528
43.98	43.99	0.02133	42.83	42.83	0.00000	0.02133
58.43	58.36	0.04893				0.04893
59.52	59.5	0.02592	59.26	59.13	0.06620	0.04028
77.73	77.75	0.02269	77.75	77.7	0.03586	0.01317
79.66	79.73	0.04193	79.85	79.79	0.03876	0.00317
83.98	83.97	0.01543	83.78	83.78	0.00000	0.01543
151.28	151.22	0.02816	151.08	151.08	0.00000	0.02816
153.73	153.73	0.00000	153.16	153.3	0.04277	0.04277

Table 22: Resulting coupling factors and variations undamaged vs damaged 10 kg mass addition at node 6

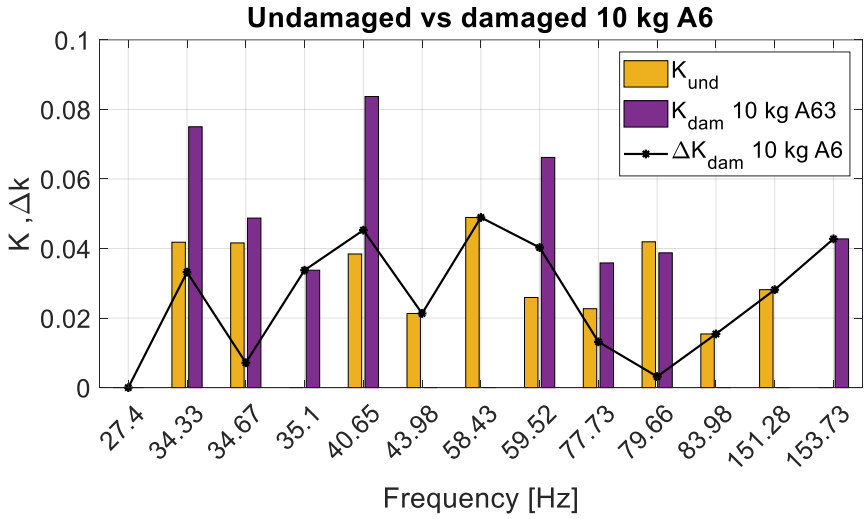

Figure 74: Undamaged vs 10 kg at node 6 damaged coupling factors and variation comparison

As in the previous cases, the coupling factors increase from undamaged to damaged, although this increment is lower than in the earlier cases. This can be observed in Figure 75where the resulting k and Δk from damaged configurations with the same mass addition (10 kg) but at different placements are compared. These factors are generally higher when the distance from the piezo is shorter. Numerical results are also reported in Table 23.

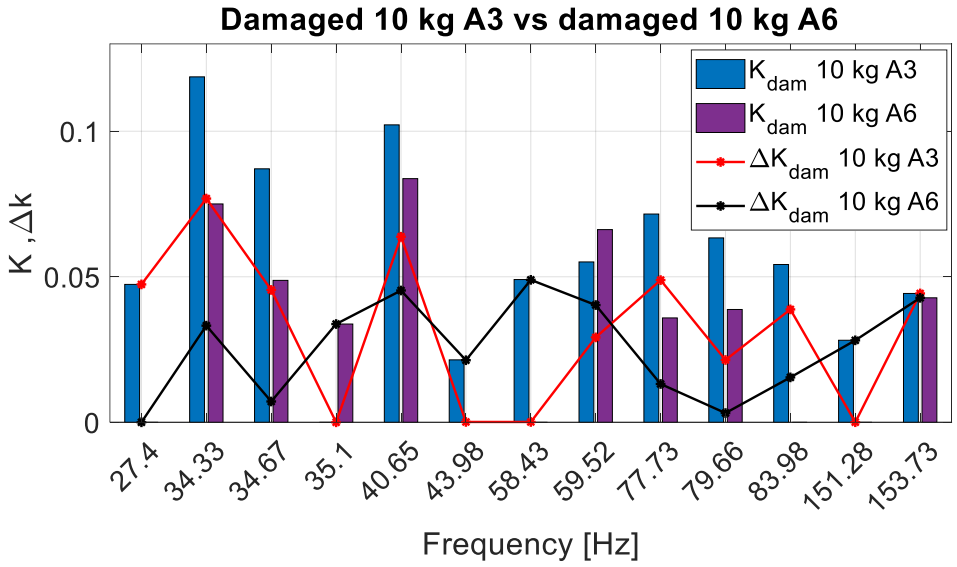

Figure 75: 10 kg at A3 vs 10 kg at A6 damaged coupling factors and variation comparison

Damaged 10 kg A3			Damaged 10 kg A6			Δ und-dam 10 kg	Δ und-dam 10 kg A6
SC [Hz]	OC [Hz]	K	SC [Hz]	OC [Hz]	K	ΔK	ΔK
26.75	26.78	0.04737	27.1	27.1	0.00000	0.04737	0.00000
33.96	33.72	0.11868	32.03	32.12	0.07502	0.07686	0.03320
34.22	34.09	0.08708	33.63	33.59	0.04876	0.04547	0.00715
			35.1	35.12	0.03376	0.00000	0.03376
40.12	39.91	0.10218	40.03	40.17	0.08371	0.06376	0.04528
43.48	43.49	0.02145	42.83	42.83	0.00000	0.00012	0.02133
58.24	58.31	0.04904				0.00011	0.04893
59.35	59.44	0.05509	59.26	59.13	0.06620	0.02917	0.04028

78.24	78.44	0.07155	77.75	77.7	0.03586	0.04886	0.01317
79.83	79.99	0.06334	79.85	79.79	0.03876	0.02141	0.00317
81.72	81.84	0.05421	83.78	83.78	0.00000	0.03878	0.01543
151	150.94	0.02819	151.08	151.08	0.00000	0.00003	0.02816
153.19	153.34	0.04426	153.16	153.3	0.04277	0.04426	0.04277

Table 23: Resulting coupling factors and variations 10 kg at different placements comparison

9.5. Configurations comparison and identification of damage indices

Starting from the results discussed in the previous sections, it is possible to make some assessments of the coupling factors obtained and estimate useful damage indices. All the coupling factors k evaluated in the different health status of the structure are reported in Figure 76, where also the variations between the undamaged and the various damaged configurations are plotted.

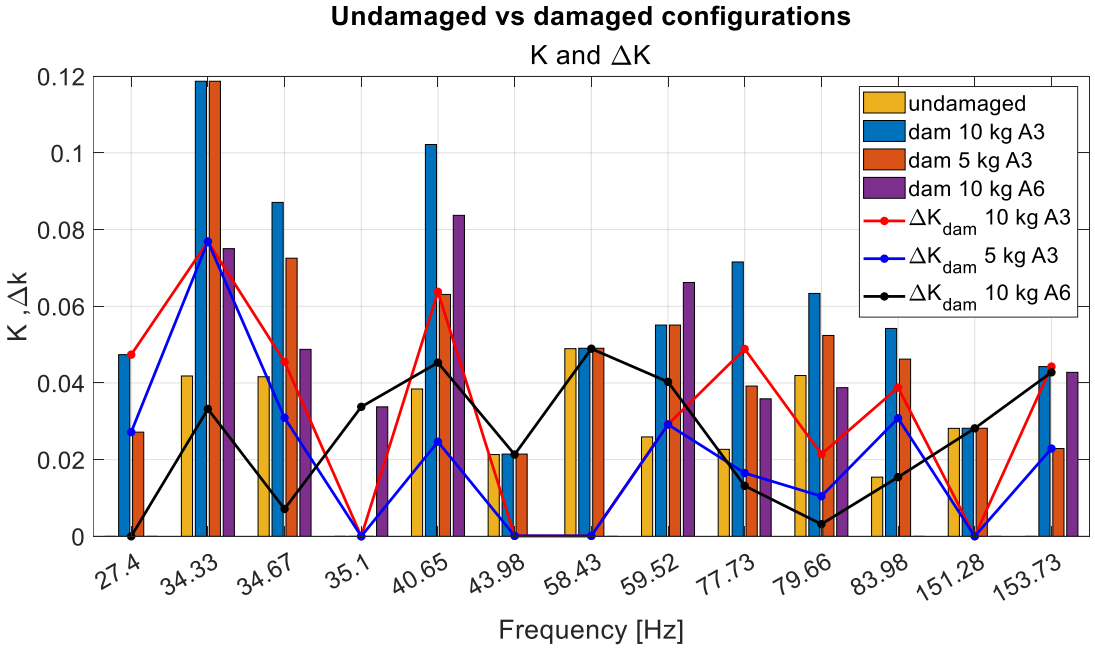

Figure 76: Undamaged vs damaged configurations coupling factors and variation comparison resume

It can be observed that there is a trend for the coupling factors to increase as the severity of the damage increases. The undamaged configuration results in the lowest coupling factors, while the configuration with the 10 kg mass near the piezo results in the highest.

These results show that the index Δk can be a good parameter to track any change in the MEMCFs due to the presence of structural alteration. Despite this, in some cases K values can be very small, that is short- and open-circuit eigenfrequencies close to each other and thus a possible high uncertainty associated with the identification of the modes.

Berardengo et al. proposed in [39] the use of a different index which incorporates information from all modes, while assigning lower weight to the less reliable ones:

$$s = \sum_{i=1}^{N} \left| |k_{dam,i}| - |k_{und,i}| \right| = \sum_{i=1}^{N} |\Delta k|$$

Eq. 22

where i=1,_N is the desired number of modes.

The higher the number of modes considered the higher increased statistical reliability.

These indices are reported in Table 24.

Total coupling factors and variations for the configurations experimentally tested				
Coupling factor K				
K Undamaged test 101	K Undamaged test 102	K Damaged 10 kg A3	K Damaged 5 kg A3	K Damaged 10 kg A6
0.32624	0.29302	0.74246	0.59592	0.42483
Variation of coupling factors Δk				
	Δk und 101-und 102	Δk und-dam 10 kg A3	Δk und-dam 5 kg A3	Δk und-dam 10 kg A6
	0.10748	0.41621	0.26968	0.33264

Table 24: Total coupling factors and variation

The undamaged test101 was used as the undamaged reference for the evaluation of the variation between undamaged and damaged configurations. As expected, the total K evaluated in the healthy status of the structure is the lowest indices, while the total k and k for the 10 kg damage near the piezo are the highest. Moreover, the total variation evaluated between the two undamaged configurations is lower (one order of magnitude smaller) than the total variations evaluated between undamaged and damaged conditions, making these indices reliable.

10. Conclusions

10.1. General conclusions

The possibility of implementing piezoelectric actuators and exploiting the variation of the Modal electromechanical Coupling Factor (MEMCF) due to the insurgence of damages to develop new SHM techniques on complex truss girder structures has been analysed. A model-based approach has been suited to do that.

First, the FE model of the structure was developed and validated by comparing modal parameters such as natural frequencies and mode shapes evaluated numerically and experimentally. For the experimental results, an Operational Modal Analysis (OMA) algorithm has been applied to the acquired signals. The MAC index was evaluated too.

Once the FE model had been validated, the electromechanical system composed of the structure and the piezoelectric actuators was analysed. The most suitable piezoelectric actuators between those available from the main producers and the best placements of them had to be estimated. To do that, the MEMCFs were evaluated in undamaged and damaged conditions of the structure. The best placements and actuators are those that ensure the greatest values of MEMCFs and of their variation between different healthy states.

The best solution estimated at the FE model provides the implementation of the P840.60P actuator produced by Physical Instruments, placed on an additional rod next to the first vertical rod or connecting the first diagonal rod and the second vertical rod of the structure.

Starting from the results of the FE model, experimental tests have been carried out. The configuration in which the piezo actuator is mounted next to the first vertical rod from the left was initially tested since it gave the best results and was also the easiest to implement. All the structure's health configurations tested were performed in short and open circuit conditions of the piezo to estimate the coupling factors and their variation. Natural frequencies have been estimated by applying an OMA algorithm to the acquired acceleration signals called PolyMAX.

Many tests were performed on the undamaged status of the structure at different environmental conditions to ensure the repeatability of the results. It turned out that the variation in the coupling factors between different tests performed in the undamaged condition is not relevant. Moreover, this variation reaches an order of magnitude greater when structural alterations are induced to the truss girder. This confirms the good robustness of the chosen damage indexes with respect to environmental and operating conditions. Coupling factors and their variation can thus be considered effective and reliable damage indexes.

Experimental results were also compared with those from the FE model. There is a good agreement between the results, as numerical modes identified with non-null coupling factors are also found experimentally. Moreover, they were found to be better than the numerical ones. Indeed, the number of modes showing a non-zero coupling factor is higher and typically with a greater magnitude than that achieved numerically. Different damaged configurations were tested too; specifically, the damages introduced were mass additions at different locations of the truss and of different entities. This kind of damage was because it was the easiest to implement and because it would not permanently damage the structure. The same structural configurations gave comparable results ensuring their validity. The coupling factors change their magnitude from undamaged to damaged configuration, based on the magnitude and the placement of the damage. More specifically, the most severe damages piezo results in the greatest variation. For the same damage instead, the proximity to the piezo results in the greatest variation of the index.

Even if coupling factors and their variation prove to be reliable damage indices, the possibility of using an additional index proposed in [39] is also considered. This index is obtained from the sum in absolute value of the variations of the coefficients between two structural configurations. The advantage of using this index is that it incorporates information from all modes while assigning lower weight to the less reliable ones.

In conclusion, the SHM methodology analysed in this thesis proves to be a reliable and effective technique Compared to other SHM techniques, it demonstrates robustness as it is based on reliable modal identification techniques. Furthermore, it should be noticed that if the piezoelectric element was implemented in a more complex acquisition system, the estimation of these parameters would not require interrupting the system's operation but only switching the piezo's electrical condition from a short circuit to an open circuit and acquire data to estimate the eigenfrequencies.

10.2. Future works

Various aspects can be further explored to deepen and enrich this research.

First of all, an interesting aspect could be to consider other types of structural damage, such as:

- Presence of cracks in the rods (as those simulated at FEM);
- Corrosion of vertical and diagonal rods;
- Loosening of bolts or clamping elements between rods and chords.

Moreover, only one mounting configuration of the piezo has been tested. Especially given that the experimental results are better than those obtained from the FEM, also the configuration in which the piezo connects the diagonal and vertical rod could be implemented and tested, expecting good results.

Finally, although the experimental results are already satisfactory, future development could involve the implementation of a shunt circuit with a negative capacity. Several studies in fact [30], [34], [39]show how this solution, optimally tuned to the mode under investigation brings higher coupling factors increasing the shift in frequency between short circuit and open circuit condition of the piezo.

11. Appendix

All the resulting coupling factor and their variation evaluated at the FE model are reported in this Chapter. Only the modes with at least one nonzero coupling factor, evaluated in the damaged or undamaged condition of the structure, are reported. Generally, the FE model of the electromechanical system composed by the structure and the PZT results in 86 eigenmodes in the frequency range between 0-200 Hz.

11.1. Piezo stack inserted in the vertical rods

11.1.1. P02590P inserted in 1st vertical rod

Table 25: Resulting MEMCFs and Δk for the configuration with 1 PZT inserted in the first vertical rod

Frequency (SC) [Hz]	K undamaged	K damaged (1 kg addition)	ΔK	Frequency (SC) [Hz]	K undamaged	K damaged (1 kg addition)	ΔK
24.18	0.03151	0.03151	0.00001	108.74	0.00000	0.01352	0.01352
48.41	0.00643	0.00647	0.00004	125.32	0.01263	0.00000	0.01263
50.72	0.00628	0.00890	0.00262	131.85	0.00000	0.01231	0.01231
55.59	0.01697	0.01897	0.00201	136.68	0.00000	0.01205	0.01205
56.94	0.02716	0.02654	0.00062	159.77	0.02960	0.02734	0.00226
57.49	0.00590	0.00590	0.00000	161.05	0.00000	0.01114	0.01114
62.74	0.01597	0.01598	0.00001	177.37	0.01062	0.00000	0.01062
66.16	0.00550	0.00000	0.00550	178.73	0.00000	0.01057	0.01057
77.48	0.00508	0.00000	0.00508	186.38	0.01465	0.01464	0.00001
80.29	0.00499	0.00499	0.00000	206.82	0.00983	0.00982	0.00001
81.27	0.00859	0.00498	0.00361	215.68	0.00000	0.00963	0.00963
106.11	0.02746	0.01363	0.01383	216.77	0.01664	0.01917	0.00253

11.1.2. P02590P inserted in 1st and 3rd vertical rods

Table 26: MEMCFs and Δk for the configuration with PZT on 1st and 3rd vertical rods, pzt1 on in OC

Frequency (SC) [Hz]	K undamaged PZT1 on	K damaged PZT1 on	ΔK PZT1 on	Frequency (SC) [Hz]	K undamaged PZT1 on	K damaged PZT1 on	ΔK PZT1 on
24.38	0.06842	0.06780	0.00062	109.35	0.03826	0.00000	0.03826
39.61	0.00711	0.01005	0.00294	122.31	0.00000	0.01263	0.01263
39.93	0.00000	0.00708	0.00708	126.24	0.01780	0.00000	0.01780
42.37	0.00000	0.00685	0.00685	132.13	0.00000	0.01214	0.01214
47.87	0.00646	0.00643	0.00004	135.63	0.01214	0.02095	0.00880
50.57	0.01406	0.01404	0.00002	137.85	0.02409	0.00000	0.02409
55.72	0.02874	0.02680	0.00194	140.94	0.00000	0.01189	0.01189
57.20	0.05485	0.03782	0.01703	144.25	0.01178	0.00000	0.01178
57.47	0.03637	0.05374	0.01737	145.11	0.00000	0.01167	0.01167
62.83	0.03869	0.03948	0.00079	147.52	0.02017	0.00000	0.02017
72.68	0.00525	0.00525	0.00000	149.88	0.00000	0.01128	0.01128
75.44	0.00728	0.00728	0.00000	157.36	0.01127	0.01577	0.00449
80.50	0.01319	0.01569	0.00251	161.08	0.01576	0.06591	0.05015
82.19	0.00000	0.00493	0.00493	162.11	0.06480	0.02190	0.04290
83.81	0.00488	0.00488	0.00000	166.94	0.02189	0.01069	0.01120
86.05	0.00000	0.00482	0.00482	175.01	0.01069	0.02123	0.01054
88.76	0.00671	0.00475	0.00197	179.07	0.02589	0.00000	0.02589
91.01	0.00469	0.00000	0.00469	185.36	0.00000	0.04139	0.04139
99.12	0.00449	0.00000	0.00449	187.05	0.04006	0.01022	0.02984
102.94	0.04183	0.05645	0.01462	191.56	0.00000	0.01703	0.01703
107.54	0.00000	0.02361	0.02361	207.50	0.01964	0.00000	0.01964
108.23	0.02355	0.02349	0.00005	215.80	0.00000	0.06042	0.06042

Table 27: MEMCFs and Δk for the configuration with PZT on 1st and 3rd vertical rods, pzt3 on in OC

Frequency (SC) [Hz]	K undamaged PZT3 on	K damaged PZT3 on	ΔK PZT3 on	Frequency (SC) [Hz]	K undamaged PZT3 on	K damaged PZT3 on	ΔK PZT3 on
24.38	0.02562	0.02396	0.00166	135.63	0.01717	0.01710	0.00007
55.72	0.00599	0.00000	0.00599	137.85	0.01205	0.00000	0.01205
62.83	0.01596	0.01381	0.00215	139.94	0.00000	0.01191	0.01191
65.93	0.05342	0.05392	0.00050	140.94	0.01191	0.00000	0.01191
72.68	0.00742	0.00742	0.00000	144.25	0.01178	0.00000	0.01178
75.44	0.00515	0.00728	0.00213	147.98	0.00000	0.02311	0.02311
80.50	0.01319	0.01404	0.00085	149.88	0.02310	0.06865	0.04555
82.19	0.00000	0.00493	0.00493	157.36	0.07223	0.04598	0.02625
83.81	0.00488	0.00488	0.00000	161.08	0.04729	0.02227	0.02502
88.48	0.00000	0.00475	0.00475	162.11	0.01111	0.00000	0.01111
88.76	0.00475	0.00000	0.00475	166.94	0.01095	0.01069	0.00025
102.94	0.02414	0.03060	0.00646	175.01	0.01069	0.01061	0.00008
107.54	0.00000	0.01363	0.01363	179.07	0.01057	0.00000	0.01057
108.23	0.01359	0.01356	0.00003	185.36	0.00000	0.02069	0.02069
109.35	0.01913	0.00000	0.01913	187.05	0.02068	0.00000	0.02068
122.31	0.00000	0.02188	0.02188	191.56	0.00000	0.04506	0.04506
126.24	0.02518	0.00000	0.02518	207.50	0.04500	0.00000	0.04500
132.13	0.00000	0.02103	0.02103				

Table 28: MEMCFs and Δk for the configuration with PZT on 1st and 3rd vertical rods, all PZT on in OC

Frequency (SC) [Hz]	K undamaged all PZT on	K damaged all PZT on	ΔK all PZT on	Frequency (SC) [Hz]	K undamaged all PZT on	K damaged all PZT on	ΔK all PZT on
24.38	0.07250	0.07248	0.00002	109.35	0.04278	0.00000	0.04278
39.61	0.00711	0.01005	0.00294	122.31	0.00000	0.02825	0.02825
39.93	0.00000	0.00708	0.00708	126.24	0.03083	0.00000	0.03083
42.37	0.00000	0.00685	0.00685	132.13	0.00000	0.02429	0.02429
47.87	0.00646	0.00643	0.00004	135.63	0.02103	0.02419	0.00315
50.57	0.01406	0.01404	0.00002	137.85	0.02694	0.00000	0.02694
55.72	0.02935	0.02746	0.00190	139.94	0.00000	0.01685	0.01685
57.20	0.05485	0.03782	0.01703	140.94	0.01685	0.01189	0.00496
57.47	0.03637	0.05374	0.01737	144.25	0.01178	0.00000	0.01178
62.83	0.04185	0.04182	0.00003	145.11	0.00000	0.01167	0.01167
65.93	0.05370	0.05392	0.00021	147.52	0.02017	0.00000	0.02017
72.68	0.00909	0.00909	0.00000	147.98	0.00000	0.02311	0.02311
75.44	0.00892	0.00892	0.00000	149.88	0.02310	0.06958	0.04647
80.50	0.01865	0.02106	0.00241	157.36	0.07223	0.05231	0.01992
82.19	0.00000	0.00493	0.00493	161.08	0.04985	0.06684	0.01699
83.81	0.00488	0.00488	0.00000	162.11	0.06480	0.02190	0.04290
86.05	0.00000	0.00482	0.00482	166.94	0.02189	0.01512	0.00677
88.48	0.00000	0.00475	0.00475	175.01	0.01512	0.02374	0.00862
88.76	0.00671	0.00475	0.00197	179.07	0.02589	0.00000	0.02589
91.01	0.00469	0.00000	0.00469	185.36	0.00000	0.04627	0.04627
99.12	0.00635	0.00000	0.00635	187.05	0.04388	0.01022	0.03366
102.94	0.04830	0.06422	0.01592	191.56	0.00000	0.04916	0.04916
107.54	0.00000	0.02726	0.02726	207.50	0.05008	0.00000	0.05008
108.23	0.02719	0.02349	0.00370	215.80	0.00000	0.06042	0.06042

11.1.3. P02590P inserted in each vertical rod

PZT1 ON				PZT2 ON				PZT3 ON			
Freq. (SC) [Hz]	K undamaged	K damaged	ΔK	Freq. (SC) [Hz]	K undamaged	K damaged	ΔK	Freq. (SC) [Hz]	K undamaged	K damaged	ΔK
24.35	0.06786	0.06788	0.00002	24.35	0.04882	0.04883	0.00001	24.35	0.02398	0.02399	0.00001
39.61	0.00711	0.01005	0.00294	39.77	0.00000	0.00709	0.00709	39.77	0.00000	0.00709	0.00709
39.71	0.00710	0.00000	0.00710	39.93	0.00708	0.00000	0.00708	55.71	0.00599	0.00599	0.00000
39.77	0.00000	0.00709	0.00709	48.40	0.00643	0.00000	0.00643	62.80	0.01693	0.01786	0.00093
39.93	0.00708	0.00708	0.00000	55.71	0.01895	0.01987	0.00093	65.84	0.05259	0.05207	0.00052

42.58	0.00000	0.00687	0.00687	57.36	0.02770	0.02774	0.00004	71.68	0.00528	0.00000	0.00528
48.40	0.00643	0.00000	0.00643	62.80	0.02258	0.02328	0.00071	72.66	0.00525	0.00525	0.00000
50.72	0.01404	0.01258	0.00146	65.84	0.03698	0.03619	0.00079	73.22	0.01169	0.01045	0.00123
55.71	0.02811	0.02936	0.00125	71.68	0.00528	0.00000	0.00528	75.55	0.00515	0.00728	0.00213
56.42	0.00842	0.00842	0.00000	72.76	0.00000	0.00524	0.00524	81.10	0.00993	0.01221	0.00228
57.36	0.06526	0.06536	0.00010	73.22	0.01383	0.01280	0.00102	81.39	0.01108	0.00000	0.01108
62.80	0.03786	0.03704	0.00083	81.10	0.00497	0.00499	0.00002	83.82	0.00000	0.00488	0.00488
71.68	0.00528	0.00000	0.00528	81.39	0.00496	0.00000	0.00496	106.63	0.03063	0.02420	0.00643
73.22	0.01169	0.01045	0.00123	83.82	0.00000	0.00488	0.00488	108.18	0.01360	0.01364	0.00004
75.55	0.00515	0.00515	0.00000	106.63	0.01370	0.01397	0.00027	112.43	0.00000	0.02345	0.02345
81.10	0.01110	0.01319	0.00209	112.43	0.00000	0.01354	0.01354	125.31	0.02527	0.00000	0.02527
81.39	0.01214	0.00000	0.01214	125.31	0.02527	0.00000	0.02527	130.44	0.00000	0.02519	0.02519
83.82	0.00000	0.00488	0.00488	130.44	0.00000	0.02519	0.02519	135.57	0.02104	0.00000	0.02104
96.81	0.00455	0.00455	0.00000	135.57	0.02975	0.00000	0.02975	136.67	0.01210	0.01718	0.00508
106.63	0.05649	0.04192	0.01457	136.67	0.01711	0.02975	0.01265	139.90	0.00000	0.01205	0.01205
108.18	0.02720	0.02362	0.00357	139.90	0.00000	0.01205	0.01205	140.91	0.01191	0.00000	0.01191
112.43	0.00000	0.04282	0.04282	146.88	0.01167	0.00000	0.01167	141.53	0.00000	0.01191	0.01191
121.08	0.01285	0.00000	0.01285	147.85	0.00000	0.01165	0.01165	146.88	0.01167	0.00000	0.01167
125.31	0.01787	0.00000	0.01787	149.75	0.02584	0.00000	0.02584	147.85	0.00000	0.01165	0.01165
130.44	0.00000	0.01781	0.01781	157.02	0.05757	0.02311	0.03446	149.75	0.02584	0.00000	0.02584
135.57	0.01215	0.00000	0.01215	160.65	0.02232	0.05972	0.03740	157.02	0.06775	0.02311	0.04464
136.67	0.01711	0.01215	0.00496	161.18	0.00000	0.01577	0.01577	160.65	0.04991	0.07049	0.02057
139.90	0.00000	0.02410	0.02410	166.62	0.03465	0.00000	0.03465	161.18	0.01929	0.04863	0.02933
142.16	0.00000	0.01189	0.01189	174.96	0.01069	0.03286	0.02217	174.96	0.01069	0.00000	0.01069
146.88	0.01650	0.00000	0.01650	177.37	0.04379	0.01512	0.02867	177.37	0.00000	0.01512	0.01512
147.85	0.00000	0.02017	0.02017	185.16	0.00000	0.04230	0.04230	185.16	0.00000	0.01057	0.01057
149.75	0.01156	0.00000	0.01156	186.60	0.04142	0.00000	0.04142	186.60	0.01793	0.00000	0.01793
157.02	0.01129	0.00000	0.01129	191.53	0.00000	0.04392	0.04392	191.53	0.00000	0.01793	0.01793
160.65	0.01578	0.00000	0.01578	206.82	0.02602	0.00000	0.02602	206.82	0.04614	0.00000	0.04614
161.18	0.06594	0.01115	0.05478	215.75	0.00000	0.02196	0.02196	215.75	0.00000	0.04608	0.04608
166.62	0.02450	0.06577	0.04127								
174.96	0.01069	0.02191	0.01122								
177.37	0.01839	0.01069	0.00770								
185.16	0.00000	0.02590	0.02590								
186.60	0.04142	0.00000	0.04142								
191.53	0.01022	0.03873	0.02851								
206.82	0.01703	0.00000	0.01703								
215.75	0.00000	0.02196	0.02196								

PZT4 ON				PZT5 ON				PZT6 ON			
Freq. (SC) [Hz]	**K undamaged**	**K damaged**	**ΔK**	**Freq. (SC) [Hz]**	**K undamaged**	**K damaged**	**ΔK**	**Freq. (SC) [Hz]**	**K undamaged**	**K damaged**	**ΔK**
24.35	0.00906	0.00907	0.00000	24.35	0.02398	0.02399	0.00001	24.35	0.04882	0.04883	0.00001
55.71	0.00599	0.00000	0.00599	39.77	0.00000	0.00709	0.00709	39.77	0.00000	0.00709	0.00709
72.59	0.00525	0.00525	0.00000	55.71	0.00599	0.00599	0.00000	39.93	0.00708	0.00000	0.00708
83.82	0.00000	0.00488	0.00488	57.36	0.00590	0.00591	0.00001	48.40	0.00643	0.00000	0.00643
106.63	0.02739	0.01976	0.00764	62.80	0.01382	0.01494	0.00112	50.72	0.00628	0.00000	0.00628
108.18	0.01360	0.01364	0.00004	65.84	0.05259	0.05207	0.00052	55.71	0.00599	0.00000	0.00599
112.43	0.00000	0.02708	0.02708	71.68	0.00528	0.00000	0.00528	56.42	0.00595	0.00595	0.00000
121.08	0.01818	0.00000	0.01818	73.22	0.01280	0.01169	0.00111	57.36	0.03180	0.03240	0.00059
122.20	0.00000	0.01814	0.01814	75.55	0.00515	0.00515	0.00000	62.80	0.03039	0.03093	0.00054
125.31	0.01787	0.00000	0.01787	81.10	0.01110	0.01319	0.00209	65.84	0.03353	0.03265	0.00088
130.44	0.00000	0.01781	0.01781	81.39	0.00991	0.00000	0.00991	72.76	0.00000	0.00524	0.00524
136.67	0.02095	0.00000	0.02095	83.82	0.00000	0.00488	0.00488	73.22	0.01280	0.01169	0.00111
139.90	0.00000	0.02410	0.02410	106.63	0.03063	0.01397	0.01666	83.82	0.00000	0.00488	0.00488
140.91	0.01191	0.00000	0.01191	108.18	0.01360	0.01929	0.00569	106.63	0.00000	0.01397	0.01397
141.53	0.00000	0.01191	0.01191	112.43	0.00000	0.02708	0.02708	108.18	0.00000	0.01364	0.01364
142.16	0.00000	0.01189	0.01189	125.31	0.02188	0.00000	0.02188	112.43	0.00000	0.01354	0.01354
142.35	0.01185	0.00000	0.01185	130.44	0.00000	0.02519	0.02519	125.31	0.01263	0.00000	0.01263
142.46	0.00000	0.01185	0.01185	131.75	0.01232	0.00000	0.01232	130.44	0.00000	0.02181	0.02181
146.88	0.02021	0.00000	0.02021	135.57	0.02104	0.00000	0.02104	131.75	0.01232	0.00000	0.01232

147.85	0.00000	0.02017	0.02017	136.67	0.02963	0.01718	0.01246	135.57	0.02429	0.00000	0.02429
149.75	0.02311	0.00000	0.02311	139.90	0.00000	0.02695	0.02695	136.67	0.03422	0.02104	0.01318
157.02	0.01596	0.02001	0.00405	146.88	0.02609	0.00000	0.02609	139.90	0.00000	0.02952	0.02952
160.65	0.05235	0.01954	0.03281	147.85	0.00000	0.02329	0.02329	146.88	0.03088	0.00000	0.03088
161.18	0.02948	0.06008	0.03061	157.02	0.03910	0.00000	0.03910	147.85	0.00000	0.02853	0.02853
166.62	0.06577	0.01111	0.05466	160.65	0.05115	0.03908	0.01206	149.75	0.01156	0.01163	0.00007
174.96	0.00000	0.06390	0.06390	161.18	0.02948	0.06008	0.03061	157.02	0.03386	0.00000	0.03386
177.37	0.02375	0.01069	0.01306	166.62	0.04383	0.01571	0.02812	160.65	0.01933	0.03385	0.01452
185.16	0.00000	0.02364	0.02364	174.96	0.01069	0.04243	0.03174	161.18	0.01114	0.02231	0.01117
186.60	0.04393	0.00000	0.04393	177.37	0.01062	0.01512	0.00450	177.37	0.00000	0.01069	0.01069
191.53	0.00000	0.04392	0.04392	185.16	0.00000	0.01057	0.01057	186.60	0.05673	0.00000	0.05673
215.75	0.00000	0.00982	0.00982	186.60	0.03434	0.00000	0.03434	191.53	0.01445	0.05671	0.04225
				191.53	0.00000	0.03433	0.03433	206.82	0.03934	0.01022	0.02912
				206.82	0.03546	0.00000	0.03546	215.75	0.00000	0.04282	0.04282
				215.75	0.00000	0.03403	0.03403				

PZT7 ON				ALL PZT ON			
Frequency (SC) [Hz]	**K undamaged**	**K damaged**	**ΔK**	**Frequency (SC) [Hz]**	**K undamaged**	**K damaged**	**ΔK**
24.35	0.06539	0.06603	0.00064	24.35	0.12351	0.12354	0.00003
39.61	0.00711	0.01005	0.00294	39.61	0.01231	0.01421	0.00190
39.77	0.00000	0.00709	0.00709	39.71	0.00710	0.00710	0.00000
39.93	0.00708	0.00708	0.00000	39.77	0.00000	0.00709	0.00709
48.40	0.00643	0.00000	0.00643	39.93	0.01001	0.01001	0.00000
50.72	0.00628	0.00000	0.00628	42.58	0.00685	0.00687	0.00002
55.71	0.01695	0.01798	0.00103	48.40	0.01113	0.00647	0.00467
56.42	0.00595	0.00842	0.00247	50.72	0.01661	0.01541	0.00121
57.36	0.06224	0.06345	0.00121	55.71	0.03790	0.03930	0.00140
62.80	0.04954	0.04892	0.00062	56.42	0.01031	0.01031	0.00000
71.68	0.00528	0.00000	0.00528	57.36	0.09963	0.10084	0.00120
73.22	0.01169	0.01169	0.00000	62.80	0.07661	0.07686	0.00026
81.10	0.01490	0.02338	0.00849	65.84	0.08981	0.08854	0.00127
81.39	0.01487	0.00496	0.00991	71.68	0.00528	0.00528	0.00000
83.82	0.00488	0.00488	0.00000	72.47	0.00000	0.00525	0.00525
96.81	0.00455	0.00455	0.00000	72.59	0.00525	0.00525	0.00000
106.63	0.05649	0.05229	0.00420	72.66	0.00525	0.00525	0.00000
108.18	0.03331	0.01929	0.01402	72.76	0.00524	0.00524	0.00000
112.43	0.00000	0.03830	0.03830	73.22	0.03048	0.02957	0.00091
121.08	0.01285	0.00000	0.01285	75.55	0.01151	0.01151	0.00000
125.31	0.01787	0.00000	0.01787	81.10	0.02329	0.03345	0.01015
135.57	0.01215	0.00000	0.01215	81.39	0.02479	0.00702	0.01777
136.67	0.02420	0.01215	0.01205	83.82	0.00691	0.00846	0.00155
139.90	0.00000	0.02087	0.02087	96.81	0.00455	0.00455	0.00000
142.16	0.00000	0.01189	0.01189	106.63	0.06988	0.07264	0.00276
144.22	0.01178	0.00000	0.01178	106.89	0.06120	0.00000	0.06120
145.09	0.00000	0.01178	0.01178	108.18	0.05441	0.03609	0.01832
146.88	0.02334	0.00000	0.02334	112.43	0.00000	0.07420	0.07420
147.85	0.00000	0.02017	0.02017	121.08	0.02226	0.00000	0.02226
149.75	0.01156	0.00000	0.01156	122.20	0.00000	0.02222	0.02222
160.65	0.02232	0.00000	0.02232	125.31	0.05211	0.00000	0.05211
161.18	0.06402	0.00000	0.06402	130.44	0.01238	0.05773	0.04534
166.62	0.01549	0.06386	0.04837	131.75	0.02134	0.00000	0.02134
174.96	0.00000	0.01897	0.01897	135.57	0.04860	0.01741	0.03119
177.37	0.03974	0.00000	0.03974	136.67	0.06404	0.04705	0.01699
185.16	0.00000	0.04487	0.04487	139.90	0.00000	0.05654	0.05654
206.82	0.02782	0.00000	0.02782	140.91	0.02064	0.00000	0.02064
215.75	0.00000	0.02778	0.02778	141.53	0.01681	0.02064	0.00382
				142.16	0.00000	0.01681	0.01681
				142.35	0.01676	0.00000	0.01676
				142.46	0.01185	0.01676	0.00491
				142.51	0.00000	0.01185	0.01185
				144.22	0.01178	0.00000	0.01178

145.09	0.00000	0.01178	0.01178
146.88	0.05220	0.00000	0.05220
147.85	0.00000	0.05078	0.05078
149.75	0.04325	0.01645	0.02680
157.02	0.10782	0.04003	0.06778
160.65	0.10055	0.11011	0.00957
161.18	0.09722	0.10234	0.00512
166.62	0.09110	0.09307	0.00197
174.96	0.02619	0.08771	0.06152
177.37	0.06886	0.02829	0.04057
185.16	0.00000	0.07175	0.07175
186.60	0.10050	0.00000	0.10050
191.53	0.01770	0.10153	0.08383
206.82	0.08175	0.01770	0.06405
215.75	0.00000	0.08224	0.08224

11.2. Piezo stack mounted on additional vertical rods

11.2.1. P02590P next to the 1st vertical rod

Table 29: Resulting MEMCFs and Δk for the configuration with 1 P012590P mounted on a vertical rod next to the first one

Frequency (SC) [Hz]	K undamaged	K damaged	ΔK	Frequency (SC) [Hz]	K undamaged	K damaged	ΔK
24.93	0.0457	0.0457	0.00001	109.66	0.0357	0.0135	0.02225
39.75	0.0071	0.0071	0.00001	110.12	0.0270	0.0380	0.01106
48.44	0.0064	0.0071	0.00067	125.56	0.0126	0.0126	0.00004
50.78	0.0063	0.0063	0.00001	131.88	0.0123	0.0121	0.00018
55.85	0.0104	0.0120	0.00160	135.81	0.0121	0.0170	0.00487
58.23	0.0083	0.0131	0.00482	137.22	0.0209	0.0119	0.00901
58.67	0.0437	0.0434	0.00034	141.64	0.0119	0.0119	0.00000
63.44	0.0327	0.0318	0.00095	144.30	0.0118	0.0116	0.00014
66.16	0.0055	0.0073	0.00178	164.85	0.0365	0.0311	0.00544
75.51	0.0051	0.0100	0.00482	168.38	0.0422	0.0422	0.00000
81.30	0.0111	0.0048	0.00634	175.13	0.0107	0.0107	0.00000
88.57	0.0048	0.0048	0.00000	177.94	0.0184	0.0211	0.00273
88.62	0.0048	0.0197	0.01496	189.85	0.0423	0.0411	0.00127
99.17	0.0045	0.0138	0.00933	191.93	0.0204	0.0228	0.00241
107.95	0.0136	0.0136	0.00000	207.51	0.0139	0.0170	0.00309

11.2.2. P02590P next to the 1st and 3rd vertical rods

Table 30:Resulting MEMCFs and Δk for the configuration with 1 P02590P PZT mounted next to the 1st and 3rd vertical rod

Freq. SC [Hz]	K PZT1 on undamaged	K PZT1 on damaged	ΔK	K PZT2 on undamaged	K PZT2 on damaged	ΔK	K PZT1, PZT2 on undamaged	K PZT1, PZT2 on damaged	ΔK
24.99	0.04562	0.04564	0.00001	0.01789	0.01790	0.00000	0.04901	0.04902	0.00001
39.64	0.00710	0.00710	0.00000	0.00000	0.00710	0.00710	0.00710	0.01005	0.00294
39.72	0.00710	0.00710	0.00000	0.00000	0.00000	0.00000	0.00710	0.00710	0.00000
39.94	0.00000	0.00687	0.00687	0.00708	0.00000	0.00708	0.00708	0.00687	0.00021
48.45	0.00643	0.00629	0.00014	0.00000	0.00000	0.00000	0.00643	0.00629	0.00014
50.78	0.00628	0.01036	0.00409	0.00000	0.00598	0.00598	0.00628	0.01197	0.00569
55.86	0.01036	0.01173	0.00136	0.00000	0.00000	0.00000	0.01197	0.01173	0.00024
58.19	0.01015	0.04337	0.03321	0.00000	0.00000	0.00000	0.01015	0.04337	0.03321
58.67	0.04370	0.03227	0.01143	0.00000	0.00973	0.00973	0.04370	0.03371	0.01000
63.48	0.03273	0.00000	0.03273	0.00794	0.02742	0.01949	0.03368	0.02742	0.00626
66.68	0.00000	0.00728	0.00728	0.02793	0.00000	0.02793	0.02793	0.00728	0.02065
75.51	0.00728	0.00863	0.00136	0.00000	0.00498	0.00498	0.00728	0.00997	0.00269
81.17	0.00993	0.00000	0.00993	0.00496	0.01686	0.01190	0.00993	0.01686	0.00693

81.79	0.00494	0.00672	0.00177	0.00000	0.00000	0.00000	0.00494	0.00672	0.00177
84.43	0.00000	0.00000	0.00000	0.01686	0.00822	0.00864	0.01755	0.00822	0.00933
88.56	0.00475	0.00000	0.00475	0.00000	0.00671	0.00671	0.00475	0.00671	0.00196
88.62	0.00672	0.00448	0.00224	0.00000	0.00000	0.00000	0.00672	0.00448	0.00224
88.75	0.00000	0.01970	0.01970	0.00822	0.00000	0.00822	0.00822	0.01970	0.01147
88.90	0.00000	0.01382	0.01382	0.00474	0.00000	0.00474	0.00474	0.01382	0.00908
108.40	0.01358	0.01358	0.00000	0.00000	0.00000	0.00000	0.01358	0.01358	0.00000
110.05	0.03814	0.01347	0.02467	0.01348	0.00000	0.01348	0.03814	0.01347	0.02467
110.47	0.02331	0.03797	0.01466	0.00000	0.01342	0.01342	0.02331	0.04027	0.01696
121.18	0.01285	0.00000	0.01285	0.00000	0.00000	0.00000	0.01285	0.01282	0.00003
125.69	0.01261	0.01257	0.00004	0.01261	0.01257	0.00004	0.01784	0.01778	0.00006
135.85	0.01213	0.01213	0.00000	0.00000	0.00000	0.00000	0.01213	0.01213	0.00000
137.25	0.01707	0.01700	0.00007	0.00000	0.00000	0.00000	0.01707	0.01700	0.00007
141.17	0.01190	0.01190	0.00000	0.00000	0.00000	0.00000	0.01190	0.01190	0.00000
141.64	0.01188	0.01188	0.00000	0.00000	0.00000	0.00000	0.01188	0.01188	0.00000
144.46	0.00000	0.00000	0.00000	0.01177	0.00000	0.01177	0.01177	0.00000	0.01177
147.10	0.01166	0.01163	0.00003	0.00000	0.00000	0.00000	0.01166	0.01163	0.00003
150.03	0.01155	0.00000	0.01155	0.00000	0.00000	0.00000	0.01155	0.01155	0.00000
159.36	0.00000	0.00000	0.00000	0.01120	0.01119	0.00001	0.01120	0.01119	0.00001
164.58	0.03308	0.02912	0.00396	0.01102	0.00000	0.01102	0.03487	0.02912	0.00575
168.38	0.04222	0.04222	0.00000	0.00000	0.00000	0.00000	0.04222	0.04222	0.00000
172.70	0.01076	0.01076	0.00000	0.06460	0.06460	0.00001	0.06549	0.06549	0.00001
176.40	0.02381	0.02129	0.00252	0.05637	0.05833	0.00196	0.06212	0.06301	0.00089
177.94	0.01499	0.02359	0.00860	0.01060	0.00000	0.01060	0.01836	0.02359	0.00523
190.31	0.03697	0.03551	0.00146	0.01776	0.02050	0.00274	0.04101	0.03971	0.00131
192.03	0.02282	0.02282	0.00000	0.01021	0.01021	0.00000	0.02500	0.02500	0.00000
214.05	0.00967	0.01365	0.00398	0.06701	0.06691	0.00010	0.06770	0.06760	0.00010

11.2.3. P01690P next to the 1st vertical rod

P01690P - DAMAGE ON ROD 2							
Frequency (SC) [Hz]	**K undamaged**	**K damaged**	**ΔK rod2**	**Frequency (SC) [Hz]**	**K undamaged**	**K damaged**	**ΔK rod2**
25.21	0.04543	0.04484	0.00059	110.67	0.04252	0.04036	0.00216
39.64	0.00710	0.00000	0.00710	121.18	0.01285	0.00000	0.01285
39.72	0.00710	0.00000	0.00710	131.61	0.03262	0.00000	0.03262
39.76	0.00709	0.00000	0.00709	131.93	0.02463	0.00000	0.02463
39.78	0.00709	0.00000	0.00709	137.58	0.01206	0.01205	0.00001
39.78	0.00709	0.00000	0.00709	141.81	0.01188	0.00000	0.01188
39.93	0.00708	0.00000	0.00708	147.16	0.01166	0.01166	0.00000
48.55	0.00642	0.00000	0.00642	157.47	0.00000	0.01127	0.01127
50.83	0.00627	0.00627	0.00000	165.57	0.02198	0.01904	0.00295
55.88	0.00846	0.00846	0.00000	170.30	0.04469	0.04470	0.00000
59.27	0.04190	0.04236	0.00046	175.27	0.01511	0.01068	0.00442
63.83	0.03714	0.03226	0.00487	178.28	0.01835	0.01835	0.00000
75.53	0.00728	0.00728	0.00000	190.05	0.01026	0.01026	0.00000
81.34	0.00992	0.00992	0.00001	193.32	0.04879	0.05089	0.00209
88.58	0.00000	0.00475	0.00475	207.03	0.00983	0.00000	0.00983
88.68	0.00950	0.00950	0.00000	207.92	0.01699	0.01699	0.00000
92.22	0.00000	0.00466	0.00466				
P01680P - DAMAGE ON ROD 1							
Frequency (SC) [Hz]	**K undamaged**	**K damaged**	**ΔK rod1**	**Frequency (SC) [Hz]**	**K undamaged**	**K damaged**	**ΔK rod1**
25.21	0.04543	0.04573	0.00029	112.16	0.00000	0.01335	0.01335
39.64	0.00710	0.00710	0.00000	121.18	0.01285	0.01285	0.00001
39.72	0.00710	0.00000	0.00710	125.59	0.00000	0.01264	0.01264
39.76	0.00709	0.00000	0.00709	131.61	0.03262	0.03020	0.00242
39.78	0.00709	0.00000	0.00709	131.93	0.02463	0.02462	0.00000
39.78	0.00709	0.00709	0.00000	137.58	0.01206	0.00000	0.01206
39.93	0.00708	0.00000	0.00708	138.56	0.00000	0.01201	0.01201
48.55	0.00642	0.00000	0.00642	141.81	0.01188	0.00000	0.01188
50.83	0.00627	0.00627	0.00000	147.16	0.01166	0.01167	0.00001
55.88	0.00846	0.01036	0.00190	165.57	0.02198	0.02199	0.00000

59.27	0.04190	0.04190	0.00000	170.3	0.04469	0.04473	0.00004
63.83	0.03714	0.03549	0.00164	175.27	0.01511	0.01068	0.00442
66.14	0.00000	0.00551	0.00551	178.28	0.01835	0.01836	0.00001
75.53	0.00728	0.00728	0.00000	190.05	0.01026	0.01451	0.00425
81.34	0.00992	0.00992	0.00000	193.32	0.04879	0.04666	0.00213
88.68	0.00950	0.00950	0.00000	207.03	0.00983	0.00983	0.00000
108.57	0.00000	0.01357	0.01357	207.92	0.01699	0.01388	0.00311
110.67	0.04252	0.04255	0.00003				

11.2.4. P01040P next to the 1st vertical rod

P01040P - DAMAGE ON ROD 2							
Frequency (SC) [Hz]	**K undamaged**	**K damaged**	**ΔK rod2**	**Frequency (SC) [Hz]**	**K undamaged**	**K damaged**	**ΔK rod2**
25.18	0.04085	0.04013	0.00072	125.62	0.00000	0.01262	0.01262
38.12	0.00000	0.00725	0.00725	135.81	0.01214	0.00000	0.01214
39.64	0.00710	0.00000	0.00710	137.37	0.01706	0.01205	0.00501
42.59	0.00000	0.00685	0.00685	140.96	0.01191	0.01205	0.00014
48.51	0.00642	0.00642	0.00000	141.68	0.00000	0.01188	0.01188
50.83	0.00627	0.00627	0.00000	144.25	0.01178	0.00000	0.01178
55.88	0.00846	0.00846	0.00000	147.21	0.00000	0.01166	0.01166
59.21	0.03856	0.03861	0.00005	149.69	0.01635	0.00000	0.01635
63.78	0.03313	0.02919	0.00394	152.28	0.02563	0.03036	0.00473
75.53	0.00515	0.00728	0.00213	157.47	0.01127	0.00000	0.01127
81.34	0.00992	0.00859	0.00132	161.03	0.01114	0.00000	0.01114
85.07	0.00485	0.00000	0.00485	165.51	0.01904	0.01904	0.00000
88.68	0.00823	0.00823	0.00000	170.12	0.03910	0.03910	0.00000
88.86	0.00000	0.00474	0.00474	175.26	0.01068	0.01068	0.00000
99.91	0.00000	0.00447	0.00447	178.24	0.01835	0.01498	0.00336
107.96	0.01361	0.01361	0.00000	190.3	0.01025	0.01450	0.00425
108.65	0.00000	0.01357	0.01357	193.16	0.04318	0.04319	0.00001
110.60	0.04035	0.03806	0.00229	207.81000	0.01387	0.013875178	1.00161E-06
121.18	0.01285	0.00000	0.01285				

P01040P - DAMAGE ON ROD 1							
Frequency (SC) [Hz]	**K undamaged**	**K damaged**	**ΔK rod1**	**Frequency (SC) [Hz]**	**K undamaged**	**K damaged**	**ΔK rod1**
25.18	0.04085	0.04112	0.00026	135.81	0.01214	0.00000	0.01214
39.64	0.00710	0.00000	0.00710	137.37	0.01706	0.02085	0.00379
39.76	0.00000	0.00709	0.00709	140.96	0.01191	0.01188	0.00003
39.78	0.00000	0.00709	0.00709	143.71	0.00000	0.01181	0.01181
48.51	0.00642	0.00642	0.00000	144.25	0.01178	0.00000	0.01178
50.83	0.00627	0.00627	0.00000	147.02	0.00000	0.01167	0.01167
55.88	0.00846	0.00846	0.00000	149.69	0.01635	0.01638	0.00004
59.21	0.03856	0.03812	0.00044	152.28	0.02563	0.02563	0.00000
63.78	0.03313	0.03176	0.00138	157.47	0.01127	0.00000	0.01127
66.15	0.00000	0.00551	0.00551	161.03	0.01114	0.00000	0.01114
75.53	0.00515	0.00728	0.00213	165.51	0.01904	0.02199	0.00295
81.34	0.00992	0.00859	0.00133	170.12	0.03910	0.03913	0.00003
85.07	0.00485	0.00000	0.00485	175.26	0.01068	0.01068	0.00000
88.68	0.00823	0.00823	0.00000	178.24	0.01835	0.01836	0.00001
107.96	0.01361	0.01361	0.00000	190.3	0.01025	0.01450	0.00425
110.60	0.04035	0.04038	0.00003	193.16	0.04318	0.04074	0.00244
121.18	0.01285	0.01285	0.00001	207.81	0.01387	0.01388	0.00001
125.62	0.00000	0.01264	0.01264				

11.2.5. P03520P next to the 1st vertical rod

P03520P - DAMAGE ON ROD 2				P03520P - DAMAGE ON ROD 1			
Frequency (SC) [Hz]	**K undamaged**	**K damaged**	**ΔK rod2**	**Frequency (SC) [Hz]**	**K undamaged**	**K damaged**	**ΔK rod1**
25.26	0.01541	0.01551	0.00010	25.26	0.01541	0.01551	0.00010
59.37	0.01298	0.01300	0.00002	59.37	0.01298	0.01298	0.00000
63.89	0.01119	0.00972	0.00147	63.89	0.01119	0.01122	0.00003
88.69	0.00475	0.00000	0.00475	75.54	0.00000	0.00515	0.00515

110.76	0.00000	0.01344	0.01344
111.11	0.00000	0.01342	0.01342
120.91	0.01286	0.00000	0.01286
141.82	0.01188	NaN	0.01188
165.62	0.01099	0.00000	0.01099
170.66	0.01531	0.01083	0.00448
190.11	0.00000	0.01026	0.01026
193.92	0.01436	0.01437	0.00000

81.34	0.00000	0.00496	0.00496
88.69	0.00475	0.00475	0.00000
110.76	0.00000	0.01344	0.01344
111.11	0.00000	0.01342	0.01342
120.91	0.01286	0.01286	0.00000
121.37	0.00000	0.01284	0.01284
141.82	0.01188	0.00000	0.01188
165.62	0.01099	0.01099	0.00000
170.66	0.01531	0.01532	0.00001
193.92	0.01436	0.01438	0.00001

11.2.6. P02540P next to the 1st vertical rod

P02540P - DAMAGE ON ROD 2			
Frequency (SC) [Hz]	**K undamaged**	**K damaged**	**ΔK rod2**
25.24	0.01991	0.01792	0.00199
55.88	0.00598	0.00598	0.00000
59.32	0.01642	0.01744	0.00102
63.87	0.01583	0.01375	0.00208
81.35	0.00496	0.00496	0.00000
88.54	0.00000	0.00475	0.00475
88.58	0.00475	0.00000	0.00475
110.84	0.01343	0.01901	0.00558
125.62	0.00000	0.01262	0.01262
132.76	0.01227	0.00000	0.01227
165.59	0.00000	0.01099	0.01099
170.46	0.01532	0.01532	0.00000
175.29	0.00000	0.01068	0.01068
178.3	0.01059	0.00000	0.01059
190.3	0.01025	0.00000	0.01025
193.61	0.02033	0.02033	0.00000
207.85	0.00981	0.00981	0.00000

P02540P - DAMAGE ON ROD 1			
Frequency (SC) [Hz]	**K undamaged**	**K damaged**	**ΔK rod1**
25.24	0.01991	0.01792	0.00199
39.78	0.00000	0.00709	0.00709
39.79	0.00000	0.00709	0.00709
55.88	0.00598	0.00000	0.00598
59.32	0.01642	0.01742	0.00100
63.87	0.01583	0.01484	0.00099
81.35	0.00496	0.00496	0.00000
88.58	0.00475	0.00000	0.00475
88.68	0.00000	0.00475	0.00475
110.84	0.01343	0.01901	0.00558
132.76	0.01227	0.01227	0.00000
146.98	0.00000	0.01167	0.01167
165.59	0.00000	0.01099	0.01099
170.46	0.01532	0.01533	0.00001
178.3	0.01059	0.01060	0.00001
190.3	0.01025	0.01025	0.00000
193.61	0.02033	0.02035	0.00002
207.85000	0.00981	0.00000	0.00981

11.2.7. P01680P next to the 1st vertical rod

P01680P - DAMAGE ON ROD 2			
Frequency (SC) [Hz]	**K undamaged**	**K damaged**	**ΔK rod2**
25.21	0.03673	0.03587	0.00086
39.64	0.00710	0.00710	0.00000
39.72	0.00710	0.00000	0.00710
39.76	0.00709	0.00000	0.00709
39.78	0.00709	0.00000	0.00709
42.60	0.00685	0.00000	0.00685
48.55	0.00642	0.00000	0.00642
50.83	0.00627	0.00627	0.00000
55.88	0.00846	0.00598	0.00248
59.26	0.03388	0.03491	0.00103
63.79	0.02800	0.02574	0.00226
64.50	0.01245	0.00788	0.00458
75.53	0.00515	0.00515	0.00000
81.34	0.00859	0.00859	0.00001
88.58	0.00475	0.00475	0.00000
88.68	0.00823	0.00823	0.00000
108.00	0.00000	0.01361	0.01361
110.74	0.03292	0.03294	0.00002

P01680P - DAMAGE ON ROD 2			
Frequency (SC) [Hz]	**K undamaged**	**K damaged**	**ΔK rod2**
125.63	0.00000	0.01262	0.01262
135.75	0.01214	0.00000	0.01214
137.27	0.02091	0.01205	0.00886
139.95	0.02071	0.00000	0.02071
141.63	0.00000	0.01187	0.01187
142.13	0.00000	0.01187	0.01187
142.35	0.00000	0.02373	0.02373
143.03	0.01183	0.00000	0.01183
147.21	0.01166	0.00000	0.01166
165.53	0.01904	0.01555	0.00349
168.69	0.01089	0.01089	0.00000
170.64	0.03424	0.03591	0.00167
175.28	0.01068	0.01068	0.00000
178.28	0.01498	0.01498	0.00000
190.28	0.01025	0.01025	0.00000
193.27	0.03941	0.04071	0.00130
207.77	0.01388	0.00981	0.00406

P01680P - DAMAGE ON ROD 1			
Frequency (SC) [Hz]	**K undamaged**	**K damaged**	**ΔK rod1**
25.21	0.03673	0.03697	0.00024
39.64	0.00710	0.00710	0.00000

P01680P - DAMAGE ON ROD 1			
Frequency (SC) [Hz]	**K undamaged**	**K damaged**	**ΔK rod1**
110.74	0.03292	0.03558	0.00266
125.63	0.00000	0.01264	0.01264

39.72	0.00710	0.00000	0.00710	135.75	0.01214	0.01213	0.00001
39.76	0.00709	0.00000	0.00709	137.27	0.02091	0.02695	0.00604
39.78	0.00709	0.00000	0.00709	139.19	0.00000	0.01199	0.01199
42.60	0.00685	0.00000	0.00685	139.95	0.02071	0.01686	0.00385
48.55	0.00642	0.00000	0.00642	143.03	0.01183	0.01184	0.00002
50.83	0.00627	0.00627	0.00000	144.39	0.00000	0.01178	0.01178
55.88	0.00846	0.00846	0.00000	147.21	0.01166	0.00000	0.01166
59.26	0.03388	0.03438	0.00050	165.53	0.01904	0.01555	0.00349
63.79	0.02800	0.02806	0.00006	168.69	0.01089	0.01089	0.00000
64.50	0.01245	0.00965	0.00281	170.64	0.03424	0.03426	0.00002
66.14	0.00000	0.00551	0.00551	175.28	0.01068	0.01068	0.00000
75.53	0.00515	0.00728	0.00213	178.28	0.01498	0.01499	0.00001
81.34	0.00859	0.00859	0.00000	190.28	0.01025	0.01025	0.00000
88.58	0.00475	0.00000	0.00475	193.27	0.03941	0.03810	0.00131
88.68	0.00823	0.00823	0.00000	207.77	0.01388	0.01388	0.00001

11.2.8. P01080 P next to the 1st vertical rod

P01080P - DAMAGE ON ROD 2							
Frequency (SC) [Hz]	**K undamaged**	**K damaged**	**ΔK rod2**	**Frequency (SC) [Hz]**	**K undamaged**	**K damaged**	**ΔK rod2**
25.15	0.05500	0.05536	0.00036	125.60	0.01785	0.01262	0.00522
39.64	0.00710	0.00000	0.00710	130.53	0.00000	0.01745	0.01745
39.76	0.00709	0.00000	0.00709	135.60	0.02429	0.00000	0.02429
39.78	0.00709	0.00000	0.00709	136.93	0.03198	0.02089	0.01109
50.83	0.00887	0.00887	0.00000	139.17	0.02076	0.02670	0.00594
55.88	0.01036	0.01197	0.00160	141.57	0.01189	0.00000	0.01189
59.14	0.05203	0.05275	0.00072	147.17	0.01166	0.01166	0.00000
63.73	0.04412	0.03894	0.00518	157.47	0.00000	0.01127	0.01127
75.53	0.00891	0.01029	0.00138	165.46	0.02693	0.02693	0.00000
81.33	0.01312	0.01109	0.00203	169.74	0.02427	0.02427	0.00000
88.58	0.00475	0.00000	0.00475	170.01	0.04729	0.04852	0.00123
88.67	0.01062	0.01062	0.00000	175.24	0.01511	0.01511	0.00000
99.84	0.00000	0.00448	0.00448	178.19	0.02369	0.02119	0.00250
107.94	0.01361	0.01361	0.00000	190.17	0.01776	0.02051	0.00275
108.47	0.01358	0.00000	0.01358	192.85	0.05853	0.06029	0.00176
110.46	0.05384	0.05387	0.00003	207.76	0.01962	0.01963	0.00000
121.18	0.00000	0.01285	0.01285				
P01080P - DAMAGE ON ROD 1							
Frequency (SC) [Hz]	**K undamaged**	**K damaged**	**ΔK rod1**	**Frequency (SC) [Hz]**	**K undamaged**	**K damaged**	**ΔK rod1**
25.15	0.05500	0.05608	0.00108	125.60	0.01785	0.01264	0.00520
39.64	0.00710	0.00710	0.00000	135.60	0.02429	0.02101	0.00328
39.76	0.00709	0.00000	0.00709	136.93	0.03198	0.04007	0.00809
39.78	0.00000	0.01003	0.01003	139.17	0.02076	0.01690	0.00386
39.78	0.00709	0.01003	0.00294	141.57	0.01189	0.00000	0.01189
50.83	0.00887	0.00887	0.00000	144.61	0.00000	0.01179	0.01179
55.88	0.01036	0.01036	0.00000	147.17	0.01166	0.01166	0.00001
59.14	0.05203	0.05236	0.00032	157.47	0.00000	0.01128	0.01128
63.73	0.04412	0.04240	0.00172	165.46	0.02693	0.02910	0.00217
66.15	0.00000	0.00780	0.00780	169.74	0.02427	0.04064	0.01637
75.53	0.00891	0.01029	0.00138	170.01	0.04729	0.03432	0.01297
81.33	0.01312	0.01312	0.00000	175.24	0.01511	0.01511	0.00000
88.58	0.00475	0.00475	0.00000	178.19	0.02369	0.02120	0.00249
88.67	0.01062	0.01163	0.00101	190.17	0.01776	0.01776	0.00000
99.84	0.00000	0.00448	0.00448	192.85	0.05853	0.05584	0.00269
107.94	0.01361	0.01361	0.00000	207.76	0.01962	0.02196	0.00233
108.47	0.01358	0.01358	0.00000				
110.46	0.05384	0.05554	0.00170				

11.3. P840-60 results

P840-60 next to the first vertical rod

Freq. (SC) [Hz]	Freq. (OC) [Hz]	K undamaged	Freq. (SC) [Hz]	Freq. (OC) [Hz]	K damaged	ΔK
24.81	24.81	0.02540	23.04	23.05	0.03090	0.00550
39.63	39.63	0.00710	39.62	39.62	0.00000	0.00710
50.83	50.83	0.00627	50.82	50.82	0.00000	0.00627
55.83	55.83	0.00846	54.71	54.72	0.02180	0.01334
58.36	58.38	0.02414	54.71	54.72	0.02180	0.00234
58.36	58.38	0.02414	61.71	61.71	0.00000	0.02414
63.29	63.30	0.01687	61.71	61.71	0.00000	0.01687
55.83	55.83	0.00846	56.81	56.82	0.01876	0.01030
	no matching mode		64.64	64.65	0.01244	0.01244
81.28	81.28	0.00702	81.24	81.24	0.00496	0.00205
88.55	88.55	0.00475	88.55	88.55	0.00475	0.00000
88.60	88.60	0.00475	88.51	88.51	0.00475	0.00000
99.25	99.26	0.00449	98.72	98.72	0.00000	0.00449
107.77	107.78	0.01362	107.09	107.12	0.02367	0.01005
108.89	108.93	0.02711	108.52	108.53	0.01358	0.01353
112.55	112.56	0.01333	113.23	113.25	0.01880	0.00547
130.52	130.52	0.00000	130.89	130.90	0.01236	0.01236
131.83	131.83	0.00000	132.27	132.28	0.01230	0.01230
137.26	137.27	0.01207	136.52	136.52	0.00000	0.01207
141.27	141.27	0.00000	143.18	143.19	0.01182	0.01182
144.37	144.37	0.00000	143.18	143.19	0.01182	0.01182
147.08	147.09	0.01166	147.27	147.28	0.01165	0.00001
164.50	164.54	0.02205	164.22	164.25	0.01912	0.00294
168.01	168.04	0.01890	166.06	166.10	0.02195	0.00305
177.82	177.83	0.01061	175.72	175.73	0.01067	0.00006
189.27	189.30	0.01781	186.55	186.59	0.02071	0.00290
190.79	190.81	0.01448	190.57	190.57	0.00000	0.01448

P840-60 between the first diagonal rod and the second diagonal rod						
Freq. (SC) [Hz]	Freq. (OC) [Hz]	K undamaged	Freq. (SC) [Hz]	Freq. (OC) [Hz]	K damaged	ΔK
46.132	46.132	0.00000	46.999	47.000	0.00652	0.00652
48.403	48.403	0.00000	48.416	48.417	0.00643	0.00643
54.150	54.177	0.03158	47.526	47.570	0.04304	0.01146
55.860	55.862	0.00846	54.034	54.034	0.00000	0.00846
55.860	55.862	0.00846	56.494	56.495	0.00595	0.00251
57.893	57.896	0.01018	57.515	57.515	0.00000	0.01018
58.067	58.068	0.00587	57.515	57.515	0.00000	0.00587
121.090	121.090	0.00000	121.750	121.750	0.00000	0.00000
122.750	122.780	0.02211	126.730	126.760	0.02176	0.00035
131.920	131.920	0.00000	132.200	132.210	0.01230	0.01230
136.050	136.050	0.00000	130.120	130.130	0.01240	0.01240
219.590	219.590	0.00000	216.580	216.590	0.00961	0.00961

P840-60 between the upper chord and the diagonal rod						
Freq. (SC) [Hz]	Freq. (OC) [Hz]	K undamaged	Freq. (SC) [Hz]	Freq. (OC) [Hz]	K damaged	ΔK
50.569	50.57	0.00629	50.538	50.538	0.000000	0.00629
53.161	53.161	0.00000	53.629	53.631	0.008636	0.00864
54.179	54.186	0.01608	54.667	54.672	0.013525	0.00255
153.39	153.41	0.01615	155.25	155.27	0.016052	0.00010
163.71	163.72	0.01105	163.71	163.72	0.011053	0.00000
168.09	168.1	0.01091	165.73	165.73	0.000000	0.01091
188.7	188.71	0.01030	186.1	186.1	0.000000	0.01030

Bibliography

[1] C. R. Farrar and K. Worden, "An introduction to structural health monitoring," *Philosophical Transactions of the Royal Society A: Mathematical, Physical and Engineering Sciences*, vol. 365, no. 1851, pp. 303–315, Feb. 2007, doi: 10.1098/rsta.2006.1928.

[2] C. R. Farrar and K. Worden, *Structural Health Monitoring*. Wiley, 2012. doi: 10.1002/9781118443118.

[3] Wei Fan and Pizhong Qiao, "Vibration-based Damage Identification Methods: A Review and Comparative Study," *Struct Health Monit*, vol. 10, no. 1, pp. 83–111, Jan. 2011, doi: 10.1177/1475921710365419.

[4] P. Cawley and R. D. Adams, "The location of defects in structures from measurements of natural frequencies," *J Strain Anal Eng Des*, vol. 14, no. 2, pp. 49–57, Apr. 1979, doi: 10.1243/03093247V142049.

[5] B. Peeters and G. De Roeck, "One-year monitoring of the Z24-Bridge: environmental effects versus damage events," *Earthq Eng Struct Dyn*, vol. 30, no. 2, pp. 149–171, Feb. 2001, doi: 10.1002/1096-9845(200102)30:2<149::AID-EQE1>3.0.CO;2-Z.

[6] O. S. Salawu, "Detection of structural damage through changes in frequency: a review," *Eng Struct*, vol. 19, no. 9, pp. 718–723, Sep. 1997, doi: 10.1016/S0141-0296(96)00149-6.

[7] Pavoni Stefano, "Development of a damage detection technique with a strong immunity to environmental influence implemented on a laboratory truss girder subjected to ambient variations," 2024.

[8] C. R. Farrar and G. H. James, "SYSTEM IDENTIFICATION FROM AMBIENT VIBRATION MEASUREMENTS ON A BRIDGE," *J Sound Vib*, vol. 205, no. 1, pp. 1–18, Aug. 1997, doi: 10.1006/JSVI.1997.0977.

[9] O. ~S. Salawu and C. Williams, "Damage Location Using Vibration Mode Shapes," in *Proceedings of the 12th International Modal Analysis*, D. J. DeMichele, Ed., in Society of Photo-Optical Instrumentation Engineers (SPIE) Conference Series, vol. 2251. Mar. 1994, p. 933.

[10] O. Huth, G. Feltrin, J. Maeck, N. Kilic, and M. Motavalli, "Damage Identification Using Modal Data: Experiences on a Prestressed Concrete Bridge," *Journal of Structural Engineering*, vol. 131, no. 12, pp. 1898–1910, Dec. 2005, doi: 10.1061/(ASCE)0733-9445(2005)131:12(1898).

[11] J. Zenisek, F. Holzinger, and M. Affenzeller, "Machine learning based concept drift detection for predictive maintenance," *Comput Ind Eng*, vol. 137, p. 106031, Nov. 2019, doi: 10.1016/J.CIE.2019.106031.

[12] C. Papadimitriou, E. Ntotsios, D. Giagopoulos, and S. Natsiavas, "Variability of updated finite element models and their predictions consistent with vibration measurements," *Struct Control Health Monit*, vol. 19, no. 5, pp. 630–654, Aug. 2012, doi: 10.1002/stc.453.

[13] P. Seventekidis, D. Giagopoulos, A. Arailopoulos, and O. Markogiannaki, "Structural Health Monitoring using deep learning with optimal finite element model generated data," *Mech Syst Signal Process*, vol. 145, p. 106972, Nov. 2020, doi: 10.1016/J.YMSSP.2020.106972.

[14] P. Jiao, K.-J. I. Egbe, Y. Xie, A. Matin Nazar, and A. H. Alavi, "Piezoelectric Sensing Techniques in Structural Health Monitoring: A State-of-the-Art Review," *Sensors*, vol. 20, no. 13, p. 3730, Jul. 2020, doi: 10.3390/s20133730.

[15] W. Yan and W. Q. Chen, “Structural Health Monitoring Using High-Frequency Electromechanical Impedance Signatures,” *Advances in Civil Engineering*, vol. 2010, pp. 1–11, 2010, doi: 10.1155/2010/429148.

[16] A. J. Croxford, P. D. Wilcox, B. W. Drinkwater, and G. Konstantinidis, “Strategies for guided-wave structural health monitoring,” *Proceedings of the Royal Society A: Mathematical, Physical and Engineering Sciences*, vol. 463, no. 2087, pp. 2961–2981, Nov. 2007, doi: 10.1098/rspa.2007.0048.

[17] F. Baptista, D. Budoya, V. Almeida, and J. Ulson, “An Experimental Study on the Effect of Temperature on Piezoelectric Sensors for Impedance-Based Structural Health Monitoring,” *Sensors*, vol. 14, no. 1, pp. 1208–1227, Jan. 2014, doi: 10.3390/s140101208.

[18] G. Park and D. J. Inman, “Structural health monitoring using piezoelectric impedance measurements,” *Philosophical Transactions of the Royal Society A: Mathematical, Physical and Engineering Sciences*, vol. 365, no. 1851, pp. 373–392, Feb. 2007, doi: 10.1098/rsta.2006.1934.

[19] V. Giurgiutiu and A. N. Zagrai, “Characterization of Piezoelectric Wafer Active Sensors,” *J Intell Mater Syst Struct*, vol. 11, no. 12, pp. 959–976, Dec. 2000, doi: 10.1106/A1HU-23JD-M5AU-ENGW.

[20] W. Na and J. Baek, “Adhesive Defect Monitoring of Glass Fiber Epoxy Plate Using an Impedance-Based Non-Destructive Testing Method for Multiple Structures,” *Sensors*, vol. 17, no. 6, p. 1439, Jun. 2017, doi: 10.3390/s17061439.

[21] V. Giurgiutiu, “Tuned Lamb Wave Excitation and Detection with Piezoelectric Wafer Active Sensors for Structural Health Monitoring,” *J Intell Mater Syst Struct*, vol. 16, no. 4, pp. 291–305, Apr. 2005, doi: 10.1177/1045389X05050106.

[22] V. T. Rathod, D. Roy Mahapatra, and S. Gopalakrishnan, “Lamb wave based identification and parameter estimation of corrosion in metallic plate structure using a circular PWAS array,” T. Kundu, Ed., Mar. 2009, p. 72951C. doi: 10.1117/12.816558.

[23] S. O. Reza Moheimani Andrew John Fleming, *Piezoelectric Transducers for Vibration Control and Damping*. London: Springer-Verlag, 2006. doi: 10.1007/1-84628-332-9.

[24] “IEEE Standard on Piezoelectricity,” *ANSI/IEEE Std 176-1978*, pp. 1–58, 1978, doi: 10.1109/IEEESTD.1978.8941331.

[25] B de Marneffe and A Preumont, *Active Control of Vibration*. Elsevier, 1996. doi: 10.1016/B978-0-12-269440-0.X5000-6.

[26] “www.PicaCeramic.com.”

[27] “Modal Analysis Conference 2006 : IMAC-XXIV; a Conference & Exposition on Structural Dynamics; held January 30 - February 2, 2006, St. Louis, Missouri, USA / Society for Experimental Mechanics ; Vol. 3,” Bethel, Conn.: SEM; , 2006. [Online]. Available: https://www.tib.eu/de/suchen/id/TIBKAT%3A512462380

[28] C. Ayela, L. Nicu, C. Soyer, E. Cattan, and C. Bergaud, “Determination of the d31 piezoelectric coefficient of PbZrxTi1−xO3 thin films using multilayer buckled micromembranes,” *J Appl Phys*, vol. 100, no. 5, Sep. 2006, doi: 10.1063/1.2338139.

[29] H. Li, B. Piekarski, D. L. DeVoe, and B. Balachandran, “Nonlinear oscillations of piezoelectric microresonators with curved cross-sections,” *Sens Actuators A Phys*, vol. 144, no. 1, pp. 194–200, May 2008, doi: 10.1016/J.SNA.2007.12.015.

[30] M. Berardengo, O. Thomas, C. Giraud-Audine, and S. Manzoni, “Improved resistive shunt by means of negative capacitance: new circuit, performances and multi-mode control,” *Smart Mater Struct*, vol. 25, no. 7, p. 075033, Jul. 2016, doi: 10.1088/0964-1726/25/7/075033.

[31] C. L. Davis and G. A. Lesieutre, “A modal strain energy approach to the prediction of resistively shunted piezoceramic damping,” *J Sound Vib*, vol. 184, no. 1, pp. 129–139, Jul. 1995, doi: 10.1006/JSVI.1995.0308.

[32] G. A. Lesieutre and C. L. Davis, “Can a Coupling Coefficient of a Piezoelectric Device be Higher Than Those of Its Active Material?,” *J Intell Mater Syst Struct*, vol. 8, no. 10, pp. 859–867, Oct. 1997, doi: 10.1177/1045389X9700801005.

[33] M. Trindade and A. Benjeddou, “Effective Electromechanical Coupling Coefficients of Piezoelectric Adaptive Structures: Critical Evaluation and Optimization,” *Mechanics of Advanced Materials and Structures*, vol. 16, no. 3, pp. 210–223, Apr. 2009, doi: 10.1080/15376490902746863.

[34] M. Berardengo, S. Manzoni, O. Thomas, and M. Vanali, “Piezoelectric resonant shunt enhancement by negative capacitances: Optimisation, performance and resonance cancellation,” *J Intell Mater Syst Struct*, vol. 29, no. 12, pp. 2581–2606, Jul. 2018, doi: 10.1177/1045389X18770874.

[35] M. Berardengo, O. Thomas, C. Giraud-Audine, and S. Manzoni, “Improved resistive shunt by means of negative capacitance: new circuit, performances and multi-mode control,” *Smart Mater Struct*, vol. 25, no. 7, p. 075033, Jul. 2016, doi: 10.1088/0964-1726/25/7/075033.

[36] S. Hamay Cole et al., “Experimental damage identification of carbon/epoxy composite beams using curvature mode shapes,” *Structural Health Monitoring (2004)*, Jan. 2004.

[37] M. BRAMBILLA, “Detection of structural alterations by means of a piezoelectric pattern,” 2018.

[38] Schena N., “Identification of structural alterations in truss structures by means of piezoelectric stacks,” 2021, doi: https://hdl.handle.net/10589/183294.

[39] M. Berardengo, M. Brambilla, A. Codina, N. Schena, and S. Manzoni, “Piezoelectric coupling as a feature sensitive to structural alterations,” *Mech Syst Signal Process*, vol. 224, p. 112012, Jan. 2025, doi: 10.1016/j.ymssp.2024.112012.

[40] M. Berardengo, S. Manzoni, M. Brambilla, M. Vanali, A. Codina, and others, “The use of piezoelectric coupling in structural monitoring as a feature robust to EOV,” *THE E-JOURNAL OF NONDESTRUCTIVE TESTING*, pp. 1–8, 2024.

[41] T. Wu, Z. Chen, J. Qu, and D. Yu, “The optimal placement of piezoelectric actuator and sensor for active structural noise control of plates,” *Smart Mater Struct*, vol. 31, no. 9, p. 095028, Sep. 2022, doi: 10.1088/1361-665X/ac8210.

[42] X. Liu, G. Cai, F. Peng, and H. Zhang, “Piezoelectric Actuator Placement Optimization and Active Vibration Control of a Membrane Structure,” *Acta Mechanica Solida Sinica*, vol. 31, no. 1, pp. 66–79, Feb. 2018, doi: 10.1007/s10338-018-0005-y.

[43] “Mounting_Handling_Instructions_for_Piezo_Actuators. https://www.pi-usa.us”.

[44] “https://www.physikinstrumente.com/en/products/linear-actuators/nanopositioning-piezo-actuators/p-840-preloaded-piezo-actuators-101000#downloads”.

[45] B. Peeters, H. Van der Auweraer, P. Guillaume, and J. Leuridan, “The PolyMAX Frequency-Domain Method: A New Standard for Modal Parameter Estimation?,” *Shock and Vibration*, vol. 11, no. 3–4, pp. 395–409, Jan. 2004, doi: 10.1155/2004/523692.

[46] “LMS International, The LMS Theory and Background Book, Leuven, Belgium, 2000”.

[47] H. Van der Auweraer and B. Peeters, “Discriminating physical poles from mathematical poles in high order systems: use and automation of the stabilization diagram,” in *Proceedings of the 21st IEEE Instrumentation and Measurement Technology Conference (IEEE Cat. No.04CH37510)*, IEEE, pp. 2193–2198. doi: 10.1109/IMTC.2004.1351525.

[48] “Modal_Analysis_Theory_and_Testing”.